



Characterization of Nisin-regulating NisR  
and Nisin-modifying NisC from  
*Lactococcus lactis*

Inaugural-Dissertation

For the attainment of the title of doctor  
in the Faculty of Mathematics and Natural Sciences  
at the Heinrich Heine University Duesseldorf

Presented by

Siai Zhang

From Tianjin, P.R. China

Düsseldorf, May 2018

From the Institute of Biochemistry  
At the Heinrich Heine University Düsseldorf

Published by permission of the  
Faculty of Mathematics and Natural Sciences at  
Heinrich Heine University Düsseldorf

Supervisor: Prof. Dr. Lutz Schmitt  
Co-supervisor:

Date of the oral examination: 28.06.2018

That which does not kill us makes us stronger.

(Friedrich Nietzsche)





## Abstract

Lantibiotics are ribosomally synthesized and posttranslationally modified peptide (RiPPs) antibiotics. Nisin (NisA), produced by *Lactococcus lactis*, is a 34-residue long peptide and contains five cyclic thioether rings which have been proven to be crucial for activity. The precursor of nisin was initially biosynthesized from ribosome and later on further processed by a series of maturation steps to achieve a fully functional nisin molecule. The biosynthesis process is regulated via a two-component system, consisting of a histidine kinase (NisK) and a response regulatory protein (NisR). And for the later-on maturation process, five lanthionine rings are installed by a two-step process that first involves dehydration (NisB) of Ser and Thr residues to the corresponding dehydroalanines and dehydrobutyrines, followed by regioselective addition (NisC) of C-terminal Cys residues to the dehydroamino acids.

The NisK/NisR two-component machinery can regulate not only the biosynthesis of Nisin; in the Nisin-controlled gene expression system (NICE), it is also used for heterologous protein expression. To perform a thorough study on this pathway, both of the proteins are required. In this work, NisR was successfully expressed in *E. coli*, purified and proved to be homogeneous at both, pH 9 and pH 11. As a regulatory protein, its binding affinity was verified through electrophoretic mobility shift assay. Additionally, a series of crystallization trials were performed on NisR.

On the other hand, due to the fact that peptides are usually vulnerable to the acid-mediated hydrolysis and proteolytic degradation, their applications for therapeutic and industrial purpose are highly restricted. The thioether installing enzymes, such as NisC, on the other hand, has been demonstrated of stabilizing a broad range of peptides by introducing thioether bridges. Thus, with a goal of improving the feasibility of designing novel peptides with high bioavailability, obtaining the structural information of NisC in complex with NisA (AC complex) is considered to be the most straightforward way for understanding the mechanism of cyclization. Both co-crystallization and soaking were used to obtain the crystal of AC complex. Meanwhile, crystals of NisC in complex with phosphoenol pyruvate were obtained and the structure was solved by X-ray crystallography. The structure revealed PEP located in the active site of NisC, being anchored by His<sup>212</sup>, and was therefore suggested to be an activating agent for NisC modification reaction.



## Zusammenfassung

Lantibiotica sind ribosomal synthetisierte und posttranslational modifizierte Peptidantibiotika (RiPPs). Nisin (NisA) wird vom Bakterium *Lactococcus lactis* produziert und ist 34 Aminosäuren lang. Es enthält fünf Thioetherringe, die für die antimikrobielle Aktivität verantwortlich sind. Die Nisin Vorstufe wird initial am Ribosom synthetisiert und durchläuft mehrere Reifungsprozesse bis es seine biologisch aktive Form erreicht hat. Der Biosynthese-Prozess wird von einem zwei Komponenten System kontrolliert, bestehend aus der Histidin Kinase (NisK) und dem Regulator (NisR). Im Laufe der Reifung werden durch die Dehydratase NisB die Serin- und Threoninreste im Kernpeptid dehydratisiert, wodurch die korrespondierenden Aminosäuren Didehydroalanin und Didehydrobutyrin entstehen. Danach erfolgt der regioselektive Ringschluss dieser dehydratisierten Aminosäuren mit einem C-terminalen Cysteinrest durch die Zyklase NisC.

Das NisK/NisR zwei Komponenten System reguliert nicht nur die Biosynthese von Nisin. Im *Nisin-controlled gene expression system* (NICE) dient es auch der Expression heterologer Proteine. Für eine umfassende Studie dieses Regulationsweges sind demnach beide Proteine notwendig. In dieser Arbeit wurde NisR erfolgreich heterolog in *E. coli* exprimiert und konnte bis zur Homogenität bei pH 9 und pH 11 gereinigt werden. Da es sich um ein regulatorisches Protein handelt, wurde die Bindungsaffinität zu Nisin mittels *electrophoretic mobility shift assay* (EMSA) verifiziert. Des weiteren wurden verschiedene Ansätze durchgeführt um NisR zu kristallisieren.

Der Einsatz von Peptiden in industriellen oder therapeutischen Ansätzen ist aufgrund der sauren Hydrolyse oder dem proteolytischen Abbau eingeschränkt. Durch den Einsatz von Zyklasen, wie der Zyklase NisC, konnte gezeigt werden, dass ein breites Spektrum an Peptiden durch die Einführung von Thioetherringen eine erhöhte Stabilität aufwiesen. Das Ziel ist es durch die Verbesserung der Prozessierung neue, veränderte Substanzen mit hoher Bioaktivität zu generieren. Hierfür sind strukturelle Information über das NisA gebundene NisC (AC Komplex) wichtig, um ein besseres Verständnis für den Mechanismus der Zyklisierung zu erhalten. Es wurden sowohl Co-Kristallisationen von NisA/NisC versucht als auch später das *soaking* eines NisC Kristalls mit NisA. Währenddessen konnten NisC Kristalle gefunden werden, in

welchen sich nach der Strukturaufklärung ein Phosphoenolpyruvat (PEP) Molekül im aktiven Zentrum von NisC befand. Dieses PEP war an der Aminosäure His212 gebunden, was impliziert, dass es einen verstärkten Effekt auf die Zyklisierung haben könnte.

# Contents

1. Introduction .....	1
1.1 Ribsomally-synthesized and post-translationally modified peptides.....	1
1.2 Bacteriocins.....	2
1.3 Lantibiotics.....	3
1.3.1 Leader peptide of lantibiotics .....	6
1.3.2 Biological activities of lantibiotics .....	6
1.4 The nisin system.....	8
1.5 NisR/NisK – the two-component regulation system.....	11
1.5.1 The nisin-controlled gene expression system (NICE).....	11
1.6 Post-translational modifications of nisin.....	12
1.6.1 NisB – the nisin dehydratase .....	13
1.6.2 NisC – the nisin cyclase .....	15
2. Aims.....	17
3. Materials and Methods .....	18
3.1 Materials.....	18
3.1.1 Chemicals .....	18
3.1.2 Enzymes, standards and antibodies.....	20
3.1.3 Buffers .....	21
3.1.4 Chromatographic materials and others.....	22
3.1.5 Instruments .....	22
3.2 Microbiological methods.....	23
3.2.1 Overexpression of NisC, non-spacer NisC and its mutant H331A .....	23
3.2.2 Overexpression of dehydrated prenisin.....	24
3.2.3 Overexpression of NisR (N-terminal His-tagged and C-terminal His-tagged).....	24
3.3 Biochemical methods.....	24
3.3.1 Purification of NisC, non-spacer NisC and its mutant H331A .....	24
3.3.2 Purification of dehydrated prenisin .....	25
3.3.3 RP-HPLC analysis of prenisin .....	25
3.3.4 Purification of NisR (C-terminal and N-terminal).....	26
3.3.5 SDS-polyacrylamide gel electrophoresis (SDS-PAGE).....	26
3.3.6 Western blot .....	27
3.3.7 Electrophoretic Mobility Shift Assay (EMSA) of NisR.....	28
3.3.8 AC complex formation analysis using Multi-Angle Light Scattering (MALS-SEC).....	28
3.3.9 Binding assay of NisC to PEP by ITC .....	29
3.4 Crystallographic methods.....	29
3.4.1 Fundamental theory of crystallization .....	29
3.4.2 Crystallization techniques.....	31
3.4.3 Soaking and co-crystallization .....	35
3.4.4 Co-crystallization of NisC with PEP .....	36
3.4.5 Finding optimal conditions for crystallization.....	36
3.4.6 Basics of x-ray crystallography .....	37
3.4.7 Harvesting and mounting of crystals.....	41
3.4.8 Data collection and processing.....	43

3.4.9 Reconstruction of electron density .....	43
3.4.10 Phase determination .....	44
3.4.11 Model building and refinement .....	52
4. Results .....	52
4.1 Characterization of response regulator NisR .....	52
4.1.1 Overexpression and purification of NHis-NisR and CHis-NisR.....	52
4.1.2 Crystallization of NisR .....	60
4.1.3 DNA binding assay of NisR.....	61
4.2 Characterization of NisC .....	63
4.2.1 Overexpression and purification of NisC in <i>E. coli</i> .....	63
4.2.2 NisC with three Zn <sup>2+</sup> ions .....	66
4.2.2.1 Crystallization .....	67
4.2.2.2 Data collection and processing .....	67
4.2.2.3 Overall structure .....	68
4.2.2.4 Active site possessing three Zn <sup>2+</sup> .....	69
4.2.2.5 Crystal packing of NisC.....	70
4.2.3 Extra Zn <sup>2+</sup> ions removal .....	71
4.2.3.1 Crystallization and data processing.....	71
4.2.3.2 Overall structure .....	73
4.2.3.3 A structure revealing extra density.....	74
4.2.4 PEP binding to NisC.....	75
4.2.4.1 Co-crystallization of NisC in complex with PEP .....	75
4.2.4.2 Data collection and processing .....	76
4.2.4.3 PEP binding site .....	77
4.2.4.4 Binding property of NisC to PEP .....	78
4.2.5 Crystallization of NisC in complex with NisA.....	79
4.2.5.1 Expression of prenisin (NisA) in <i>L. lactis</i> .....	79
4.2.5.2 MALS-SEC analysis of AC complex formation and its stability .....	80
4.2.5.3 Crystallization of AC complex using the NisC construct with the four amino acid spacer .....	83
4.2.5.4 AC complex crystallization using the NisC construct without spacer	85
4.2.5.5 AC complex crystallization using NisC H331A.....	85
4.2.6 The stability of AC complex with PEP adding-in .....	86
5. Discussion.....	87
5.1 NisR.....	87
5.1.1 NisR with N-terminal His-tag .....	89
5.1.2 NisR with C-terminal His-tag.....	90
5.1.3 Whether or not NisR can bind to its corresponding promoter? .....	91
5.2 AC complex .....	91
5.2.1 Formation of AC complex.....	92
5.2.2 Crystallization.....	92
5.2.3 Is AC complex stable enough?.....	93
5.3 NisC with PEP.....	94
5.3.1 Crystallization.....	94
5.3.2 Why is PEP surely in the structure? .....	94
6. Summary .....	97
7. Literature .....	97
8. Curriculum vitae .....	106
9. Acknowledgements.....	109

10. Declaration .....	112
-----------------------	-----





# **1. Introduction**

## **1.1 Ribsomally-synthesized and post-translationally modified peptides**

Ribsomally-synthesized and post-translationally modified peptides (RiPPs) are produced in all three kingdoms of life, archaea, bacteria, and eukaryotes, respectively. RiPPs have been subdivided based on either the producing organism or their biological activities [1]. Microcins, for example, are gene-encoded antibacterial peptides produced by enterobacteria, Gram negative bacteria [2]. Another example is bacteriocins, the antimicrobial peptides responsible for killing closely related bacteria [3, 4]. They are produced mainly by Gram positive bacteria [5]. Nisin, as one of the most famous bacteriocins, has been used as a food preservative for over 50 years [6]. The extensive post-translational modifications (PTMs) of RiPPs provide greater structural diversity and more rigid structures compared to linear peptides [7]. Moreover, via PTMs, RiPPs can be equipped with expanded chemical functionalities (e.g. cyanobactins), improved target recognition (e.g. thiopeptides), and increased metabolic and chemical stability (e.g. lanthipeptides) [1, 8, 9].

The biosynthesis of RiPPs is initiated with a ribosomally generated precursor peptide encoded by the structural gene of the operon. The precursor peptide usually contains an N-terminal leader peptide that is important for recognition by PTM enzymes and for subsequent secretion. Sometimes, a C-terminal recognition sequence (RS) is also present for initiating the proteolysis and cyclization of the core peptide (cyanobactins) [1] (Figure 1). Upon the binding of precursor peptide to the modifying enzyme(s), various post-translational modifications are installed in the core peptide. The leader peptide will be afterwards removed by proteolytic cleavage in the last step of the maturation process, which releases the mature peptide with full functionality [9].

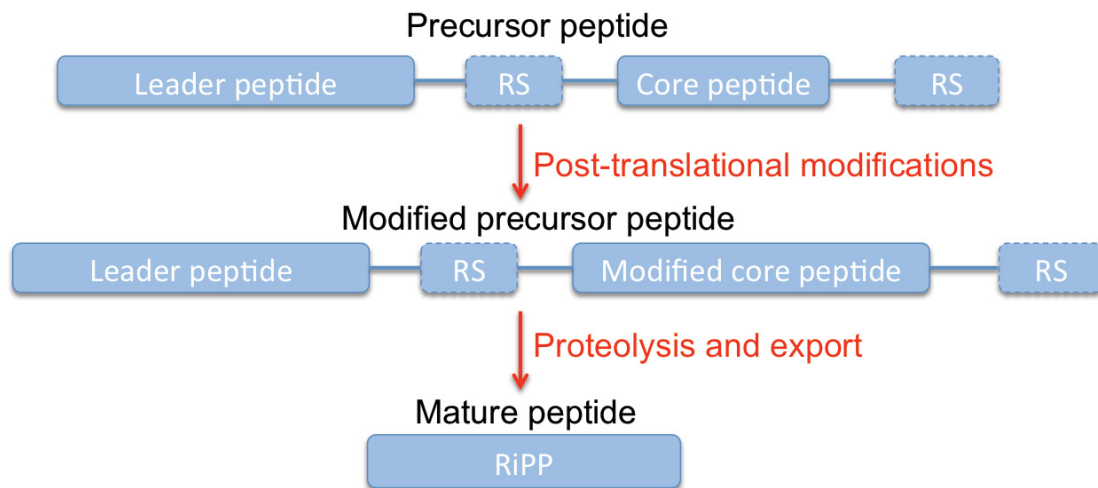


Figure 1. The pathway of RiPPs biosynthesis. Created based on [9]. RS: recognition sequence.

## 1.2 Bacteriocins

Bacteriocins are ribosomally produced antimicrobial peptides from bacteria, either post-translationally modified or not, that can help the producer organism to outcompete other bacterial species [10]. In general, bacteriocins are active against a wide spectrum of Gram-positive bacteria [11]. And 99% of all bacteria may synthesize at least one bacteriocin and the only reason why we haven't isolated more is that few researchers have searched for them [5, 12]. Lactic acid bacteria (LAB), a type of Gram positive bacteria with great biotechnological potential in the food industry, are one of the major producers of bacteriocins. Therefore, bacteriocins produced by LAB are generally considered as safe compounds with interesting properties, such as stability, antimicrobial activity, lack of toxicity, no flavor alteration, etc. [3, 13].

According to the biosynthesis mechanism, bacteriocins can be classified into three classes (Figure 2):

**Class I: RiPPs (less than 10 kDa)** This class contains all the peptides that are processed by PTM enzymes. These enzymatic modifications would endow peptides with uncommon amino acids and structures that have an impact on their properties. Lanthipeptides are a typical example as they possess lanthionine rings in their structures, which dramatically prolong their biostability [14].

**Class II: unmodified bacteriocins (less than 10 kDa)** This class of bacteriocins does not contain unusual modifications. Therefore, enzymes for maturations are not required except a leader peptidase and a transporter.

**Class III:** They are unmodified bacteriocins larger than 10 kDa with bacteriolytic or non-lytic mechanism of actions [3].

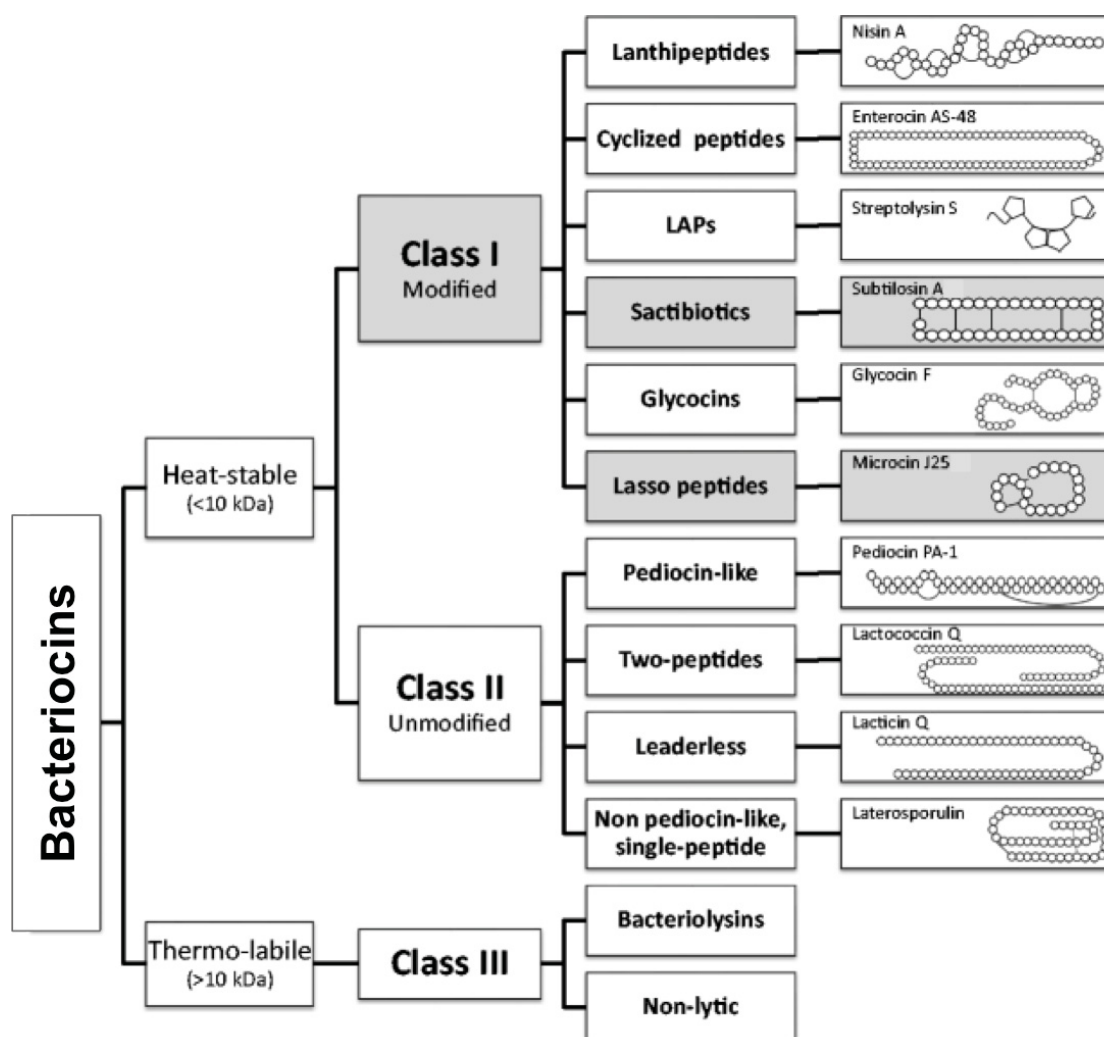


Figure 2. Classifications of bacteriocins and their structures. Classes identified in silico are depicted in gray. Structure of non-lytic bacteriocins of class III still remains uncharacterized. Adapted from [3].

### 1.3 Lantibiotics

Lantipeptides are a class of post-translationally modified peptides containing characteristic thioether cross-links imperative for bioactivity and stability. Based on

PTM enzymes involved in the maturation process, lantipeptides can be divided into four classes (Figure 3). For class I, serine/threonine dehydration and thioether cyclization are performed by the dehydratase LanB and the cyclase LanC, respectively. The most well-known example for class I lantipeptide is Nisin, which will be described in detail later. For class II, these reactions are carried out by a single bifunctional lantipeptide synthetase, LanM, containing an N-terminal dehydratase and a C-terminal LanC-like cyclase domains. Lacticin 3147 from *Lactococcus lactis* is one of the best-studied type II lantipeptides, which consists of two peptides, LtnA1 and LtnA2 that are processed by LtnM1 and LtnM2, respectively. [15]. Class III lantipeptides are modified by a trifunctional synthetase bearing an N-terminal lyase domain, a central kinase domain, and a putative C-terminal cyclase domain, which lacks many of the conserved active site residues found in LanC/LanM [16, 17]. Finally, class IV lantipeptides are synthesized by LanL, which contains N-terminal lyase and kinase domains as in class III, but its C-terminal cyclase domain is analogous to LanC [18, 19]. Among these, only types I and II can be considered as lantibiotics due to their confirmed antimicrobial activities.

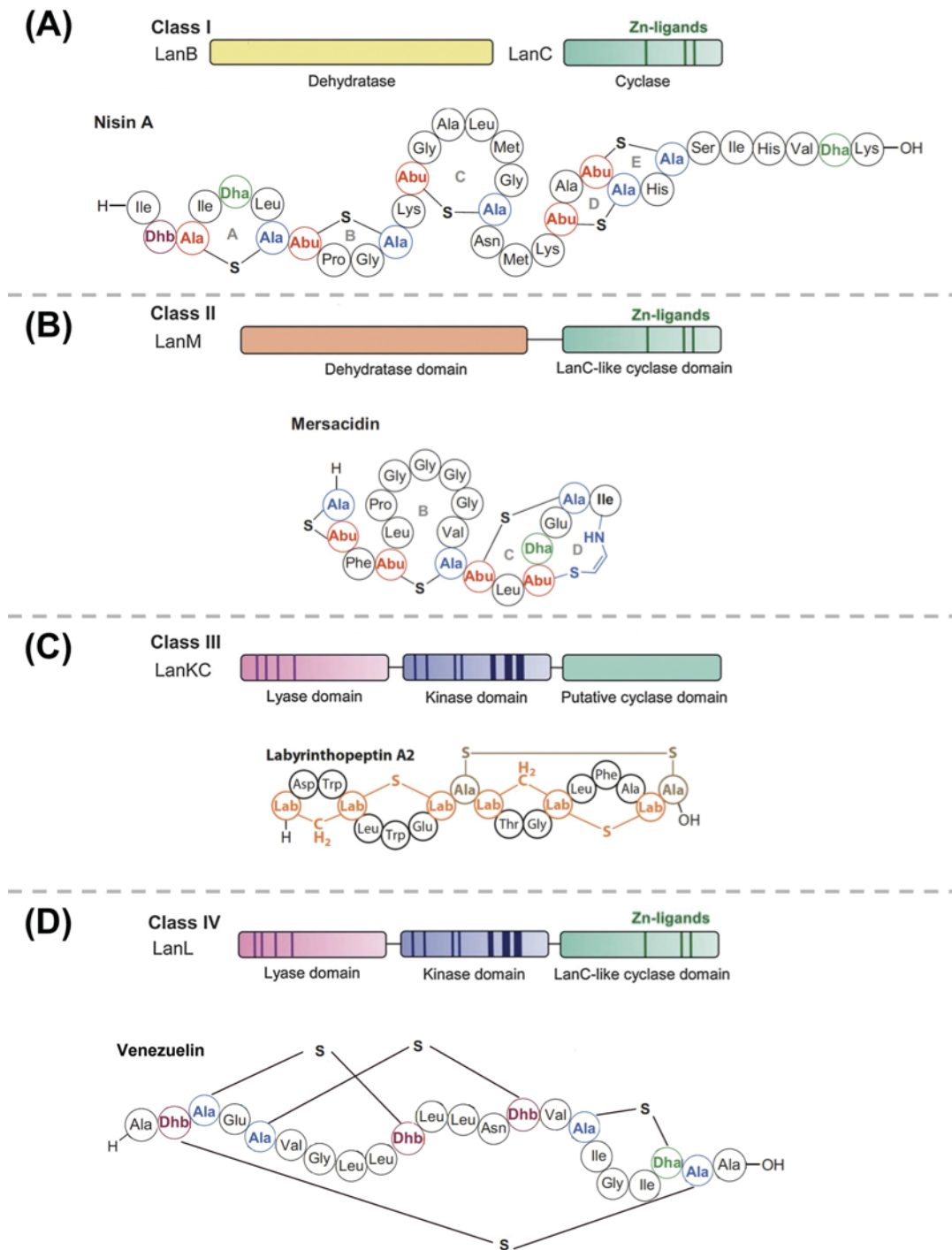


Figure 3. The four classes of lanthionine generating enzymes, highlighting conserved motifs. Abbreviations: LabKC, labionin synthetase; LanB, lantipeptide dehydratase; LanC, lanthipeptide cyclase; LanL, class IV lanthipeptide synthetase; LanM, class II lanthipeptide synthetase; RamC, SapB-modifying synthetase. Based on [14].

### **1.3.1 Leader peptide of lantibiotics**

Although the mechanism of how the leader peptide facilitates lantipeptide maturation is still not clear [20], the conserved FNLD box of class I leader peptides is clearly important for its maturation process as simultaneous replacement of the FNLD amino acids by four alanines would strongly reduce export and even lead to a complete loss of the capacity to induce modifications [21]. However, it appears that single substitutions on FNLD box would not hurt the efficiency of LanB/C modification [21, 22]. A similar phenomenon was observed for class II [23-25] and class III [26] leader peptides. A distinction between leader peptides of different classes is that the N-terminal residues are critical for modification in class I [21] and class III [26]. Whereas the C-terminus appears more important for class II given that the N-terminus could be truncated from class II precursor peptides without losing modification activity [27]. Leader peptide binding was shown not to be very tight in a few cases [28, 29], which is possibly designed on purpose to prevent product inhibition. This would ensure that the product leaves once the reaction is finished so that the enzyme is ready for another substrate, as a result to enhance the enzyme efficiency. Although identification of exact binding interactions has been challenging, recognition of the leader peptide is clearly different between the synthetase and protease in both, class I and II [21, 24, 25, 30], and thus different parts of the leader peptide may be involved in different steps of modification process.

### **1.3.2 Biological activities of lantibiotics**

Most lantibiotics target components of the plasma membrane of bacteria, with more than one-third of the known lantibiotics targeting lipid II. Among these, Nisin is the best known and most extensively studied lantibiotic [31, 32]. It was discovered that nisin uses lipid II as a ‘docking molecule’ to form pores in a targeted manner with high efficiency [33, 34].

Thus, nisin can permeabilize membranes by two different mechanisms: through a low-affinity permeation mechanism; and through a lipid-II-dependent targeted pore-formation mechanism, which is much more efficient. In the first mechanism, which requires micromolar concentrations of nisin and the presence of anionic lipids in the

target membrane, nisin binds to anionic lipids, and then inserts between the phospholipid head groups. The accumulation of nisin in the outer lipid leaflet of the target membrane drives aggregation of nisin monomers, which is followed by formation of short-lived pore-like structures. The pore formation process usually involves translocation of the C-terminal region of the molecule across the membrane [35, 36].

The second working mechanism of nisin, which operates in the presence of lipid II in the membrane (as in Gram positive bacteria), can be described as follows: specific recognition and binding of lipid II, followed by assembly and pore formation (Figure 4). If nisin can interact with lipid II in the target membrane of a bacterium, it will follow the lipid II dependent pathway for pore formation, as the affinity of nisin for lipid II ( $2 \times 10^7 \text{ M}^{-1}$ ) is much higher than the affinity of nisin for membranes containing anionic lipids (about  $1,800 \text{ M}^{-1}$ ) [34, 37]. It was supported by the observation that, in the presence of lipid II, nisin activity was not dependent on the membrane lipid composition [38]. Furthermore, several experiments have shown that the pores formed by nisin in the presence of lipid II are much more stable than pores formed in the absence of the receptor [39-42]. Nisin has a stable transmembrane orientation in the presence of lipid II, indicating that stable pores are formed [41] and also, in the nisin-mediated pore formation process, lipid II is not only a receptor. Indeed, two independent approaches have shown that lipid II is a constituent of the pore complex [43, 44], the stoichiometry of which is four lipid II molecules and eight nisin molecules [45] (Figure 4).

However, it is demonstrated that only some of the lantibiotics can use lipid II as a docking molecule to facilitates the formation of pores in the cytoplasmic membrane, such as nisin and epidermin. Pep5, on the other hand, did not show a similar interaction, and possibly uses another unidentified compound as docking molecule [33].

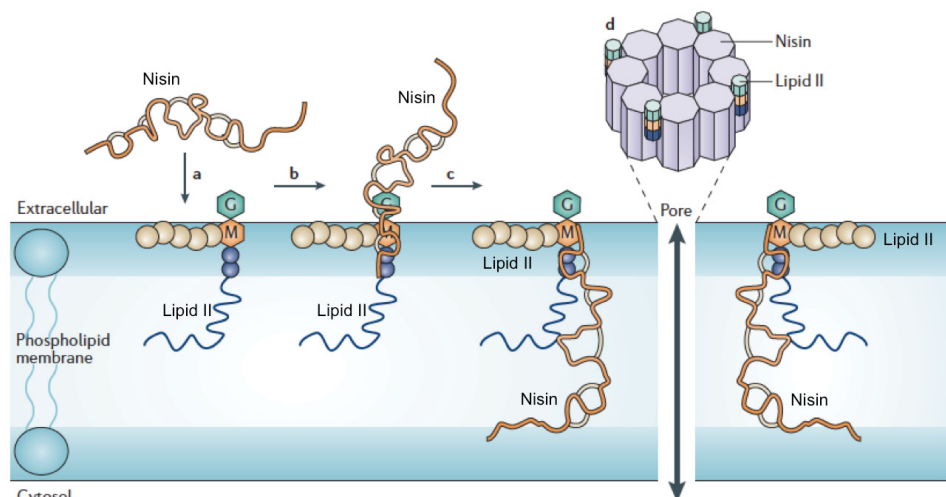


Figure 4. Model for the target-directed pore formation mechanism of nisin. First, nisin reaches the bacterial plasma membrane (a), where it binds to lipid II via two of its amino-terminal rings (b). This is then followed by pore formation (c), which involves a stable transmembrane orientation of nisin. During or after assembly of four 1:1 (nisin: lipid II) complexes, four additional nisin molecules are recruited to form the pore complex (d). Adapted from [46].

Moreover, it was discovered that several members of these lipid II-targeted lantibiotics are too short to span the lipid bilayer and cannot form pores, such as mutacin 1140. For these lantibiotics, even including nisin, an alternative mechanism by which members of the lantibiotic family kill Gram-positive bacteria by removing lipid II from the cell division site (or septum) and thus block cell wall synthesis was thus proposed [47].

## 1.4 The nisin system

The antimicrobial peptide, nisin, produced by several strains of *Lactococcus lactis*, belongs to type I lantibiotics [4, 48]. Nisin is a small (3353 Da), cationic, hydrophobic, and 34-amino acid peptide that contains one lanthionine and four  $\beta$ -methyl-lanthionine rings, and unusual residues as dehydroalanine and dehydrobutyrine. (Figure 5 b) [49-52]. There are two natural variants of nisin, nisin A and Z, which have similar structures and antimicrobial spectra however differ in a single residue at position 27 (His in nisin A and Asp in nisin Z). A new variant of nisin, nisin H, was recently discovered, possessing five different amino acids compared to nisin A (Phe1,



Met6, Dhb18, Tyr21, and Lys31) [53]. Production of nisin by *Lactococcus lactis* is regulated in a growth-phase-dependent manner [52, 54-57].

A cluster of 11 genes, *nisA(Z)BTCIPRKFE*G, is required for nisin biosynthesis, development of immunity, and regulation of gene expression [51, 58-60]. Of these genes, the *nisA(Z)* gene encodes nisin A(Z) precursor peptide consisting of 57-amino acid residues, the first 23 residues of which is called leader peptide, directing the modification and targeting process of nisin precursor [56, 61] (Figure 5a). *nisB* and *nisC* encode proteins involved in the intracellular post-translational modification reactions. The ribosomally synthesized nisin precursor is post-translationally modified such that serine and threonine residues are dehydrated to become dehydroalanine and dehydrobutyrine. Subsequently, five of the dehydrated residues are coupled to C-terminally located cysteines, thus form the thioether bonds that produce the characteristic ( $\beta$ -methyl)lanthionine rings [50, 59, 60, 62]. *nisT* encodes an ABC transporter that is involved in the translocation of the fully modified nisin precursor across the cytoplasmic membrane [63]. *nisP* encodes a protease involved in extracellular proteolytic activation. During or shortly after translocation of the nisin precursor, the leader peptide is removed by NisP to form the mature nisin peptide extracellularly [61, 63] (Figure 5b). Four proteins, NisI and NisFEG, are involved in immunity function to nisin-producing cells. *nisI* encodes a lipoprotein involved in the self-protection of the producing bacterium against nisin [60] and Nis-FEG encodes an ABC transporter, which is believed to export nisin to the extracellular space [51]. *nisR* and *nisK* encode a response regulator [61] and a sensor kinase of the histidine protein kinase family [49, 51, 59, 64], respectively. They belong to the class of two-component regulatory systems [65], responsible for the regulation of nisin biosynthesis [50, 60, 61]. The biosynthetic pathway of nisin in *L. lactis* is summarized in Figure 6.

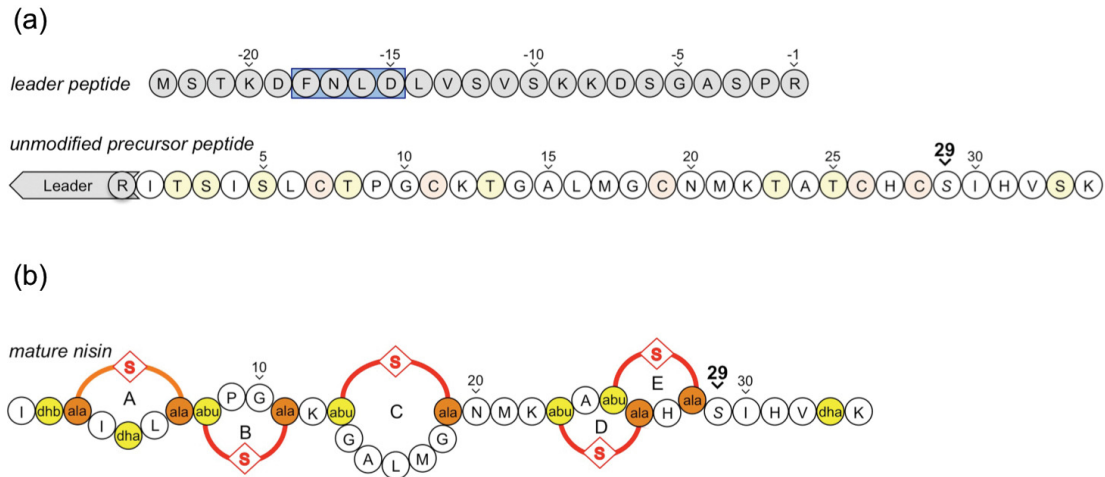


Figure 5. The structures of nisin precursor (a) and mature nisin (b). The molecule shown is nisin A. The residues, which will be dehydrated by NisB, are indicated in yellow. Dehydrated residues are coupled by NisC to cysteine residues (highlighted in orange) forming one lanthionine (A, orange) and four methyllanthionine rings (B-E, red). Dha is dehydroalanine, Dhb is dehydrobutyrine, Ala-S-Ala is lanthionine and Abu-S-Ala is  $\beta$ -methyl-lanthionine. Based on [66, 67].

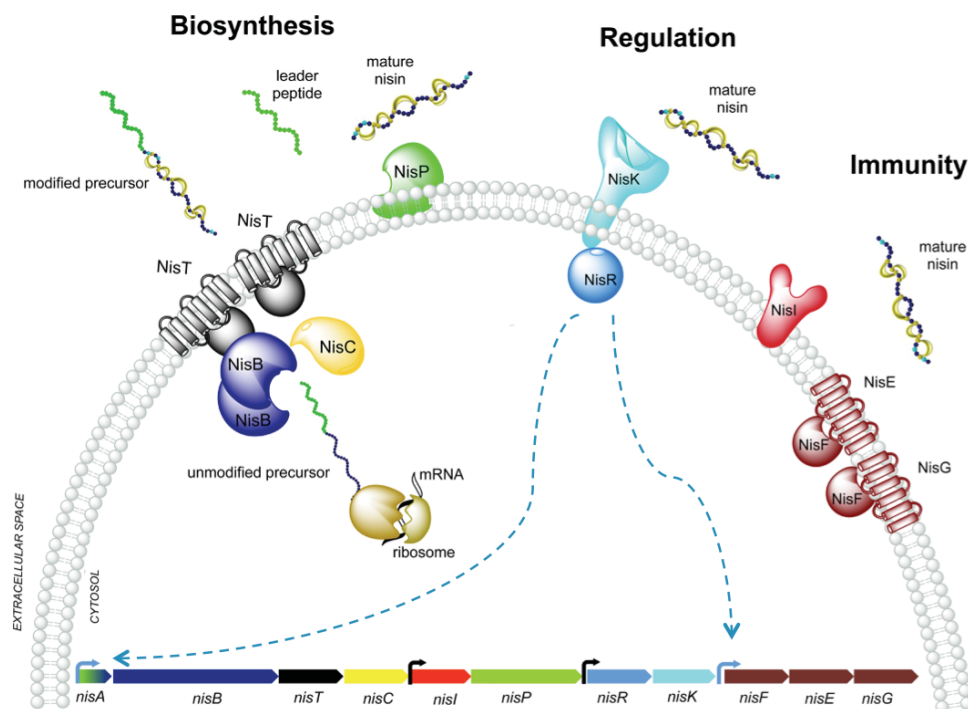


Figure 6. Nisin biosynthesis and regulation in *Lactococcus lactis*. The nisin precursor (encoded by the *nisaA/Z*) is ribosomally synthesized and subsequently modified (NisB and NisC) and translocated (NisT), followed by leader peptide processing (NisP), finally resulting in the mature nisin molecule. The extracellular mature nisin acts as

an antimicrobial peptide, and producing cells are protected against nisin activity by the immunity system composed of NisI and NisFEG. Moreover, this mature nisin acts as peptide pheromones involved in activation of their own biosynthesis via a two-component signal transduction machinery composed of NisK and NisR. Adapted from [66].

## **1.5 NisR/NisK – the two-component regulation system**

Most prokaryotic signal-transduction systems and a few eukaryotic pathways use phosphotransfer systems involving two conserved components, a histidine protein kinase and a response regulator (RR) protein. The histidine protein kinase, which is regulated by environmental stimuli, autophosphorylates a histidine residue, creating a high-energy phosphoryl group that is subsequently transferred to an aspartate residue in the response regulator protein. Phosphorylation induces a conformational change in the regulatory domain of RR that results in activation of its effector domain triggering downstream responses [68]. In the nisin system, these proteins are NisK and NisR, respectively. NisK resides in the cytoplasmic membrane and acts as a receptor for the mature nisin molecule. Upon binding of nisin to NisK it autophosphorylates and transfers the phosphate group to NisR, which is a response regulator that becomes activated upon phosphorylation by NisK. Activated NisR\* (phosphorylated form of NisR) induces transcription from two of the three promoters in the nisin gene cluster:  $P_{\text{nisA}}$  and  $P_{\text{nisF}}$  (Figure 6). The promoter that drives the expression of *nisR* and *nisK* is not affected [50, 52, 69].

### **1.5.1 The nisin-controlled gene expression system (NICE)**

Because of the large progress that has been made in the development of genetic engineering tools and the molecular characterization of this species, a versatile and tightly controlled gene expression system, based on the auto-regulation mechanism of the bacteriocin nisin, was developed approximately 20 years ago—the NIsin Controlled gene Expression system, called NICE [70].

The applications of NICE system can be classified into: (1) over-expression of homologous and heterologous genes for functional studies and to obtain large

quantities of specific gene products, (2) metabolic engineering, (3) expression of prokaryotic and eukaryotic membrane proteins, (4) protein secretion and anchoring in the cell envelope, (5) expression of genes with toxic products and analysis of essential genes and (6) industrial-scale expression [70].

## **1.6 Post-translational modifications of nisin**

The post-translational modifications of nisin are introduced by two enzymes: NisB and NisC. They involve dehydration of several serine and threonine residues followed by intramolecular conjugate additions of cysteines, resulting in the extensively cross-linked polycyclic structure of nisin. Both *in vivo* and *in vitro* studies indicate low substrate specificity of the modification machinery [71]. The pathway of post-translational modifications of nisin is presented in Figure 8. Although it was demonstrated that NisB and NisC can function independently, these two enzymes were proposed to work in a complex *in vivo* in an N- to C- direction, with alternating activities [72, 73]. And the formation of the NisABC complex *in vitro* has been achieved by another colleague in our laboratory. Thus, the complex is composed of a NisB dimer, a monomer of NisC and one prenisin molecule [74].

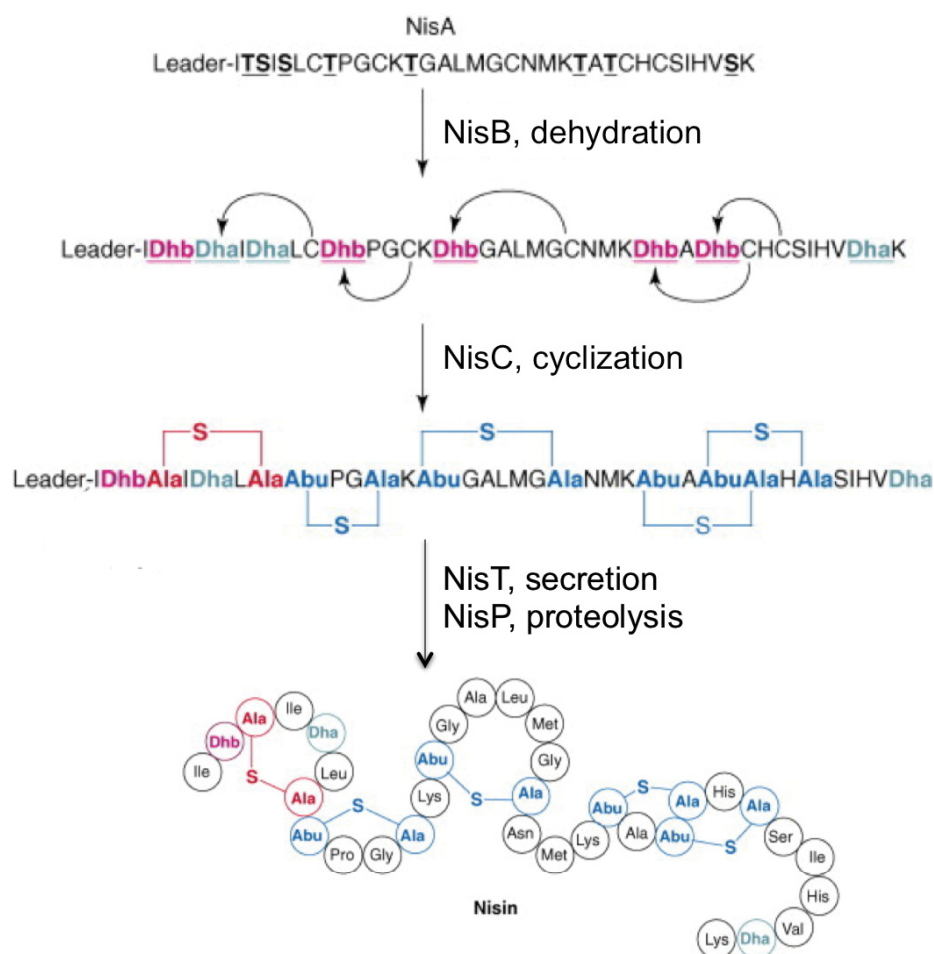


Figure 8. Following ribosomal synthesis, NisB dehydrates serine and threonine residues in the nisin precursor. NisC subsequently catalyzes the intramolecular addition of cysteines onto the dehydroamino acids in a stereo- and regioselective manner. This leads to the formation of one lanthionine and four methylanthionine rings, respectively. Subsequent transport of the final product across the cell membrane by NisT and proteolytic cleavage of the leader sequence by NisP produces the mature lantibiotic. Adapted from [28].

### 1.6.1 NisB – the nisin dehydratase

NisB is a lantibiotic dehydratase, with a size of 117 kDa that is responsible for dehydrating Ser/Thr residues of NisA into Dha and Dhb, respectively. It was demonstrated to be a dimer in solution [29]. The leader peptide of NisA, especially the highly conserved FNLD box, is essential for initial recognition and binding to NisB [29]. Glutamylation was discovered to be a necessary step for NisB dehydration activity and the glutamylated peptide is an intermediate in dehydration [75]. Based on

this observation, a mechanism of a two-step reaction, including glutamylation and elimination, was proposed for NisB [76] (Figure 9).

The crystal structure of NisB in complex with NisA reveals the two domains that are suggested to catalyze the Ser/Thr glutamylation and glutamate elimination steps separately [76] (Figure 10). As shown in Figure 10, NisB is a homodimer in the crystal, consistent with the oligomeric status in solution [76]. The 700 residues N-terminal region of NisB is suggested to be the glutamylation domain [76]. And glutamyl-tRNA<sup>Glu</sup> was reported to be the key component, as glutamate provider, which is used to activate Ser/Thr residues in NisA [29, 75, 76].

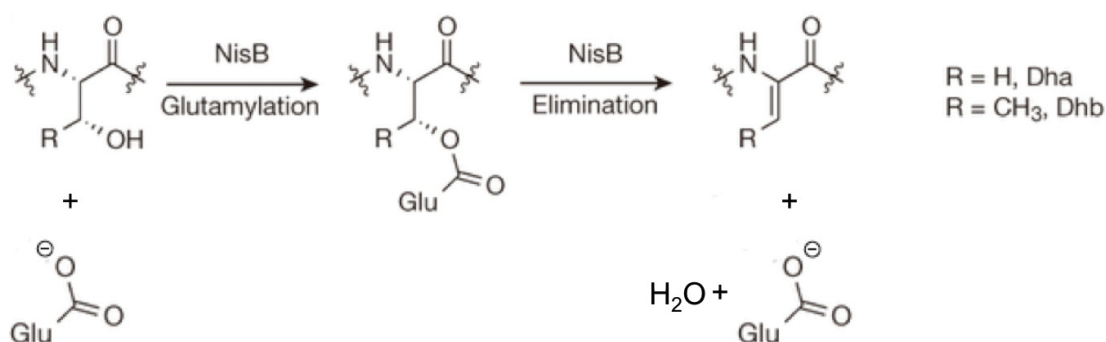


Figure 9. NisB dehydrates Ser/Thr residues in NisA by glutamylation, forming Dha and Dhb, respectively. Adapted from [76].

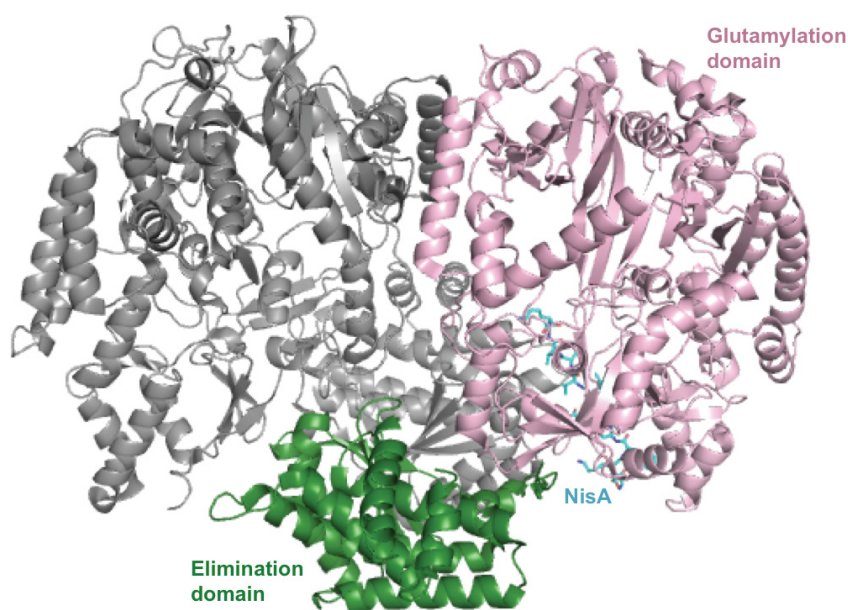


Figure 10. Crystal structure of the lantibiotic dehydratase NisB. Overall structure of the NisB homodimer in complex with its substrate peptide NisA, showing the

disposition of the glutamylation (light pink) and glutamate elimination (green) domains; the other monomer is shown in grey. The NisA peptide is shown in cyan. Based on [76] and created by PyMol [77].

### 1.6.2 NisC – the nisin cyclase

Nisin contains five thioether rings formed by the intramolecular Michael-type addition of cysteine residues to dehydroalanine (Dha) or dehydrobutyrine (Dhb) (Figure 8). The size of these rings in nisin varies from four amino acids in the case of rings B, D, and E to seven amino acids in the case of the C ring. The cyclase enzyme NisC is believed to be responsible for the formation of all rings. A X-ray crystal structure of NisC (resolution of 2.5 Å) was published in 2006, which showed an  $\alpha$ -toroid core consisting of 14  $\alpha$ -helices and a SH2-like extension domain [72]. It also displayed an active site containing a zinc ion coordinated by 3 conserved residues (His331, Cys284 and Cys330) and a water molecule and also two other conserved residues, His212 and Asp141, respectively (Figure 11). Here,  $\text{Zn}^{2+}$  is demonstrated to be essential for activity and believed to activate the cysteines in the substrate for nucleophilic attack and so do all the mentioned residues, as mutation of any of them abolished the enzymatic activity of NisC. Moreover, a water molecule was proposed as the Cys-activating agent in NisC mechanism [28, 72]. Furthermore, within the highly conserved -FNLD- box, two amino acids (F-18 and L-16) were demonstrated to be essential for NisC binding [67].



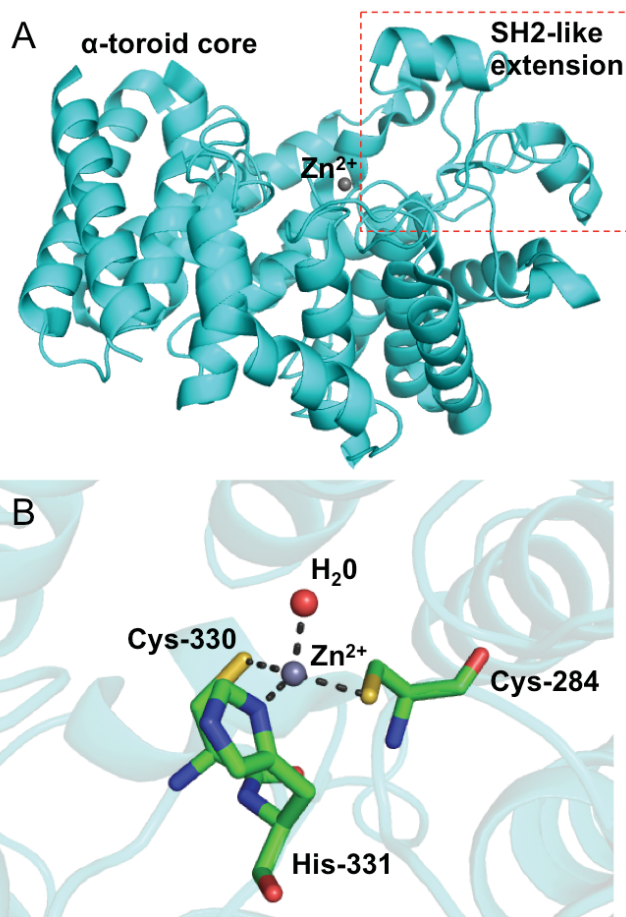


Figure 11. A. Overall structure of NisC, showing the bound the zinc ion and the extended domain. B.  $\text{Zn}^{2+}$  site supported by tetrahedral coordination, consisting of Cys<sup>284</sup>, Cys<sup>330</sup>, His<sup>331</sup> and  $\text{H}_2\text{O}$ . Two other residues His<sup>212</sup> and Arg<sup>280</sup> are highly conserved. Based on [72] and created by PyMol [77].

Several previous studies have demonstrated that cyclic lanthionines also increase the stability and activity of non-lantibiotic peptides [78, 79], suggesting that this structural motif has much potential for engineering of bioactive peptides. An example is the enzymatically synthesized thioether angiotensin displaying 34-fold enhanced bioavailability [80]. Moreover, introducing the thioether bridges could even open up novel delivery options for medically important peptides [80]. Up to now, the utility of the lanthionine conformational constraint has been underexplored, however, predominantly because chemical approaches to prepare lanthionine-containing peptides are currently still challenging when applied to larger peptides with multiple ring structures [81, 82]. Enzymatic cyclization is a promising alternative in this context and lantibiotic biosynthesis enzymes appear to be well-suited candidates for both, reprogramming the structure of lantibiotics and introducing lanthionines into



non-lantibiotic peptides [83-85]. A better understanding of the mechanism of the cyclization step will provide important information for these bioengineering studies [86].

## 2. Aims

Two proteins are in the focus of this thesis: NisR and NisC. The first protein, NisR is a response regulator protein involved in the Nisin-controlled gene expression system (NICE). The second protein, NisC is a cyclase involved in the maturation process of the lantibiotic nisin.

It is known that the NisR/NisK system is a two-component phosphotransfer machinery. As in all other phosphor-transfer systems, it is believed that NisK, the histidine protein kinase, which is regulated by environmental stimuli, auto-phosphorylates a histidine residue, creating a high-energy phosphoryl group that is subsequently transferred to an aspartate residue in the response regulator protein NisR. Phosphorylation induces a conformational change in the regulatory domain of NisR that results in activation of its effector domain, which triggers downstream responses. However, the question of how NisR and NisK interacts stays mysterious, and to solve the question, uncovering the structures for both NisK and NisR would be the key. For NisC, on the other hand, the X-ray structure and the *in vitro* activity were described in 2006. Nevertheless, the binding site within the enzyme NisC, due to the reason that no substrate bound to the structure, was not identified. Furthermore, in 2011, the FNLD region of the leader was identified to bind to NisC. Despite all these discoveries, to elucidate the interaction between NisC and its substrate, further structural and biochemical characterization are inevitable.

In order to obtain structural information for NisR, the first aim of this thesis was the establishment of a reliable purification strategy. Additionally, the activity of the purified protein had to be demonstrated. The second aim of the thesis was to solve NisR structure by determining crystallization conditions that produce diffracting crystals. The third aim was to obtain crystals of NisC in complex with NisA via either co-crystallization or soaking and to solve the structure accordingly, in which way to

elucidate the interaction between NisC and NisA.

### 3. Materials and Methods

#### 3.1 Materials

##### 3.1.1 Chemicals

Acetic acid	Merck
Acrylamide/N,N'-Methylenbisacrylamide solution 30% (w/v) / 0.8% (w/v)	Roth
Aluminum sulfate (AlSO <sub>4</sub> )	Acros Organics
Ammonium peroxodisulfate (APS)	Grüssing
Ammonium sulfate	AppliChem
Ascorbic acid	Roth
L-Asparagin	Sigma
Biotin	Sigma-Aldrich
Bovine Serum Albumin (BSA); Fraction V, proteasefree	Roth
Bromphenolblue	Merck
Calcium acetate	Fluka
Calcium chloride	Grüssing
Chloramphenicol	Sigma
Coomassie Brilliant Blue R250	Serva
Coomassie Brilliant Blue G250	Serva
Cacodylic acid	Fluka
Disodium phosphate	AppliChem
Erythromycin	Merck
Ethanol (EtOH)	Roth
Ferric chloride	J.T.Baker
Folic acid	Roth
Glucose	Caelo
Glycerol	Fisher Scientific
Hydrochloric acid	Roth

HEPES	VWR Chemicals
Imidazole	Sigma
Isopropyl $\beta$ -D-1-thiogalactopyranoside (IPTG)	Roth
Kanamycin	Roth
Lactic acid	Fluka
2-Methyl-2,4-pentanediol(MPD)	Merck
Magnesium chloride (MgCl <sub>2</sub> )	Acros Organics
Magnesium sulfate	Merck
Methanol	Roth
$\beta$ -Mercaptoethanol	Roth
Milk powder	Roth
Monopotassium phosphate	AppliChem
Nisin-Powder	Sigma
Nicotinic acid	Roth
Phosphoric acid	AppliChem
Pantothenic acid (Vitamin B5)	Sigma
PEG 600	Fluka
PEG 4000	Fluka
PEG 8000	Fluka
Pyridoxal (Vitamin B6)	TCL
Riboflavin	Roth
Sodium acetate	Grüssing
Sodium azide (NaN <sub>3</sub> )	Roth
Sodium chloride (NaCl)	Fisher Scientific
Sodium dodecyl sulfate (SDS)	Serva
Sodium hydroxide	AppliChem
Tetramethylethylenediamine (TEMED)	Merck
Tween 20	Fluka
TRIS	VWR Chemicals
Trypton/Peptone-Casein	Roth
Western Lightning Ultra	PerkinElmer
Yeast extract	Roth
Zinc chloride	Fluka

### *Kits for protein crystallization*

Nextal Classics I	Qiagen
Nextal Classics II	Qiagen
Nextal ComPAS	Qiagen
Nextal Cryos	Qiagen
Nextal JCSG Core I	Qiagen
Nextal JCSG Core II	Qiagen
Nextal JCSG Core III	Qiagen
Nextal JCSG Core IV	Qiagen
Nextal JCSG+	Qiagen
Nextal Mb Class I	Qiagen
Nextal Mb Class II	Qiagen
Nextal MPD	Qiagen
Nextal PACT	Qiagen
Nextal Protein Complex	Qiagen
Nextal PEGs I	Qiagen
Nextal PEGs II	Qiagen
Nextal pH Clear Suite I	Qiagen
MD MIDAS	Molecular Dimensions
MD MemGold	Molecular Dimensions
MD MemGold2	Molecular Dimensions
MD MemPlus/MD MemSys	Molecular Dimensions
MD PGA	Molecular Dimensions
HR Crystal Screen I + II	Hampton Research

### **3.1.2 Enzymes, standards and antibodies**

Thrombin clean cleave kit	Sigma
Anti-Histag from rabbit/mouse	GE life science
Anti-mouse/Anti-rabbit	GE life science
Prestained protein ladder	Fisher Scientific

### 3.1.3 Buffers

All the buffers are prepared with MiliQ water.

#### Low IMAC buffer for NisC

50mM HEPES, pH 8

1M NaCl

10% Glycerol

20mM Imidazole

#### High IMAC buffer for NisC

50mM HEPES, pH 8

1M NaCl

10% Glycerol

150mM Imidazole

#### SEC buffer for NisC

50mM HEPES, pH 7.5

1M NaCl

10% Glycerol

#### MALS buffer

50 mM HEPES, pH 7.0

500 mM NaCl

#### Low IMAC buffer for NisR

20mM Tris, pH 8.0

250mM NaCl

5% Glycerol

20mM Imidazole

#### High IMAC buffer for NisR

20mM Tris, pH 8.0

250mM NaCl

5% Glycerol

400mM Imidazole

#### SEC buffer 1 for NisR

20 mM CAPS, pH 11.0

50 mM NaCl

5% Glycerol

#### SEC buffer 2 for NisR

20 mM Tris, pH 9

50 mM NaCl

5% Glycerol

#### LOW LA (equi buffer)

50mM lactic acid, pH 2-3

#### HIGH LA (wash buffer)

50 mM lactic acid

1M NaCl

#### LOW HEPES (wash buffer)

#### HIGH HEPES (elution buffer)

50 mM HEPES, pH 7

50mM HEPES, pH 7

1M NaCl

10% glycerol

Resuspension buffer

10x binding buffer

50 mM Tris, pH 8.0

200 mM HEPES

50 mM NaCl

1 M KCl

10% Glycerol

10 mM EDTA

100 mM MgCl<sub>2</sub>

### 3.1.4 Chromatographic materials and others

#### *Chromatography*

HiTrap Chelating column, 5ml

GE life science

Talon preppacked column, 5ml

GE life science

HiTrap SP HP column, 5ml

GE life science

Superdex 200 10/300, 16/60, 26/60

GE life science

LiChrospher WP 300 RP-18 end capped column

Merck

#### *Others*

Amicon ultra 15 (MWCO 100kDa)

Milipore

Cryo Loop

Hampton Research

Crystal Clear sealing tape

Jena Bioscience

Crystal Drop lid

Hampton research

PD 10 column

GE life science

PVDF membrane

GE life science

Whatman paper

Schleicher & Schüll

Whatman filter membrane

GE life science

24-well crystallization plate

Hampton research

3553 sitting drop plate

Corning

### 3.1.5 Instruments

Äkta System

GE life science

Balances

Satorius

Cell disrupter	BANDELIN SONPULS
Dewar	Taylor Wharton
Electrophoresis unit	University of Düsseldorf
Eppendorf 5417R centrifuge	Eppendorf
Incubator	Heraeus
ITC200	GE life science
HPLC	Agilent technologies
Multi-angle light scattering	Wyatt technology
Mili-Q <sup>50</sup> plus	Milipore
NT8 robot	Formulatrix
pH meter	VWR
Semidry Blot transfer cell	BIO-RAD
SDS-PAGE gel casting unit	University of Düsseldorf
Shaking incubator	Infors
Optima <sup>TM</sup> L-90K Ultracentrifuge	Beckman coulter
Sorvall Discovery M120 SE	Fisher Scientific
Sorvall Discovery 90 SE	Fisher Scientific

## 3.2 Microbiological methods

### 3.2.1 Overexpression of NisC, non-spacer NisC and its mutant H331A

The NisC gene, non-spacer NisC gene or its H331A mutant from *Lactococcus lactis* was cloned into pET-28b and overexpressed in *E. coli*. BL21 (DE3). The cells containing the pET-28b-NisC plasmid were used for a 200 mL LB preculture containing 30 µg/ml. kanamycin. Twelve liters of LB medium was supplemented with 100 µM zinc chloride, inoculated to an OD600 of 0.05, and grown at 37 °C with 180 rpm shaking to an OD600 of 0.8. At 18 °C, the culture was induced with 100 µM IPTG and grown overnight. After 20 h, cells were harvested at 6,000 g for 15 mins and stored at −20 °C.

### **3.2.2 Overexpression of dehydrated prenisin**

Production of prenisin was performed with *L. lactis* strain NZ9000 containing pNZnisA-E3 together with pIL3hpBT (for dehydrated prenisin). The freshly transformed cells grown on agar plates or taken from cryo-stocks were used for an overnight preculture by inoculating a 100 ml M17 media supplemented with 0.5% glucose, 5 µg/ml chloramphenicol and 5 µg/ml erythromycin. After 14-16 hours incubation at 30 °C, 50 ml of preculture were spun down and the resulting pellet was resuspended in 500 ml of minimal media to an OD<sub>600</sub> of 0.3. This main culture was induced with 25 ng/ml nisin at an OD of 0.45- 0.5, and grown at 30 °C for 24 hours. The cells were spun at 14,000 g for 30 mins. The supernatant containing secreted dehydrated prenisin was collected and diluted immediately with 50 mM lactic acid in a 1: 1 ratio (v/v).

### **3.2.3 Overexpression of NisR (N-terminal His-tagged and C-terminal His-tagged)**

A 200 ml LB preculture of BL21 (DE3) cells containing plasmid of pET16-NisR was supplemented with 100 µg/ml ampicillin and grown overnight at 37 °C with 200 rpm shaking in flask. The main culture was started by inoculating 6× 2 liters of LB media to an OD<sub>600</sub> of 0.05 and growing at 37 °C at 180 rpm until an OD of 0.3 was reached. The temperature was changed to 18 °C and the culture was grown until an OD of 0.8-1.0. The induction of the expression was performed by adding IPTG to a final concentration of 0.1 mM. The main culture was then incubated overnight and harvested afterwards at 6000 rpm for 14 mins. The cell pellets were stored -20 °C.

## **3.3 Biochemical methods**

### **3.3.1 Purification of NisC, non-spacer NisC and its mutant H331A**

NisC expressing cells were thawed on ice and resuspended in 50 mM HEPES, pH 8.0, 1 M NaCl, and 10% glycerol. The cells were then lysed with a cell sonifier and



centrifuged at 45,000 rpm, 4 °C, for 45 min. The resulting supernatant was applied to a cobalt affinity chromatography column, which had been equilibrated with 50 mM HEPES, pH 8, 1M NaCl, 10% Gly, 20 mM Imidazole. NisC was eluted with 50 mM HEPES, pH 8.0, 1 M NaCl, 10% glycerol, and 150 mM imidazole in one step. The resulting His<sub>6</sub>-NisC was digested with a thrombin clean cleave kit (Sigma) to cleave the N-terminal His<sub>6</sub>-tag. After overnight cleavage at 4 °C, non-cleaved and cleaved NisC were separated via IMAC following the procedure outlined above. NisC was then further purified by size-exclusion chromatography (SEC) pre-equilibrated with SEC buffer (50 mM HEPES, pH 7.5, 1 M NaCl, and 10% glycerol). All fractions containing NisC were pooled and concentrated with an ultracentrifugation unit (30 kDa MWCO). Tag-free NisC was concentrated to 20 mg/ml.

### **3.3.2 Purification of dehydrated prenisin**

The dehydrated prenisin containing supernatant diluted 1:1 (v/v) with 50 mM lactic acid was loaded onto a cation exchange chromatography (HiTrap SP HP, GE life science) . After peptide binding, the lactic acid buffer, pH 3, was gradually changed to 50 mM HEPES-NaOH, pH 7, by applying a gradient (0–100% 50 mM HEPES-NaOH, pH 7) for 4 column volumes at a flow rate of 2 ml/min followed by a wash step of 8 column volumes with 50 mM HEPES-NaOH, pH 7. At this stage, the eluent showed a pH of 7. Finally, bound prenisin was eluted with 50 mM HEPES NaOH, pH 7, 1 M NaCl, and 10% (v/v) glycerol. Peptide elution was monitored at 215 nm. Prenisin containing fractions were pooled and filtered through an Ultracentrifugal filter (30 kDa MWCO) to remove high molecular mass contaminants. The flow-through containing the prenisin was concentrated with an Ultracentrifugal filter (3 kDa MWCO).

### **3.3.3 RP-HPLC analysis of prenisin**

Analytical RP-HPLC was performed with a LiChrospher WP 300 RP-18 end capped column (Merck) at room temperature. Purified prenisin was injected at a concentration of 50 µM and eluted by mixing the aqueous buffer A (10% acetonitrile, 0.1% (v/v) trifluoroacetic acid) with the organic solvent buffer B (90% acetonitrile,

0.1% (v/v) trifluoroacetic acid). The elution was performed by a linear gradient over 35 min to 60% solvent B at a flow rate of 1 ml/min. Specific peptide concentrations were determined by the absorption at 205 nm.

For calibration, a certain amount of nisin or human insulin were injected, and the absorption integrals were determined with the software EZChrom Elite software V.3.3.1. and plotted against the known amount of injected material. A calibration line was calculated, and this equation was used to determine the concentration of prenisin purified from the supernatant.

### **3.3.4 Purification of NisR (C-terminal and N-terminal)**

The cells were thawed and resuspended in resuspension buffer. The resuspended cells were cracked by cell disrupter at 1.6 kBar, 4 °C, five times. Afterwards, the suspension was spun down in a ultracentrifuge (Ti 70 Rotor) for 60 mins at 45000 rpm, 4 °C and the supernatant was collected after the centrifugation. Imidazole was added to a final concentration of 20 mM. The supernatant solution was then loaded on to the IMAC column with a flow rate of 1ml/min, followed by a wash step with low IMAC buffer until a stable base line was reached. The imidazole concentration was then increased to 75 mM to wash off some non-target proteins. A final elution was carried out with a linear gradient from 75 mM to 400 mM imidazole for 60 mins at 2 ml/min. After concentrating the elution peak of the IMAC to a volume of 5 ml with an ultraspinn concentration unit (10 kDa MWCO) NisC was then further purified by SEC pre-equilibrated with SEC buffer 1 (pH 11) or SEC buffer 2 (pH 9). All fractions containing NisR were pooled and concentrated with an ultracentrifugation unit (10 kDa MWCO). NisR was concentrated to approximately 16 mg/ml.

### **3.3.5 SDS-polyacrylamide gel electrophoresis (SDS-PAGE)**

The SDS-PAGE was utilized to assess the purity of a protein sample. The protein sample is denatured by the sample buffer and concentrated in the stacking gel to form a sharp band before it enters the 10% separation gel, where the proteins are separated according to their molecular weight.

Glass plates for nine gels were placed in a SDS-PAGE casting unit. 18.75 ml of

separation buffer was mixed with 37.5 ml of 30% acrylamide solution, 18.75 ml of deionized water, 300  $\mu$ l 10% (w/v) APS solution and 70  $\mu$ l TEMED. The solution was immediately poured into the prepared casting unit. When the separation gel was polymerized the stacking gel was prepared by mixing 5 ml of stacking buffer with 5.25 ml of 30% acrylamide solution, 28 ml of deionized water, 210  $\mu$ l of 10% (w/v) APS and 70  $\mu$ l TEMED. This solution was poured on top of the separation gel and teflon spacers were fitted between two glass plates to form the sample application wells. Fully polymerized gels were stored at 4 °C. For the separation of the protein sample 20  $\mu$ l of protein solution was mixed with 5 $\mu$ l 5x sample buffer.

One polyacrylamide gel was placed into the electrophoresis unit and the chambers were filled with running buffer. The teflon spacer was removed and 20  $\mu$ l of the prepared protein sample was filled into the sample application wells. The electrophoresis was performed at beginning at 90 V for 1h, and afterwards at 160 V until the running front reached the bottom. When the electrophoresis process was finished the gel was stained with Coomassie stain for ~1 hour. Unbound Coomassie dye was removed by adding destain solution until the background of the gel became clear.

### 3.3.6 Western blot

6 Whatman papers were incubated for 1 min in Blotting buffer. 3 papers were placed on the electrode of the semi dry transfer cell. A same size PVDF membrane was activated by incubating in MeOH for 1 min. This activated membrane was then placed on the top of the papers. Afterwards, SDS-gel was placed on the membrane. In the end, the other 3 Whatman papers were used to cover on the top. The running program was started at 100mA for 60 min with a voltage of 25V. After the transfer process, the membrane was washed according to the following procedure:

Blocking solution	1x 30min (or O/N)
TBST buffer	2x 10min each
TBS buffer	1x 10 min
1° antibody (anti-Histag)	1x 1h

TBST	3x	10min each
2° antibody (anti-mouse or anti-rabbit)	1x	1h
TBST buffer	2x	10 min each
TBS buffer	2x	10 min each

The developing solution was freshly made by mixing solution A and B in a 1:1 ratio. 0.5 ml of mixed solution was put on both sides of the membrane. Afterwards, the membrane was placed under the light detection table of the Lumi-imager and the target protein can be detected after 30 s.

### **3.3.7 Electrophoretic Mobility Shift Assay (EMSA) of NisR**

EMSA assays with entire plasmid were conducted by incubating plasmid pNZ-SV-His-entero (with a concentration of 10 nM) with increasing amounts of NisR (0 nM, 1 nM, 10 nM, 100 nM, 1  $\mu$ M, 10  $\mu$ M) at various pHs (pH 7, pH 8, pH 9) and salt concentrations (5 mM, 50 mM, 500 mM) for 1 h at room temperature. For EMSA assay with PnisA DNA piece, a mixture of 45 nM PnisA, 50  $\mu$ M NisR, 10% glycerol in 1x binding buffer/SEC buffer was incubated for 1 h at room temperature.

These assays were analyzed by electrophoresis in TBE buffer (89 mM each of Tris and borate, 1 mM EDTA, pH 8) using a 0.5% agarose gel and visualized via staining with ethidium bromide. DNA binding was evidenced by a shift in the electrophoretic mobility of the DNA band in the gel upon protein binding.

### **3.3.8 AC complex formation analysis using Multi-Angle Light Scattering (MALS-SEC)**

250  $\mu$ l of 20  $\mu$ M NisC was incubated with 250  $\mu$ l of 200  $\mu$ M prenisin for 1 h at 25 °C. Afterwards, 500  $\mu$ l of the complex solution was injected on a SEC column pre-equilibrated with MALS buffer. The absorption signal at 280 nm, light scattering signal, and differential refractive index were monitored. Data were analyzed with the ASTRA software package (Wyatt Research).

### **3.3.9 Binding assay of NisC to PEP by ITC**

To minimize the noise of dilution heat produced during the measurement, the enzyme NisC were dialyzed against freshly made SEC buffer. After dialysis, the concentration of NisC was adjusted to 400  $\mu\text{M}$  and a certain amount of PEP was dissolved with the same SEC buffer to make a 40  $\mu\text{M}$  PEP solution. The ITC measurements were performed at 25 °C with 40 injections (1  $\mu\text{l}$  each). Only the first injection had a volume of 0.5  $\mu\text{l}$  and was discarded from the isotherm. The other technical parameters were reference power = 5  $\mu\text{ cal s}^{-1}$ , stirring speed = 1000 rpm, spacing time = 180 s, and a filter period = 5 s. For each measurement, 40  $\mu\text{l}$  enzyme NisC was titrated to PEP solution [67]. The control experiment (NisC to SEC buffer) was consistently subtracted from each isotherm, and the resulting isotherm was fitted with a one site binding model using the Origin 7 Microcal software.

## **3.4 Crystallographic methods**

### **3.4.1 Fundamental theory of crystallization**

Obtaining protein crystals always involves massive screening to determine suitable crystallization conditions, which also vary from protein to protein. The first necessary step in any crystallization experiment is to force the protein gently out of solution, so that in the process of phase separation crystals can form. The solubility of a protein can be reduced by adding precipitants, such as salts and polymers, to the solution, by removing solvent (water) from the protein solution, or by a combination of both. Exceeding the solubility limit of protein would cause supersaturation of the solution and eventually results in precipitation. Slow precipitation is more likely to produce larger crystals, whereas rapid precipitation may produce many small crystals, or worse, an amorphous solid.

Crystal formation occurs in two stages, nucleation, and growth. Both crystal nucleation and growth occur in supersaturated solutions where the concentration of the crystallizing species, in our case protein, exceeds its equilibrium solubility value. The region of solution parameter space suitable for crystallization is generally

represented on the phase diagram by solubility curve. The supersaturation requirements for nucleation and crystal growth differ. This is shown in the phase diagram (Figure 12) where the supersaturated region is further divided into regions of higher supersaturation (the 'labile' region), where both nucleation and initial growth occur, and lower supersaturation (the 'metastable region'), where only growth is supported. The ideal approach would be to induce the nuclei in the labile region which permits their formation. Once nuclei formed, the concentration of the protein in solution is lowered, which means the system would enter the metastable region, where nuclei continue to develop into visible crystals.

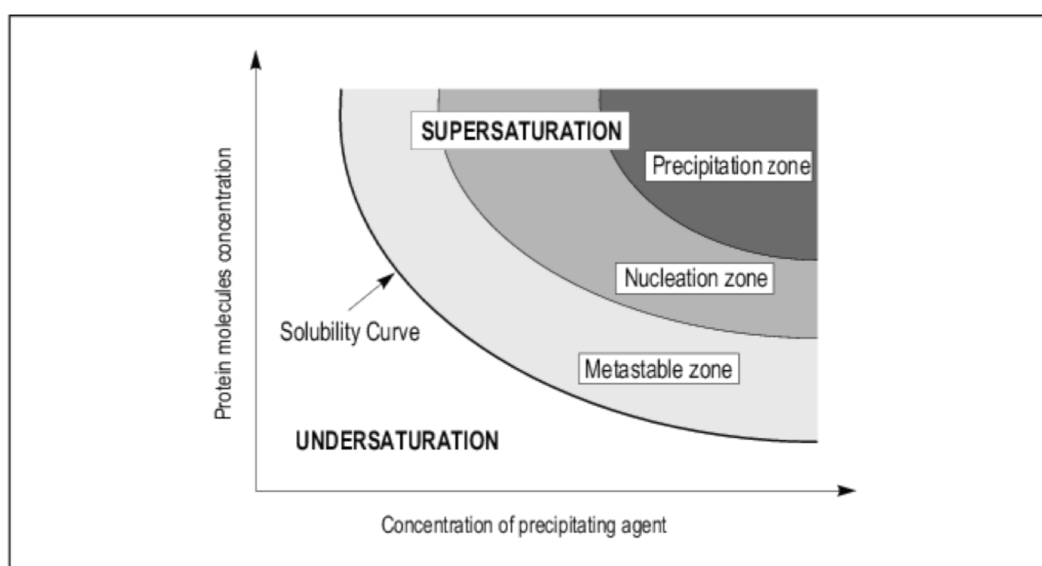


Figure 12. Crystallization phase diagram. Schematic representation of a two-dimensional phase diagram, illustrating the change of protein molecules concentration against precipitating agent concentration. The concentration space is divided by the solubility curve into two areas corresponding to undersaturated and supersaturated state of a protein solution. The supersaturated area comprises of the metastable, nucleation and precipitation zones. Taken from [87].

Other than addition of precipitants and removal of water, some other variables can also contribute in the supersaturation process of the protein:

- Temperature
- pH-value

For a successful protein crystallization process, it always involves more than one of above mentioned variable to eventually achieve a crystal.

### **3.4.2 Crystallization techniques**

A number of crystallization techniques have been developed, each with advantage and disadvantage depending on the specific application and type of research environment. Figure 13 provides three most popular methods, including vapor diffusion, batch, and dialysis. And by including the phase diagram, their corresponding processes to achieve crystals differ (Figure 14).

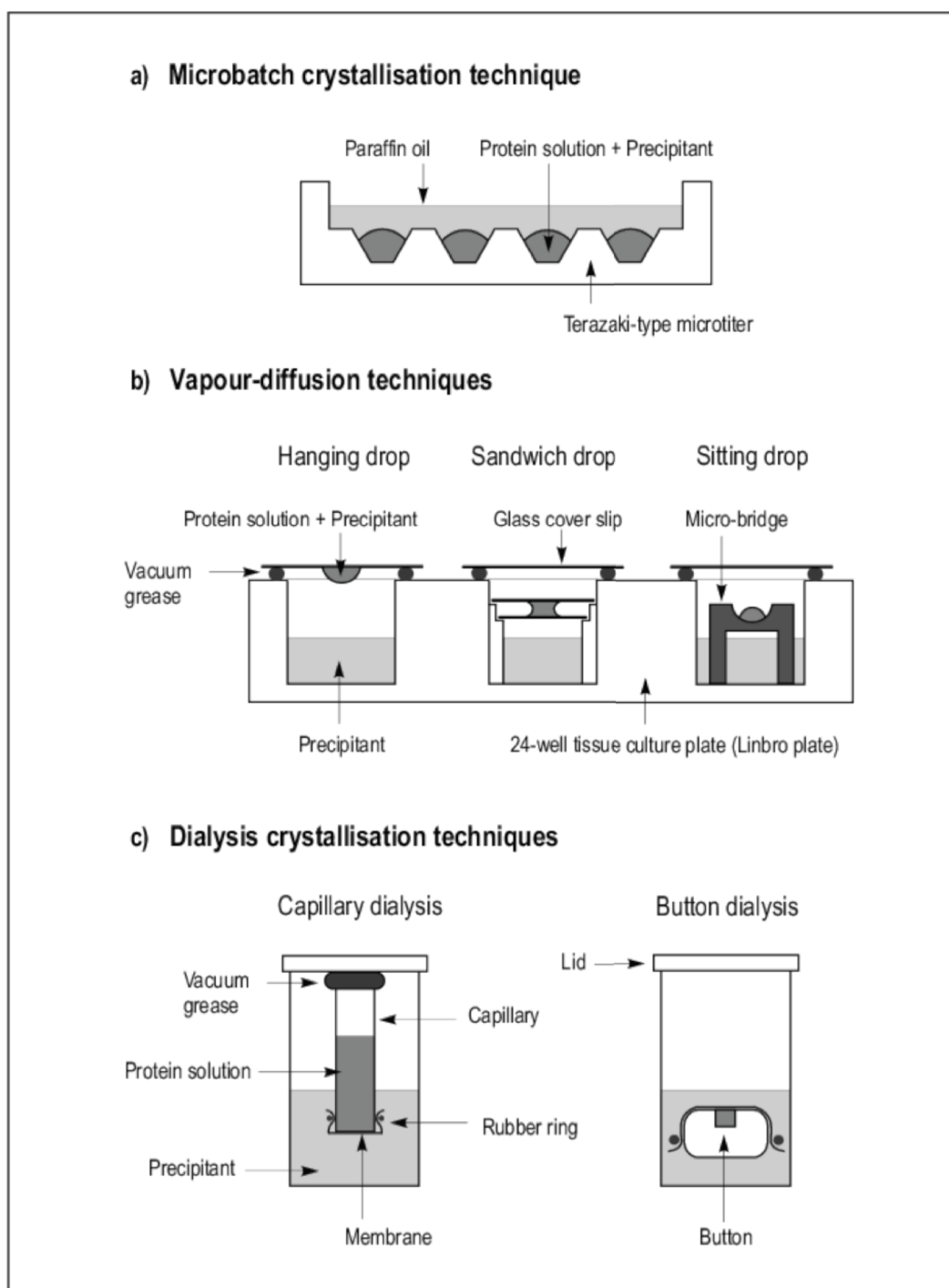


Figure 13. Protein crystallization techniques. Schematic representation of a) microbatch, b) vapor-diffusion, and c) dialysis crystallization techniques widely used in growing of protein crystals. Taken from [87].



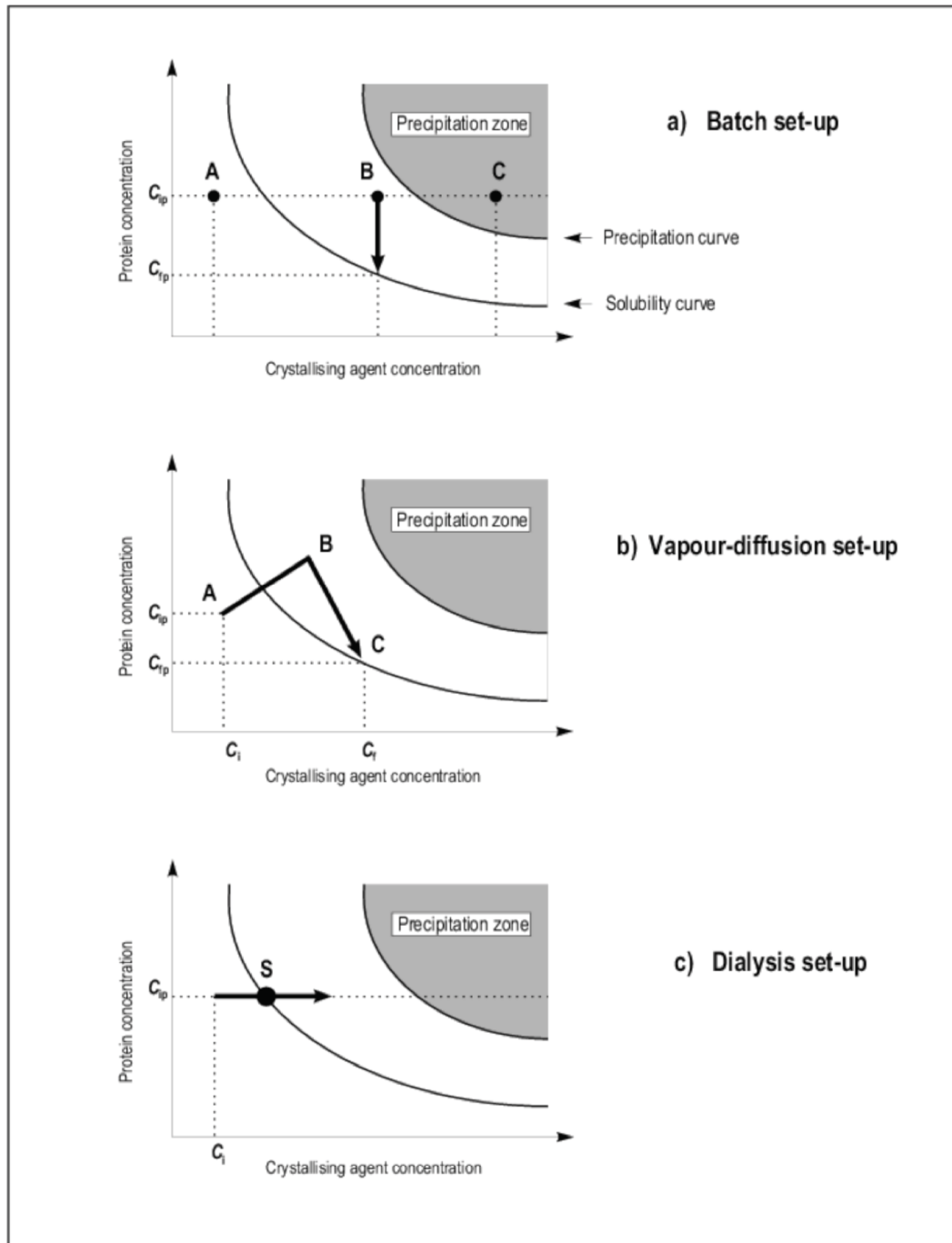


Figure 14. Various crystallization set-ups explained in terms of phase diagrams. Schematic representation of solubility phase diagram and correlation between protein and crystallizing agent concentrations in a) batch, b) vapour-diffusion and c) dialysis crystallization experiments.  $C_{ip}$  and  $C_{i}$  are the initial concentrations of protein and crystallizing agent respectively,  $C_{fp}$  and  $C_{f}$  are their final concentrations. Taken from [87].

#### *Batch crystallization*

Batch crystallization, including microbatch, is a method where the concentrated protein solution is mixed with concentrated precipitant in a closed vessel to produce a final supersaturated concentration, which may eventually lead to crystallization. It requires no equilibration with a reservoir. Therefore, the volume of the drop remains the same during the experiment. In terms of phase diagram, see Figure 14a, this condition is indicated by point A. The protein will immediately precipitate if the starting point is located in the precipitation zone of the solubility diagram, point C. Therefore, only those points in the phase diagram (point B in Figure 14a) which lie between the solubility and precipitation curves represent starting conditions for a successful crystallization experiment. This technique is very popular in the area of small molecule crystallography. The advantages to the technique are speed and simplicity. The main disadvantage of this method is that the equilibration occurs very rapidly, thus affecting the rate of crystal growth and consequently the quality of the obtained crystals.

#### *Vapor-diffusion techniques*

Vapor-diffusion method is by far the most common crystallization technique for biomolecules. As the name indicates, it relies on the presence of a reservoir of precipitant that absorbs water from the crystallization drop, thus driving the solution into a supersaturated state and enabling crystallization. The vapor-diffusion technique utilizes evaporation and diffusion of water between solutions of different concentrations as a means of approaching and achieving supersaturation of protein macromolecules. Typically, the protein solution is mixed in a 1:1 ratio with a solution containing the precipitant agent at the concentration that needs to be achieved after vapor equilibration has occurred. The drop is then suspended and sealed over the well solution, which contains the precipitant solution at the target concentration, as either a hanging or sitting drop (Figure 13b). The difference in precipitant concentration between the drop and the well solution is the driving force which causes water to evaporate from the drop until the concentration of the precipitant in the drop equals that of the well solution. Since the volume of the well solution is much larger than that of the drop (1 - 3 ml as compared to 1 - 20  $\mu$ l), its dilution by water vapor leaving the drop is insignificant. During a vapor-diffusion experiment, the protein will start to concentrate from an unsaturated state (point A, concentration  $C_{pi}$ ) to reach a supersaturated state (point B). As the first crystals appear the concentration of protein

will decrease (Figure 14b). The crystal will then grow until the concentration of the protein in the drop reaches the solubility curve (point C, at concentration  $C_{pf}$ ).

Vapor-diffusion is the optimal technique when screening a large number of conditions. Furthermore, this method can be used to increase or decrease the concentration of protein in the equilibrated state, relative to its initial concentration. Varying the ratio between the protein and well solutions when the drop is initially set up does this. Since the drop equilibrates in such a way that its precipitant concentration matches that of the well solution, the final volume of the drop will always equal that of the initial amount of well solution mixed with the protein.

As shown in the Figure 13b, there are three types of vapor-diffusion setup, sitting drop, hanging drop, and sandwich drop. Nowadays, sitting and hanging methodologies are very popular because they are easy to perform, require a small amount of sample, and allow a large amount of flexibility during screening and optimization.

#### *Crystallization by dialysis*

Dialysis crystallization involves placing the sample in a dialysis button which is sealed with a dialysis membrane. Dialysis techniques utilize diffusion and equilibration of small precipitant molecules through a semipermeable membrane as a means of slowly approaching the concentration at which the macromolecule solute crystallizes. Water and some precipitants are then allowed to exchange while retaining the sample in a cell containing the precipitant or crystallization media. The protein solution at the start of the dialysis experiment is in an undersaturated state (Figure 14c). The concentration of the precipitant agent slowly increases as its diffusion through the membrane takes place. Thus, the system goes from an undersaturated state into the metastable region through the point S on the solubility curve. The technique allows for salting-in, salting-out, as well as pH crystallization techniques. The method does not work with concentrated PEG solutions used for crystallization, which is considered as a big disadvantage as PEG is a very popular precipitant.

### **3.4.3 Soaking and co-crystallization**

Once native crystals are obtained, they frequently need to be further treated by soaking small molecule ligands such as cofactors, non-hydrolysable substrate analogs, or therapeutic drug lead compounds into the native crystal to obtain the target structure in a complex. Particularly for structure guided drug design, many ligand-target complexes must be screened. The other major application of soaking techniques to incorporate heavy atom as tools to solve the phase problem. Next to co-crystallization, where protein and binding partner are mixed and incubated before the crystallization is set up, soaking ligands into already grown crystals are the essential techniques to obtain protein ligand complexes.

#### *Protein-ligand complex*

Co-crystallization, the simultaneous crystallization of two materials, is possible with small molecule ligands as well as larger molecules such as peptides, DNA oligomers, and even other proteins. Soaking into crystals is limited to small molecules because of the slow diffusion and the limited diameter of the solvent channels. Diffusion of long peptides in crystals, for example, is a slow process. And even small molecule dyes or drugs need several hours to days to travel through the solvent channels into a crystal. Some ligands that induce conformational changes in proteins and destroy the crystals upon soaking need to be co-crystallized with the protein.

### **3.4.4 Co-crystallization of NisC with PEP**

Prior to the initial screening, NisC were pre-incubated with 10mM PEP on ice for 1hr. Crystallization initial screening was performed at 285 K using NT8 robot (Formulatrix) and sitting-drop vapor diffusion method in Corning 3553 sitting drop plates. Nanodrops consisting of 0.1  $\mu$ l each of protein and reservoir solution were mixed and equilibrated over 50  $\mu$ l reservoir solution.

### **3.4.5 Finding optimal conditions for crystallization**

Many variables influence the formation of macromolecular crystals. These include obvious ones such as protein purity, concentrations of protein and precipitant, pH, and temperature, as well as the presence of ligands. There are in general two steps for

finding optimum crystallization conditions, first, initial screening, and then fine screening as a follow-up. When starting a crystallization experiment, screening conditions should cover a wide chemical space to efficiently identify crystallization trends. Crystallization suites are usually either based on experimental conditions outlined in literature references and databases or based on a rational combination of chemical conditions. Although past experience can be used to deduce starting conditions for crystallization setup, it does not guarantee success. The initial screening is normally recommended to carry out via robotic systems. The major advantages of robotic systems involve the ability to miniaturize the crystallization drops down to 100+100 nl and significant improvement of drop-setting speed comparing to manually pipetting.

In order to fine-tune successful hit conditions and to grow larger and/or better-diffracting crystals, fine screening is necessary. One strategy involves choosing suites using chemicals that worked best in the initial screening for a second, more defined round of screening using dedicated precipitants with a certain range of gradient. And this experiment can be normally carried out by using 24-well plates.

### **3.4.6 Basics of x-ray crystallography**

#### *Crystal assembly and space group*

A crystal is a solid composed of atoms or other microscopic particles arranged in an ordered periodic array. This periodicity in the arrangement generally varies in different directions. It is very convenient to imagine points in space about which these atoms are located. Such points in space are called lattice points and the totality of such points forms a crystal lattice or space lattice. The lattice is periodic, finite assembly of unit cells. A unit cell can be completely described by three vectors  $a$ ,  $b$ ,  $c$  when the length of the vectors and the angles between them ( $\alpha$ ,  $\beta$ ,  $\gamma$ ) are specified. Each identical unit cell contains the same number of identically arranged molecules. The molecules in each unit cell can be related by internal symmetry, generating a unit cell packed with multiple copies of the molecule with symmetry equivalency. The smallest object required to generate the unit cell via applying the crystallographic operation is called asymmetric unit. The symmetry properties of the crystal are described by the concept of space groups. All possible symmetric arrangements of

particles in space may be classified into 7 categories of crystal systems, including 65 chiral space groups.

Crystal system	Lattice properties	Minimum internal symmetry
Triclinic	$a \neq b \neq c$ $\alpha \neq \beta \neq \gamma \neq 90^\circ$	None
Monoclinic	$a \neq b \neq c$ $\alpha = \gamma = 90^\circ$ $\beta \neq 90^\circ$	One 2-fold axis
Orthorhombic	$a \neq b \neq c$ $\alpha = \beta = \gamma = 90^\circ$	Three perpendicular 2-fold axes
Tetragonal	$a = b \neq c$ $\alpha = \beta = \gamma = 90^\circ$	One 4-fold axis
Trigonal	$a = b \neq c$	One 3-fold axis
Hexagonal	$\alpha = \beta = 90^\circ$ $\gamma = 120^\circ$	One 6-fold axis
Cubic	$a = b = c$ $\alpha = \beta = \gamma = 90^\circ$	Four 3-fold axes

### *The fundamental mathematics of crystallography*

X-ray diffraction is the result of electromagnetic interaction between the electrons of the atoms in the crystals. X-rays are high energy electromagnetic waves, which can interact with matter primarily through its oscillating electric field vector due to dielectric polarizability. In a scattering process, an X-ray photon excites all electrons, causing their vibrations within its coherent length. The resulting waves emitted by resonating electrons possess identical frequency and fixed phases, which will either recombine or superimpose, to form a consequent scattered wave. In this way, the photon can be scattered in a certain direction proportional to the amplitude of the recombined wave in that direction. Constructive interference increases the probability of scattering, destructive interference decreases it. By splitting the wave into amplitude and phase parts, the scattered wave can be represented in the complex number plane, and vector addition can be performed to simplify the partial wave summations.

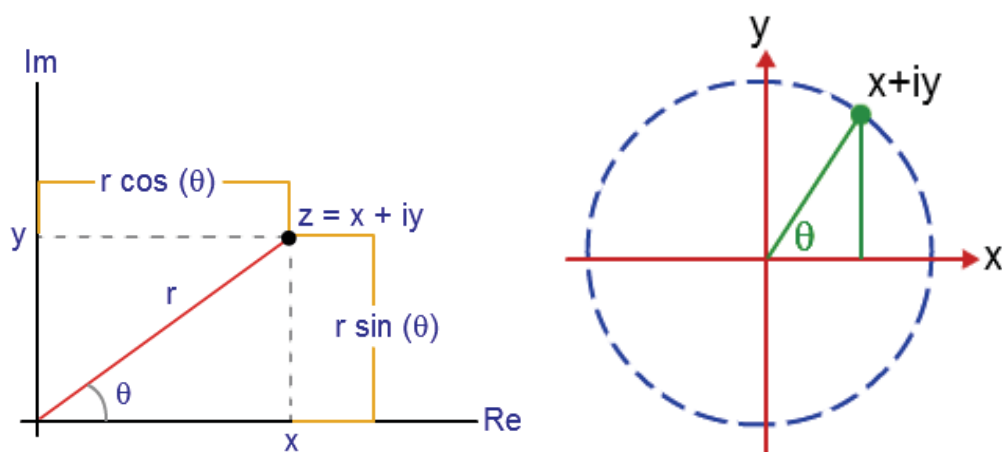


Figure 15. Representation of a complex number in an Argand diagram. Taken from [88].

As shown in Figure 15, a plane wave  $z$  of amplitude  $r$  and phase angle  $\theta$  relative to a fixed origin can be represented in a complex number of  $x+iy$ , spanned by the real part axis **Re** and the imaginary part axis **Im** (**i**). Altogether, the following equation can be easily derived:

$$z=x + iy= |r|(\cos\theta + i\sin\theta)= |r| e^{i\theta}$$

In here, the real component along **Re** is then the real part,  $x=|r|\cos\theta$ , and the imaginary part in the direction of **i** is  $y=|r|\sin\theta$ . Alternatively,  $z$  can be expressed as  $|r| e^{i\theta}$ , where  $|r|$  is the amplitude, and  $\theta$  is the phase.

The amplitude of a wave scattered by an atom is decided by the distribution of the electrons, also known as the electron density. The total scattering power is proportional to the square of the number of electrons of the atom, which means heavy atoms scatter X-ray strongly, but light atoms scatter only weakly.

For a single molecule, the scattering of x-rays is too small to be measured, but it can be amplified by arranging many molecules in a periodic lattice, which is known as the diffraction of X-rays on a crystal. In a crystal lattice, positive interference of the scattered waves occurs if all outgoing waves are in the phase with each other. Therefore, the path-difference of the incoming wave and outgoing waves has to be  $n\lambda$ . The function of the reflection conditions in a crystal was formulated first by Max von Laue and then simplified by W. Lawrence Bragg. In this well-known Bragg equation

[89], X-ray diffraction was interpreted as reflection on discrete lattice planes ( $h, k, l$ ), relating the diffraction angle  $\theta$  to the lattice spacing  $d_{hkl}$ :

$$n\lambda = 2 d_{hkl} \sin\theta$$

By using this equation, one can quantify the relation between scattering angle  $\theta$  and the interplanar distance  $d_{hkl}$  for the set of reflecting planes  $hkl$ . (Figure 16) for maximum constructive interference, the total path difference between two excited partial waves ( $2d\sin\theta$ ), which must equal  $n\lambda$ ,  $n=0,1,2$  and so on.

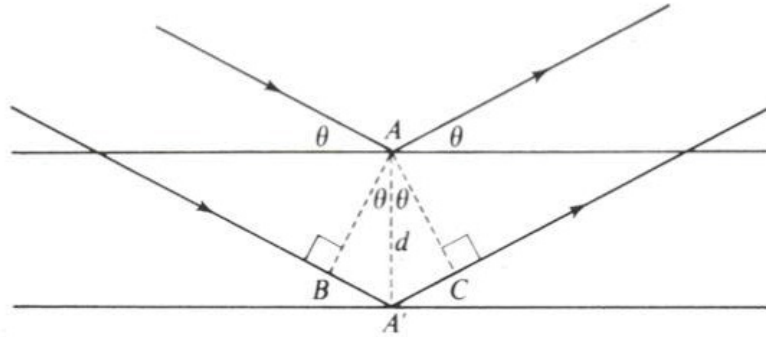


Figure 16. Reflection of parallel beams on parallel planes with interplanar spacing  $d$ . Taken from [90].

Diffraction is the Fourier transformation of the electron density from real space  $R$  into reciprocal space  $R^*$ , which is generated by the continuous molecular scattering of a crystal. The geometric relations between crystals orientation and the diffraction condition can be easily understood in reciprocal space via a graphic representation of the diffraction process called the Ewald sphere, as shown in the Figure 17 below.



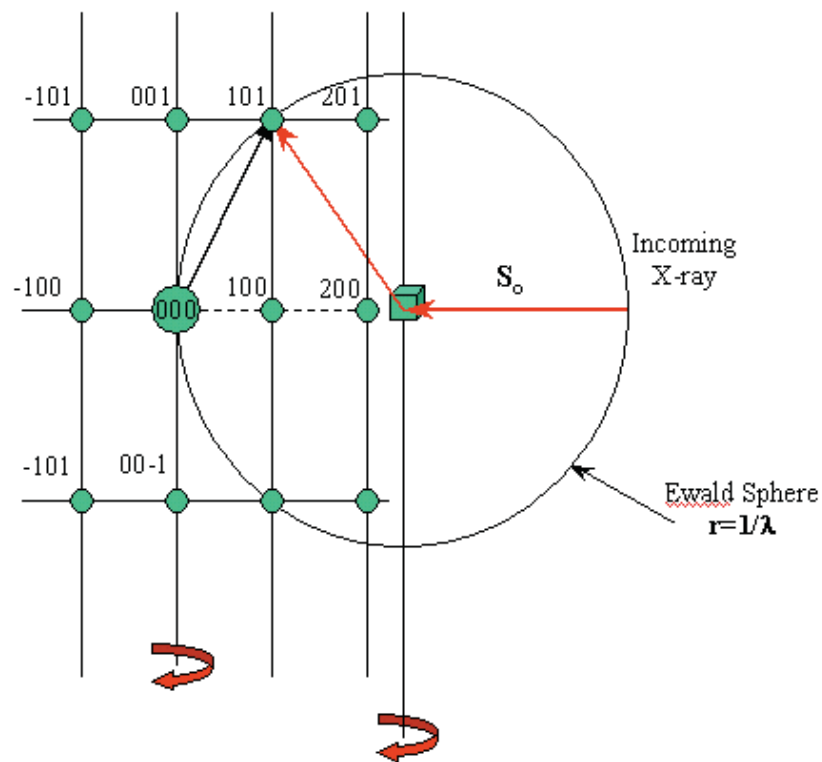


Figure 17. Reciprocal lattice and Ewald sphere. Taken from [91].

In Ewald sphere, there is a sphere of radius  $1/\lambda$ , and combining Bragg equation  $n\lambda = 2d_{hkl}\sin\theta$ , the diffraction conditions can be stated as the following equation:

$$d^*_{hkl} = 2\sin\theta/\lambda$$

Therefore, diffraction occurs under the condition of having a reciprocal lattice point lying on the Ewald sphere. At the same time, the origin of the reciprocal lattice is at the intersection of the Ewald sphere with the incoming beam direction. In order to have more reciprocal lattice points to intersect the Ewald sphere, rotating crystals in different axes is needed.

### 3.4.7 Harvesting and mounting of crystals

Successful data collection starts with proper harvesting, cryoprotection, and mounting of the delicate protein crystals. Once crystals have grown to a proper size (normally  $10\ \mu\text{m}$  to a few  $100\ \mu\text{m}$ ), they need to be harvested and put on the diffractometer.

Protein crystals need to remain in the mother liquor during the mounting process and data collection. The quality of the crystal and the data will ultimately determine the achievable quality of the final structure, and careful mounting is the first step to assure successful data collection. There are essentially two methods: capillary mounting, which is still used for room temperature data collection, and cryomounting, for data collection at cryogenic temperatures. Because of the prevention or minimization of radiation damage caused by the ionizing X-rays, cryomounting in cryoloops is the most prevalent mounting techniques.

The crystals are harvested while viewed under the microscope and a single crystal is scooped out of the mother liquor with a nylon loop or microfabricated kapton mount attached to a steel pin with a magnetic base. The captured crystal may be directly dipped into liquid nitrogen ( $\text{LN}_2$ ) if there is sufficient cryoprotectant already in the crystallization cocktail, or briefly swished through a cryoprotectant and then quickly dipped into liquid nitrogen. The cryo-pin with the crystal is then transferred into  $\text{LN}_2$ -containing vials to maintain cryogenic temperature (quenching) or the nitrogen cold-gas stream of a diffractometer with pre-cooled protective tongs, or even mounted directly on the goniostat with the cryostream deflected with card or a shutter.

A cryoprotectant acts as an anti-freeze, preventing the mother liquor water from crystallizing during the rapid cooling and the mother liquor solidifies as an amorphous phase (vitrifies). The formation of crystalline ice outside of a crystal in the surrounding mother liquor almost invariably destroys the diffraction quality of the crystal largely because of the change of density during the phase transition from water to ice. Inside the crystal, ice formation is generally hampered as protein itself acts as a cryoprotectant. Common cryoprotectant are glycerol, ethylene glycol, MPD, sucrose and low molecular weight PEGs.

The actual quenching or flash-cooling of the crystal is done by quickly dipping the mounting pin with the looped crystal into liquid nitrogen, where a storage puck is submerged. The base of the pin is held safely in place by magnetic rim of the puck or a vial located in the puck. The loaded puck can be transferred into a shipping or storage container filled with liquid nitrogen. Once cryo-cooled, the crystals are essentially permanently conserved. The actual mounting of the bases and vials are standardized. The actual mounting of the cryo-pins on the diffractometer is generally automated on synchrotrons. Automated mounting of the cryo-pins carrying the harvested and cryo-

protected crystals on the diffractometer increases reliability and enhances utilization of valuable synchrotron beam time.

### 3.4.8 Data collection and processing

Collection of diffraction data is the last physical experiment that is conducted before the *in silico* phase of structure determination. The quality of data would eventually decide the quality and informative content of the final structure, because of which, even though data collection procedure is now automated to a high degree, it is still considered important. Because X-rays generate heat and reactive free radicals in the crystal, that hurts the quality of crystals, crystallographer would like to capture as many reflections as possible.

X-ray are electromagnetic radiation of wavelength 0.1–100 Å. A monochromatic source of X-rays is desirable for crystallography because the radius of the sphere of reflection is  $1/\lambda$ . The X-ray source at synchrotron is capable of providing monochromatic X-rays at selectable wavelengths, that would allow a crystallographer collect sufficient data within minutes (compare to days with “in house”) and would be also helpful in solving the phase problem.

The most common data collection method in macromolecular crystallography is the rotation method, which involves a simple rotation of the crystal around a single axis in small increments - generally 0.1° to about 1.5° - while the crystal is exposed to X-rays and the reflections are recorded on an area detector or CCD camera.

In our case, X-ray diffraction data were collected at the ID23-1 (NisC) and BM14U (NisC with PEP) beamlines of the European Synchrotron Radiation Facility (ESRF), Grenoble. All the data sets were processed and scaled using XDS and XSCALE software package [92]. Data sets were collected at wavelengths of 0.976 Å and 0.953 Å at 100 K, respectively.

### 3.4.9 Reconstruction of electron density

As the physical source of diffraction was the scattering of X-ray photons by the electron distributed around the atoms of the molecules, a mathematical inversion of the diffraction process can be used to reconstruct the electron density distribution,  $\rho$

(**r**), of the diffracting molecules. The switching from one domain representation to its reciprocal representation can be formalized through the Fourier transformation. The electron density function  $\rho(x,y,z)$  in dependence of the coordinates  $x$ ,  $y$  and  $z$ , which is a periodic function as it repeats itself due to the regular array of a crystal.

Imagining that the electron density in the unit cell is composed of small volume elements, each structure factor can be written as a Fourier summation over these volume elements. Each term of this summation represents the diffraction of the electrons constituting this volume element. Thus, the complex structure factor  $F_{hkl}$ , can be expressed by a Fourier series with the contribution of the averaged electron density of each of these volume elements or with infinitesimal small volume elements with the average values of  $\rho(x,y,z)$ .

$$F_{hkl} = \int_V \rho(x,y,z) e^{2\pi i(hx+ky+lz)} dV$$

As this equation is a Fourier series, its transform can be written as

$$\rho(x,y,z) = \frac{1}{V} \sum_h \sum_k \sum_l F_{hkl} e^{-2\pi i(hx+ky+lz)}$$

### 3.4.10 Phase determination

In order to reconstruct the actual molecule structure from our diffraction data, two parts are demanded. First, the amplitude  $|F_{hkl}|$ , which is proportional to the square root of measured intensity  $I(hkl)$ , is already known. Second, the phases  $\alpha$  for each structure factor amplitude  $F_{hkl}$ , which is missing in intensity measurements, need to be supplied through additional phasing experiments (isomorphous replacements and anomalous diffraction) or in the form of model phases via molecular replacement. No matter which phasing method is used, the Patterson function is required in the early stage of structure determination.

*Patterson maps*

The Patterson equation was developed in 1935 by Lyndo Patterson [91]. By using the equation, the map can be constructed without knowing the phase information, but with solely squared  $F_{hkl}$  (intensities). The Patterson function is stated as follow:

$$P(uvw) = \frac{1}{V} \sum_h \sum_k \sum_l |F_{hkl}|^2 \exp[-2\pi i(hu + kv + lw)]$$

Here,  $u$ ,  $v$  and  $w$  represent a vector between two atoms at  $(x_1, y_1, z_1)$  and  $(x_2, y_2, z_2)$  in the crystal lattice, locating a point in the Patterson map. A peak in the Patterson map at  $(u, v, w)$ , corresponding to  $u = x_1 - x_2$ ,  $v = y_1 - y_2$ ,  $w = z_1 - z_2$ , can be provided by this function. Patterson map can be applied typically for locating heavy metal atoms and anomalous scatters, internal symmetry search, or finding the orientation of a molecule in molecular replacement phasing.

#### *Multiple Isomorphous Replacement (MIR)*

Isomorphous replacement means, by make a change to the crystal to perturb the structure factors and, in which way, to deduct possible phase values. Heavy atoms are normally used to achieve this change. Figure 18 illustrates the effect of adding a heavy atom to the two Bragg planes with four atoms.

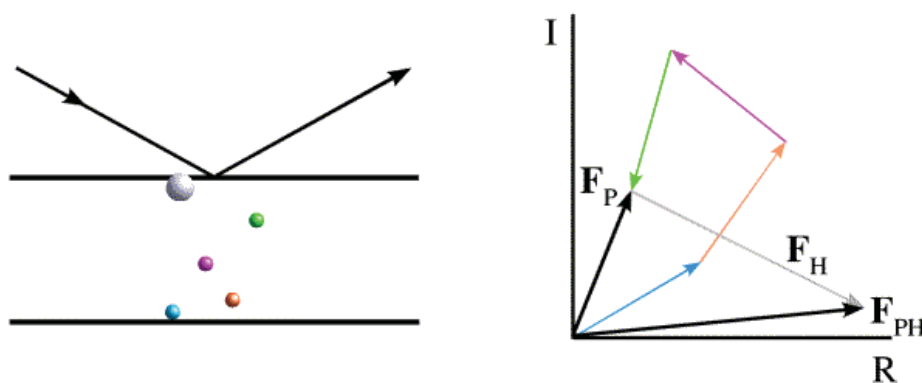


Figure 18. With a heavy atom (gray) adding-in, how the phase and amplitude of the overall scattered wave arise from the individual scattered waves. Two Bragg planes are shown, together with four atoms (pink, green, blue, orange). The atoms and their corresponding contributions to the scattering (vectors on the right side) are shown in

matching colors. The overall scattered wave, sum of the other vectors, is represented by a black vector. Taken from [93].

As shown in Figure 18, by introducing a heavy atom, the scattered intensity will be changed significantly. It means, by measuring the diffractions of two kinds of crystals, native crystal and heavy atoms containing crystal, the differences in scattered intensities, that reflects the scattering contribution of the heavy atoms, can be calculated and then used to compute a Patterson map. Given the limited number of heavy atoms in the crystal, the resulting Patterson map can be deconvoluted. And with the location of heavy atoms in the crystal, their contribution to the structure factors can be computed.

Since the structure factors can be thought of as vectors, the structure factor for the derivative crystal ( $F_{PH}$ ) equals the sum of the protein structure factor ( $F_P$ ) and the heavy atom structure factor ( $F_H$ ), represented as follow:

$$F_{PH} = F_P + F_H$$

This equation defines two kinds of triangle, as shown in the Figure 19, meaning there are two possible phases for  $F_P$ .

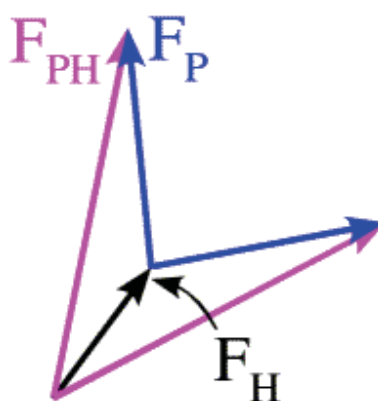


Figure 19. Two possible phases for  $F_P$ . Taken from [93].

It can be illustrated as well by a Harker construction, as shown in Figure 20. In the diagram of a Harker construction, a circle with a radius of  $|F_P|$  is drawn, centered at

the origin (color blue), which indicates all the vectors that would be obtained with all the possible phase angles for  $F_P$ . Another circle with radius  $|F_{PH}|$  centered at a point of  $-|F_H|$  (color magenta) shows all the possible phase values for  $F_{PH}$ . To fulfill the equation of  $F_{PH} = F_H + F_P$ , there are two possible phase values for  $F_P$ .

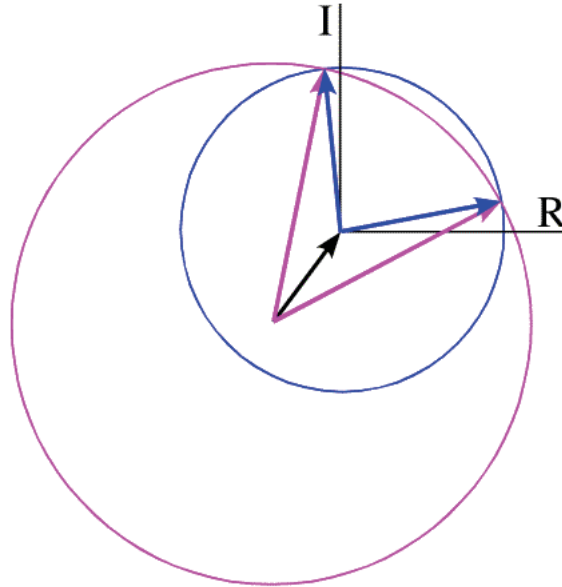


Figure 20. Diagram of Harker construction. Taken from [93].

The phase can be finally determined by applying a second derivative crystal with heavy atoms that bind at other sites. Figure 21 shows that only one phase choice can satisfy all the conditions.

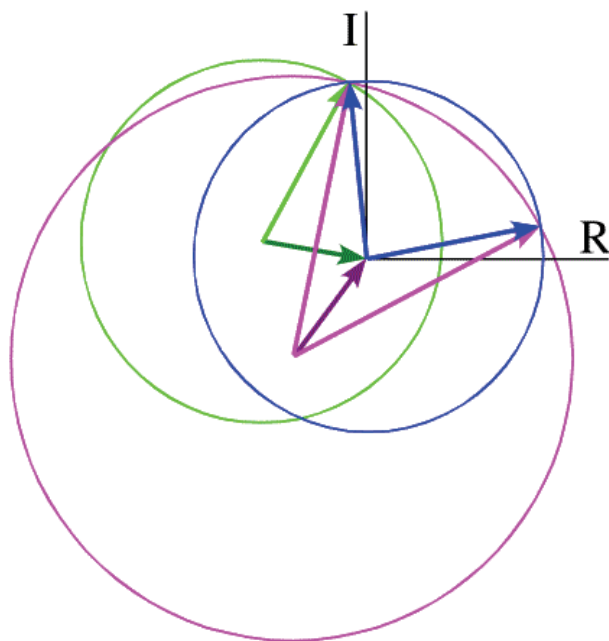


Figure 21. Harker construction when having a second derivative crystal with heavy atoms. Taken from [93].

#### *Multiple Wavelength Anomalous Diffraction (MAD)*

Most electrons in the atoms that make up a crystal will interact identically with X-rays. Because of this, pairs of diffraction spots obey Friedel's law, which is illustrated in Figure 21. On the left, two arrows, black and red, indicate two similar diffraction event from opposite sides of the Bragg planes. If the black arrows define planes with Miller indices  $(h\ k\ l)$ , the other side of the planes would be  $(-h\ -k\ -l)$ . The reflection with indices  $(-h\ -k\ -l)$  is considered as the Friedel mate of  $(h\ k\ l)$ . The respective diffraction patterns contributed by the atoms are shown on the right with opposite signs of phases.



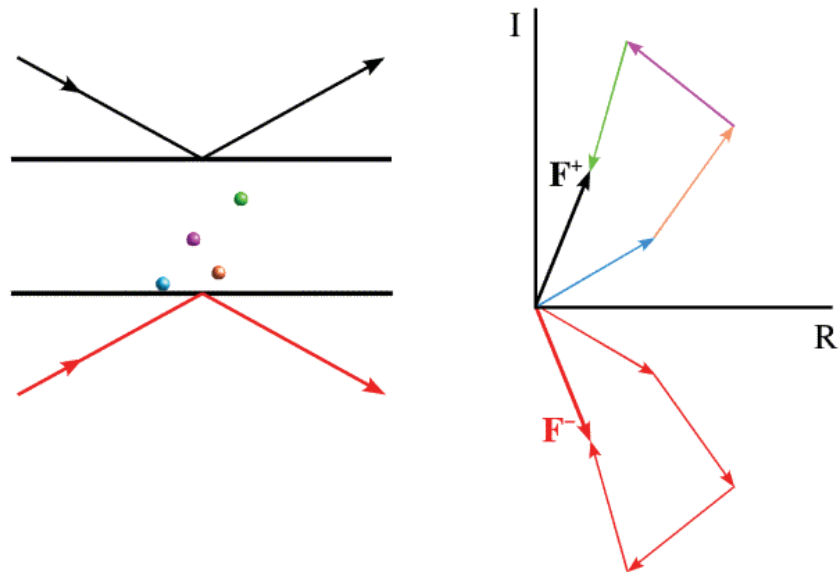


Figure 21. Pairs of diffraction spots obey Friedel's law. Taken from [93].

When the frequency of oscillation induced by X-ray is similar to the natural frequency of oscillation, then there will be a small shift in both the amplitude and phase of the induced oscillation. This phenomenon usually happens to some inner shell electrons in some atoms, where the X-ray photon energy is close to a transition energy. This shift in amplitude and phase is called anomalous scattering. The phase shift in anomalous scattering leads to a breakdown of Friedel's law, as illustrated in the Figure 22, when a heavy atom with an anomalous scattering component is added.

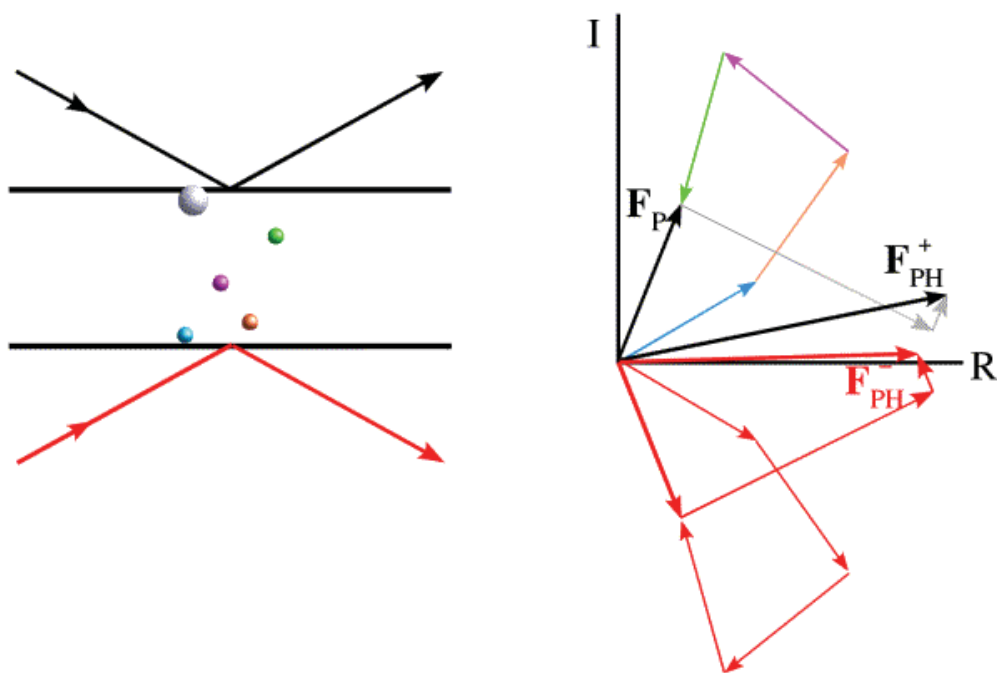


Figure 22. The phase shift in anomalous scattering. Taken from [93].

The amplitudes of the Friedel mates become different under the effect of anomalous scattering. The anomalous scattering effect depends on the frequency of oscillation being similar to the natural frequency for the atom, which means the strength of the anomalous scattering effect depends on the wavelength of the X-rays. By collecting data at several wavelengths near the absorption edge of an element in the crystal, the phase information can be obtained analogous to methods used in MIR. This technique is multiple-wavelength anomalous dispersion (MAD). Introduction of selenomethionine, the selenium atoms of which have a strong anomalous signal at a certain wavelength, to replace methionine residues in a protein is a well-known way for MAD.

### *Molecular replacement*

Molecular replacement can be used when a good model what shares a certain level of sequence identity (at least 40%) is available. To carry out molecular replacement, the model structure needs to be placed in the correct orientation and position in the unknown unit cell. For this purpose, three rotation angles and three translational parameters need to be specified, which is considered as a 6-dimensional problem and can usually be separated into two 3D problems. A rotation function can be computed

to find the three rotation angles, and then the oriented model can be placed in the cell with a 3D translation function.

An understanding of the rotation and translation functions can be obtained by considering the Patterson function. The vectors in the Patterson map can be divided into two categories, intramolecular vectors and intermolecular vectors. Intramolecular vectors, which depend only on the orientation of the molecule, can be exploited in the rotation function. Intermolecular vectors, which depend both on the orientation of the molecule and on its position so, can then be exploited in the translation function with the known orientation. Since the intramolecular vectors in average are shorter than the intermolecular vectors, the rotation function can be computed using only the part of the Patterson map near the origin. (Figure 24)

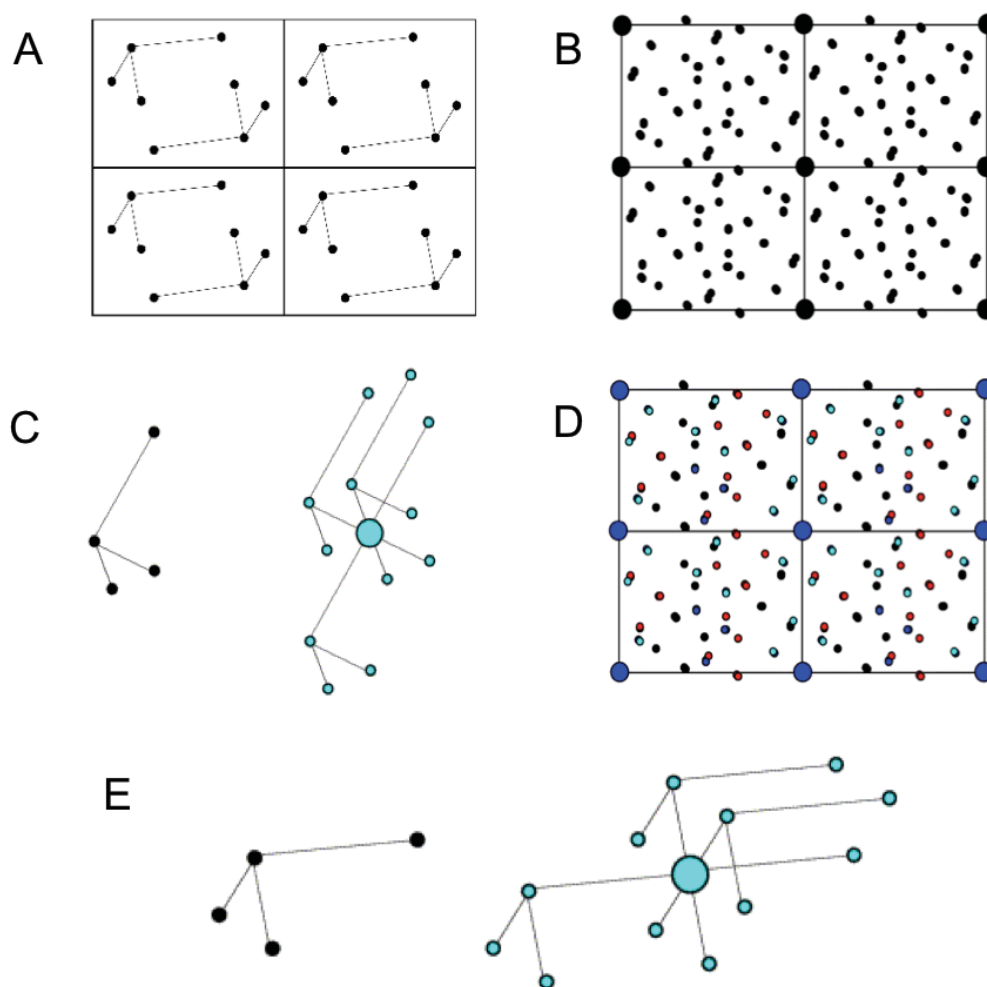


Figure 23. A. Crystal, B. Patterson map, C. Intracellular vectors before rotation, D. color-coded Patterson map, E. Intracellular vectors after rotation. Taken from [93].

### **3.4.11 Model building and refinement**

The structures were solved by molecular replacement with the phases of the published structure of NisC (PDB code: 2G02) [72]. For the structure of NisC with PEP, initial model was built and refined using COOT and PHENIX, followed by manual iterative cycles of model refinement using the program phenix.refine and ccp4.refmac. [94-96] Manual adjustments between the refinement cycles were done with the program Coot and Ramachandran validation was done using MolProbity. [97] The images of the models were prepared using MacPyMOL [98].

For the model of NisC possessing three Zn ions,  $R_{\text{work}}$  is 16.17%,  $R_{\text{free}}$  is 20.81%. For the model of NisC with extra Zn ions removed,  $R_{\text{work}}$  is 18.70%,  $R_{\text{free}}$  is 20.73%. For the model of NisC in complex with PEP,  $R_{\text{work}}$  is 16.17%,  $R_{\text{free}}$  is 19.08%.

## **4. Results**

### **4.1 Characterization of response regulator NisR**

#### **4.1.1 Overexpression and purification of NHis-NisR and CHis-NisR**

The NHis-NisR protein was overexpressed and isolated as described in Materials and Methods. After the induction with IPTG, cells were grown at 37 °C overnight. The expression of NHis-NisR was monitored by taking the same amount of cells at different time points: right before induction, 1 hour after induction, 2 hours after induction, 3 hours after induction and overnight. All samples were afterwards boiled at 95 °C for 5 minutes and analyzed by Commassie stained SDS-PAGE. As shown in Figure 24, a protein band at 28 kDa increased gradually after induction, indicating that NHis-NisR (theoretical mass: 27.54 kDa) was successfully expressed in *E.coli*.

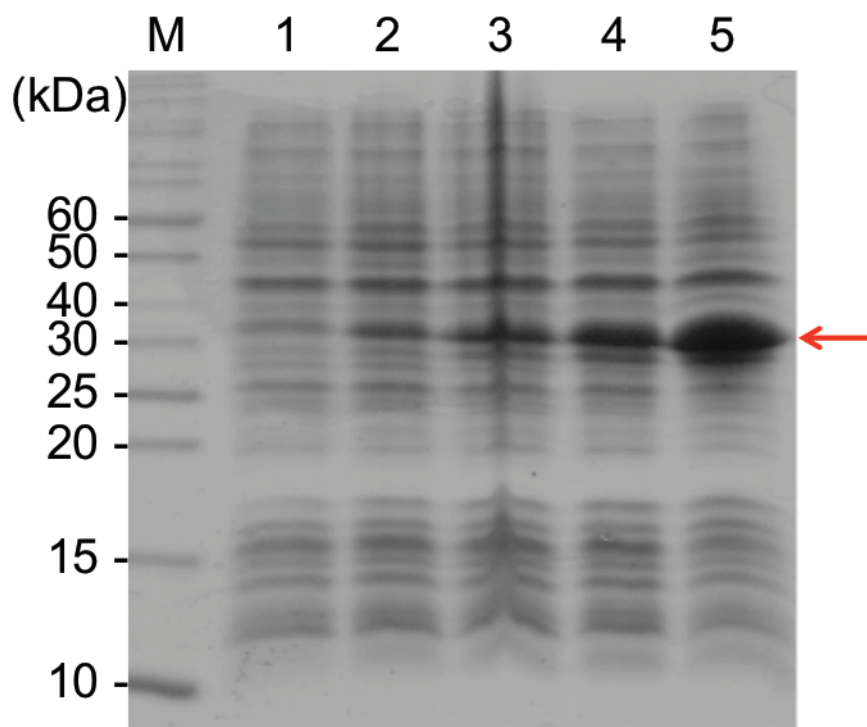


Figure 24. Expression analysis of NHis-NisR analyzed by 15 % Coomassie stained SDS-PAGE. M: PageRuler Unstained Protein Ladder; 1: Before IPTG induction; 2: 1 hour after IPTG induction; 3: 2 hours after IPTG induction; 4: 3 hours after IPTG induction; 5. Overnight after IPTG induction.

After a two-step purification, the purity of NHis-NisR reached 95%, which is demonstrated by Coomassie stained SDS-PAGE (Figure 25). The homogeneity and oligomeric state of NHis-NisR was examined by MALS, shown in Figure 26, demonstrating NHis-NisR behaves as a monomer at pH 11.

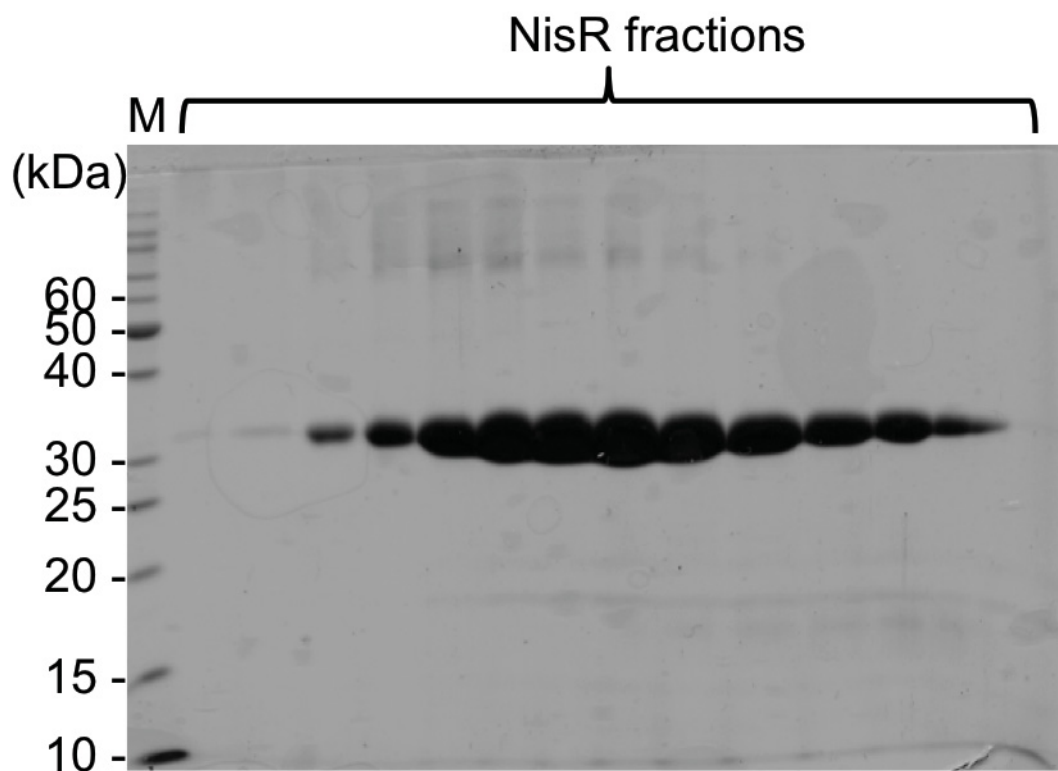


Figure 25. 15 % Commassie stained SDS-PAGE of NHis-NisR after SEC at pH 11. M: PageRuler Unstained Protein Ladder.

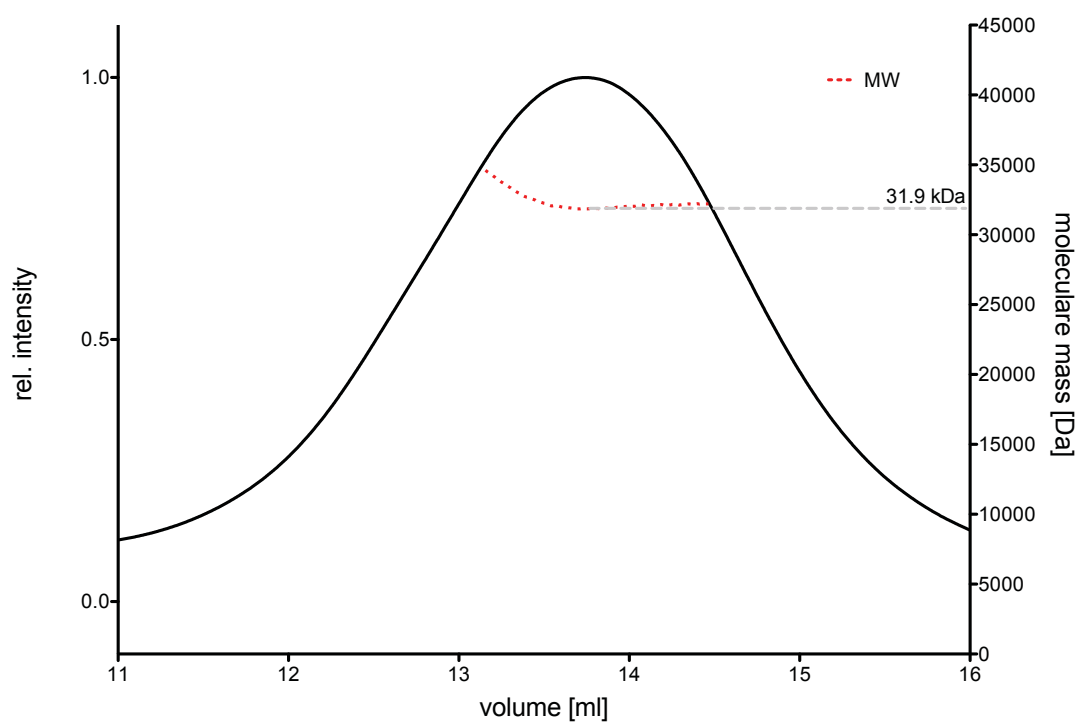


Figure 26. MALD-SEC for NHis-NisR at pH 11. The position of red dash line indicates the calculated molecular mass of NHis-NisR, as labeled (31.9 kDa). Black

line: SEC chromatogram of NisR (shown in relative intensity), illustrating NisR is behaving as a monomer in the solution at pH 11.

At pH 9.0, the elution time of NHis-NisR on SEC was shifted to an earlier elution volume, compared to pH 11, suggesting a higher oligomeric state (Figure 27). The SEC was further optimized by adding an overnight dialysis against pH 9 SEC buffer prior to SEC and the optimized chromatogram (Figure 28) illustrated the expected homogeneity of NHis-NisR at pH 9. Furthermore, the purity of NHis-NisR after SEC was confirmed to be over 95 % via Commassie stained SDS-PAGE (Figure 29). In conclusion, NHis-NisR is homogeneous at both pH 9 and pH 11, which make crystallization trials possible.

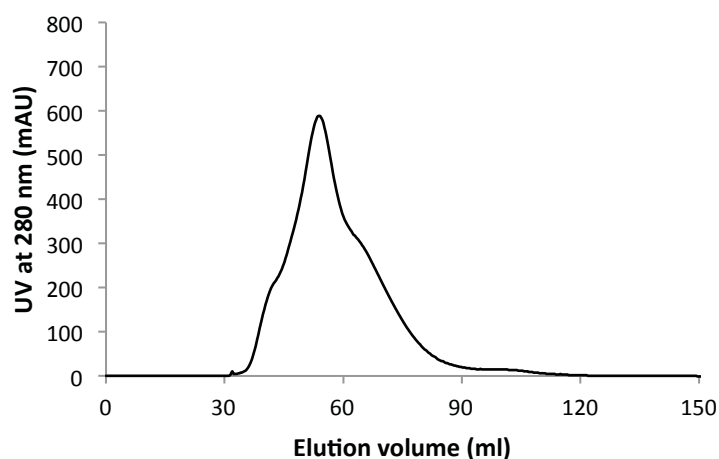


Figure 27. Diagram of the SEC for NHis-NisR at pH 9. Black line: the SEC chromatogram of NHis-NisR protein at pH 9. The void volume of the column is 40 ml.

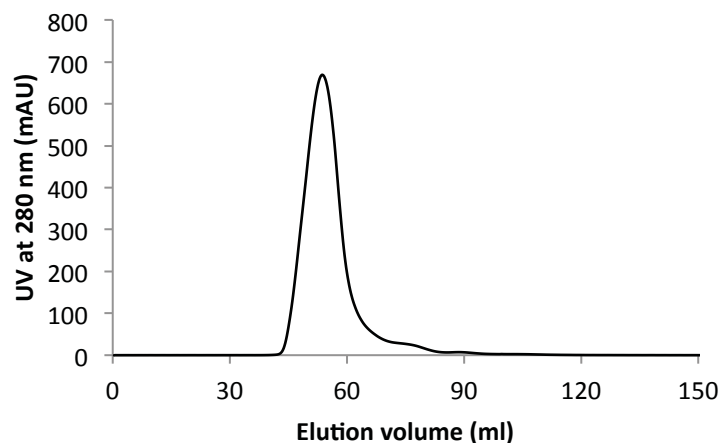


Figure 28. SEC of NHis-NisR after overnight dialysis at pH 9. Black line: the SEC chromatogram of NisR protein. The sample was pre-equilibrated against pH 9 SEC buffer overnight prior to injection. The void volume of the column is 40 ml.

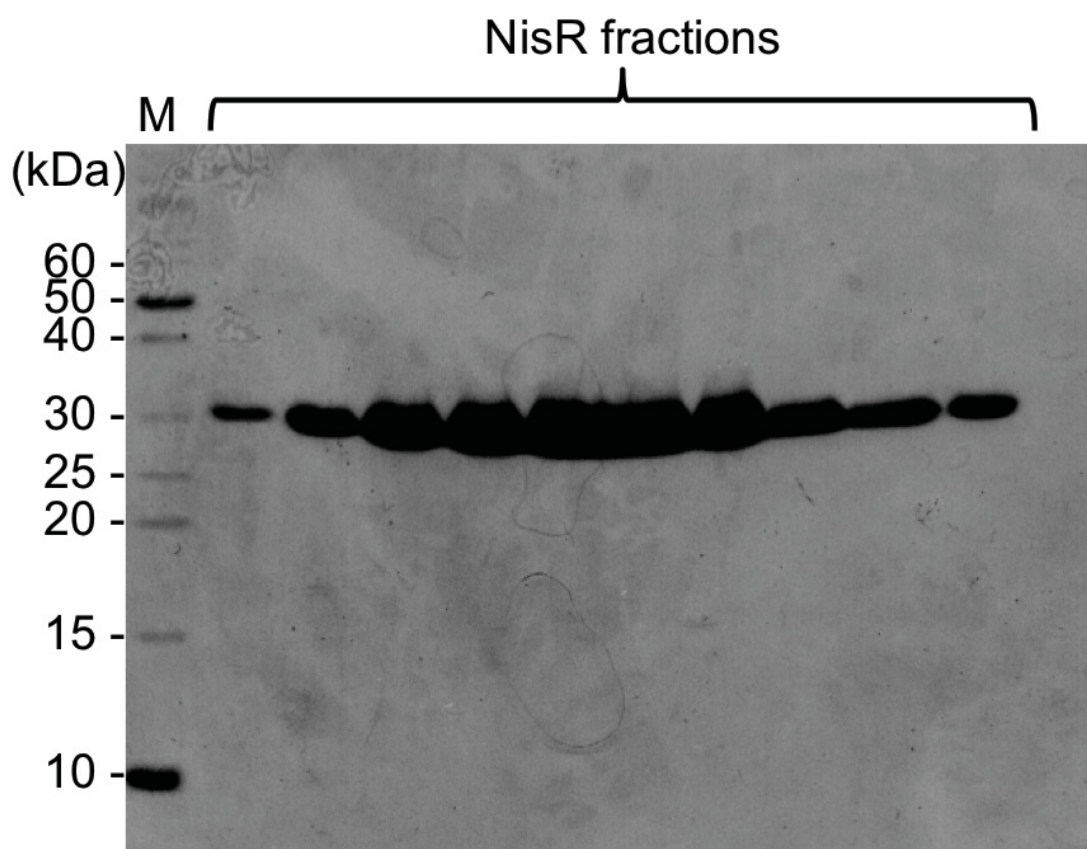


Figure 29. 15 % Commassie stained SDS-PAGE for NHis-NisR at pH 9. M: PageRuler Unstained Protein Ladder.



The expression of C-terminal His-NisR was performed by using the same protocol as the N-terminal His-tag construct. The successful expression of CHis-NisR was analyzed by SDS-PAGE (Figure 30), which shows the bands of the target protein around 28 kDa upon IPTG induction.

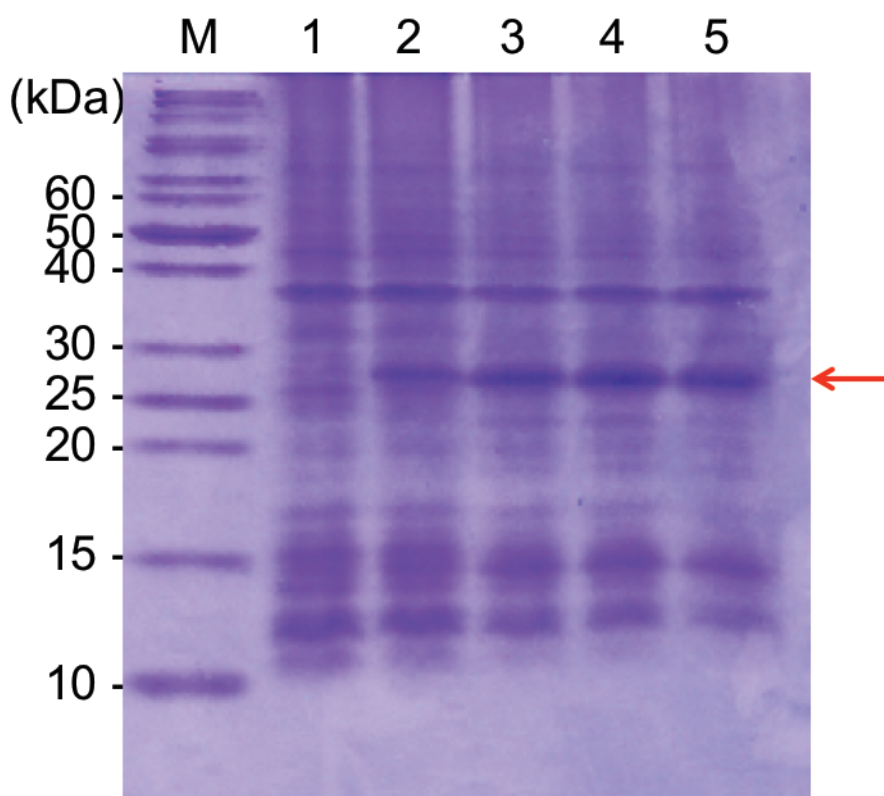


Figure 30. Expression analysis for CHis-NisR by 15% SDS-PAGE. M: PageRuler Unstained Protein Ladder; 1: Before IPTG induction; 2: 1 hour after IPTG induction; 3: 2 hours after IPTG induction; 4: 3 hours after IPTG induction; 5. Overnight after IPTG induction.

The first purification was performed with IMAC as described in Materials and Methodsgy. The target protein was eluted with a gradient of high IMAC buffer from 0 % to 100 %. The second peak from the IMAC chromatogram (Figure 31) was confirmed to be the CHis-NisR by both SDS-PAGE and Western Blot (Figure 32). The following SEC analysis showed that CHis-NisR is homogeneous at pH 11 (Figure 33). However, from the SDS-PAGE and Western blot of both IMAC (Figure 32) and SEC (Figure 34), another band at around 15kDa was always observed and could not be separated from the CHis-NisR through SEC, suggesting the presence of a “half-size” NisR protein. It is proven that, in the class of response regulator protein,

the linker connecting the regulatory domain to the effector domain is often vulnerable to proteolysis, in our case, resulting in a degradation of full size of NisR [99]. And for NisR, the situation could not be changed even with the protease inhibitors such as PMSF.

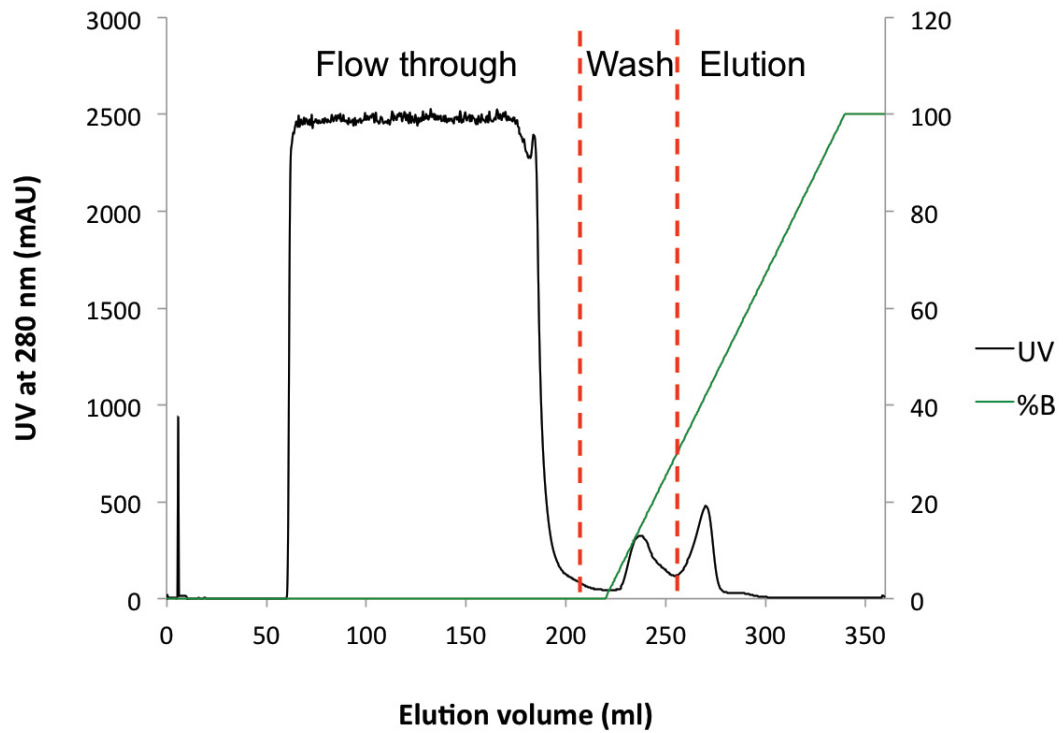


Figure 31. Diagram of IMAC of CHis-NisR.

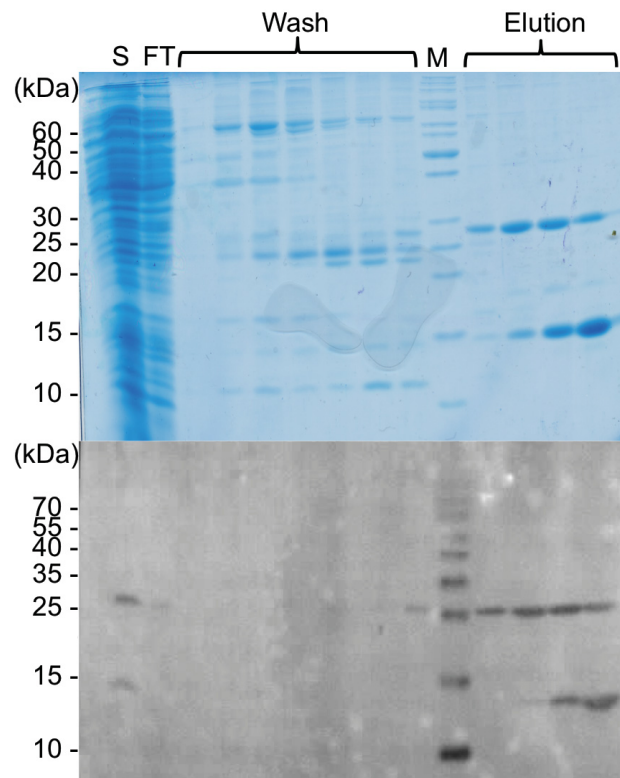


Figure 32. Coomassie stained SDS-PAGE (upper panel) and Western blot (lower panel) for IMAC of CHis-NisR. S: Supernatant. FT: Flow through. M: PageRuler Unstained Protein Ladder.

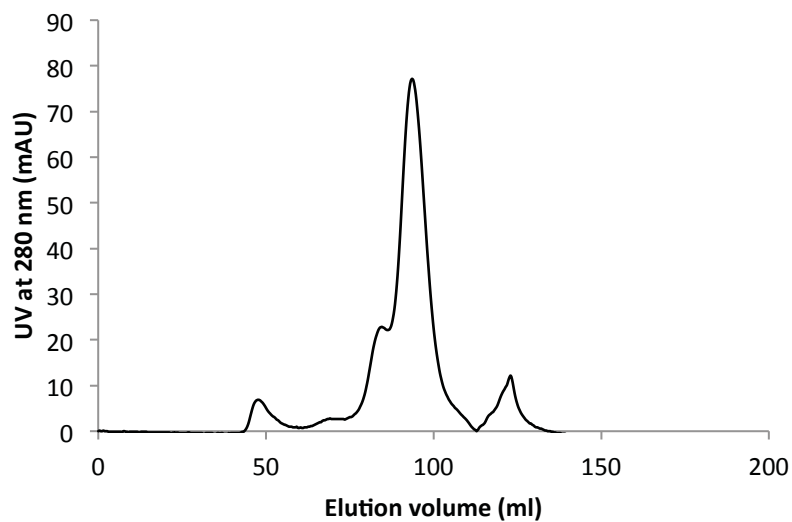


Figure 33. Diagram of SEC chromatogram for CHis-NisR at pH 11. The void volume is 40 ml.

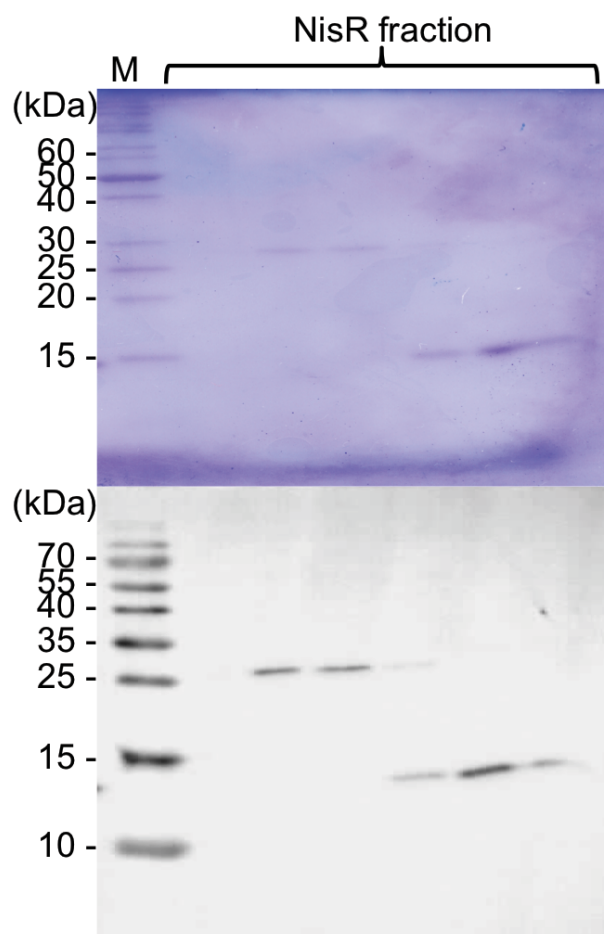


Figure 34. Coomassie stained SDS-PAGE (upper panel) and Western blot (lower panel) of SEC of CHis-NisR. M: PageRuler Unstained Protein Ladder.

#### 4.1.2 Crystallization of NisR

The crystallization trials for both N-terminal and C-terminal His-tagged NisR were performed. For NisR purified at pH 11, no crystal hits were observed. On the other hand, at pH 9, a crystalline-like hit (Figure 35A) was observed for NHis-NisR using 0.1M CAPS pH 10.5, 30% PEG 400, 12 °C. And the crystalline illuminates under UV light which is considered positive (Figure 35B). Yet the hit was not able to be reproduced.

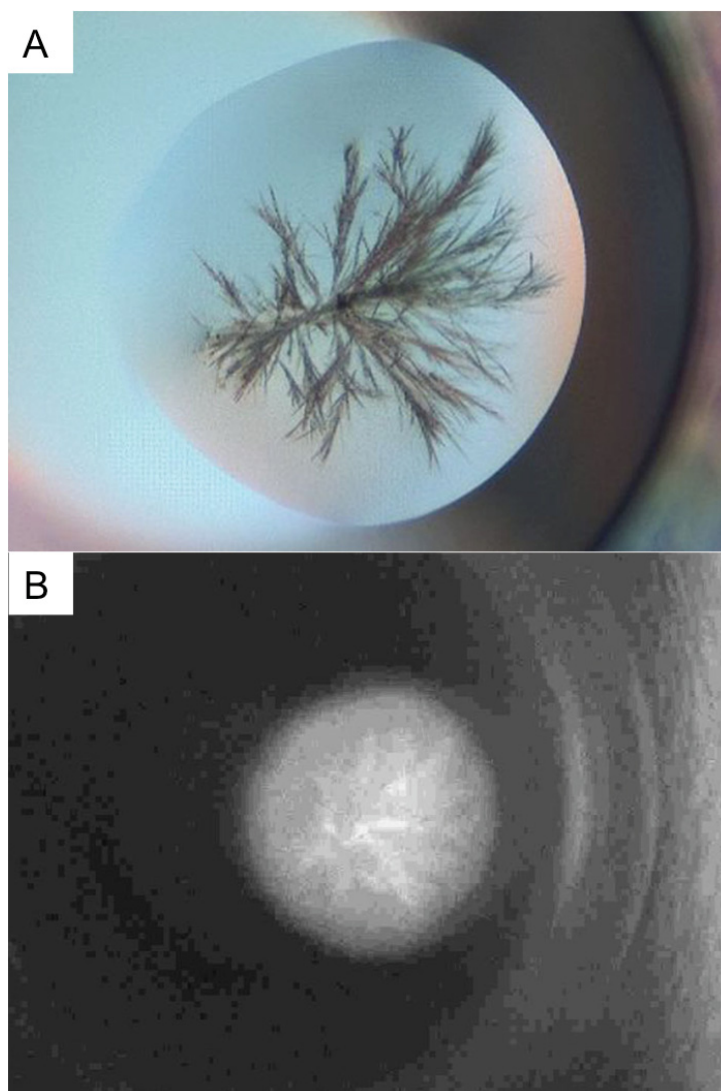


Figure 35. First crystalline of NHis-NisR at pH 9. Reservoir condition: 0.1M CAPS PH 10.5, 30% PEG 400, 12 °C, sitting drop. A) Image of the drop obtained by light microscope. B) Image of the drop obtained by under UV light.

#### 4.1.3 DNA binding assay of NisR

As a response regulator, the essential property of NisR is the ability to bind to its corresponding promoter, in this case the NisA promoter (Figure 36). The electrophoretic mobility shift assay (EMSA) was used to study the binding properties of NisR to the NisA promoter. At first, the assay was carried out by using the NisA promoter involving plasmid (pNZ-SV) as a binding target. The assay was designed to study the binding affinity of NisR under different pH, different salt concentrations, and different protein concentrations. As shown in the Figure 37, DNA binding was

evidenced by the shifts in the gel upon an increasing protein concentration (0.01-10  $\mu\text{M}$ ), suggesting that this heterologously expressed NisR is active *in vitro*. Moreover, the optimal binding condition of NisR was observed at pH 7 buffer with 50 mM NaCl at protein concentration of 10  $\mu\text{M}$ .



Figure 36. Interaction between NisR and its corresponding promoter: PnisA. PnisA is located on one circular plasmid.

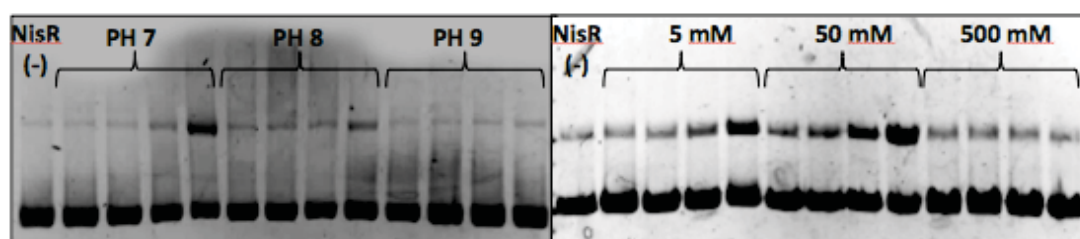


Figure 37. EMSA studies of NisR with pNZ shuttle vector on 0.5% agarose gels. Left: pNZ mobility shifts with increasing concentrations of NisR (0.001  $\mu\text{M}$ , 0.01  $\mu\text{M}$ , 0.1  $\mu\text{M}$ , 1  $\mu\text{M}$ , 10  $\mu\text{M}$ ) at different pH values (7-9). Right: Salt optimization (5-500 mM NaCl) of EMSA at pH 7 with 15 nM of pNZ and increasing concentrations of NisR (0.001  $\mu\text{M}$ , 0.01  $\mu\text{M}$ , 0.1  $\mu\text{M}$ , 1  $\mu\text{M}$ , 10  $\mu\text{M}$ ).

To further confirm the binding property of NisR, a DNA fragment of pNisA was used to perform the EMSA assay. The pNisA fragment was obtained by digesting the pNZ-SV into two pieces, and the one with pNisA (341 bps) was later separated via gel extraction. In lane 3 of Figure 38, a shifted band was observed. However, a later control sample with 50  $\mu\text{M}$  NisR only also showed a band at the same position, suggesting the previously observed band is rather a DNA contamination from the NisR protein sample. Interestingly, even though the concentration of the NisR in lane 2 was the same as in lane 3, no similar band was observed, therefore the possibility of a buffer effect cannot be ruled out.

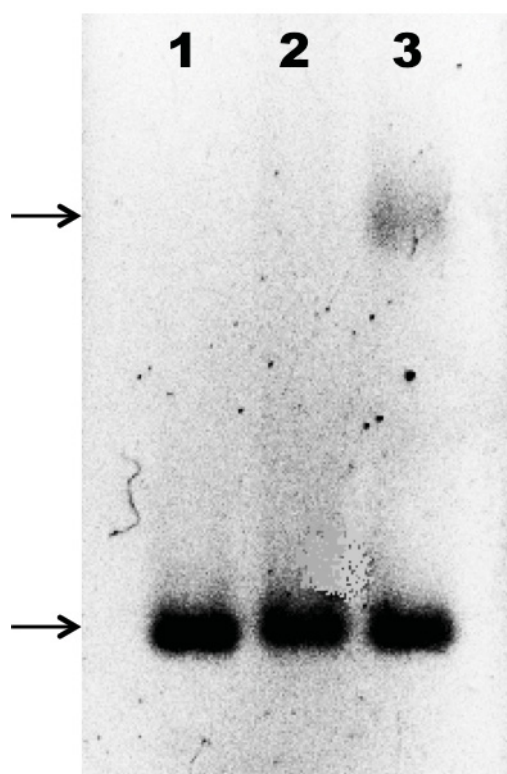


Figure 38. 1. 45 nM PnisA, no NisR in binding buffer A (20 mM HEPES, pH 7, 100 mM KCl, 1 mM EDTA, 10 mM MgCl<sub>2</sub>, 10% glycerol); 2. 45 nM PnisA, 50  $\mu$ M NisR in binding buffer A; 3. 45 nM PnisA, 50  $\mu$ M NisR in binding buffer B (20 mM phosphate, pH7, 50 mM NaCl, 10% glycerol).

In conclusion, based on the EMSA assays above, the unphosphorylated NisR is suggested to be capable of binding to the pNisA region at a high concentration.

## 4.2 Characterization of NisC

### 4.2.1 Overexpression and purification of NisC in *E. coli*

Three constructs of NisC were used to perform crystallization trial. These were NisC with a four amino acid spacer (N-HMAS-C), NisC with no spacer, and NisC H331A (with spacer). All these three forms of NisC were overexpressed and isolated with the same protocol as described in Materials and Methods. Since all three constructs behaved nearly identical during the purification, only one set of diagrams was shown as an example to represent the purification process of all three constructs. NisC was firstly purified via IMAC (Figure 39), in which Zn<sup>2+</sup> ion was used as the immobilized



metal ion. The His<sub>6</sub>-tag was removed from all three kinds of NisC by thrombin [67]. As shown in Figure 40, over 90% of the fusion protein was cleaved, causing a shift in the SDS-PAGE. The subsequent SEC demonstrated that NisC is homogeneous in SEC buffer, which is prerequisite for crystallization (Figure 41).

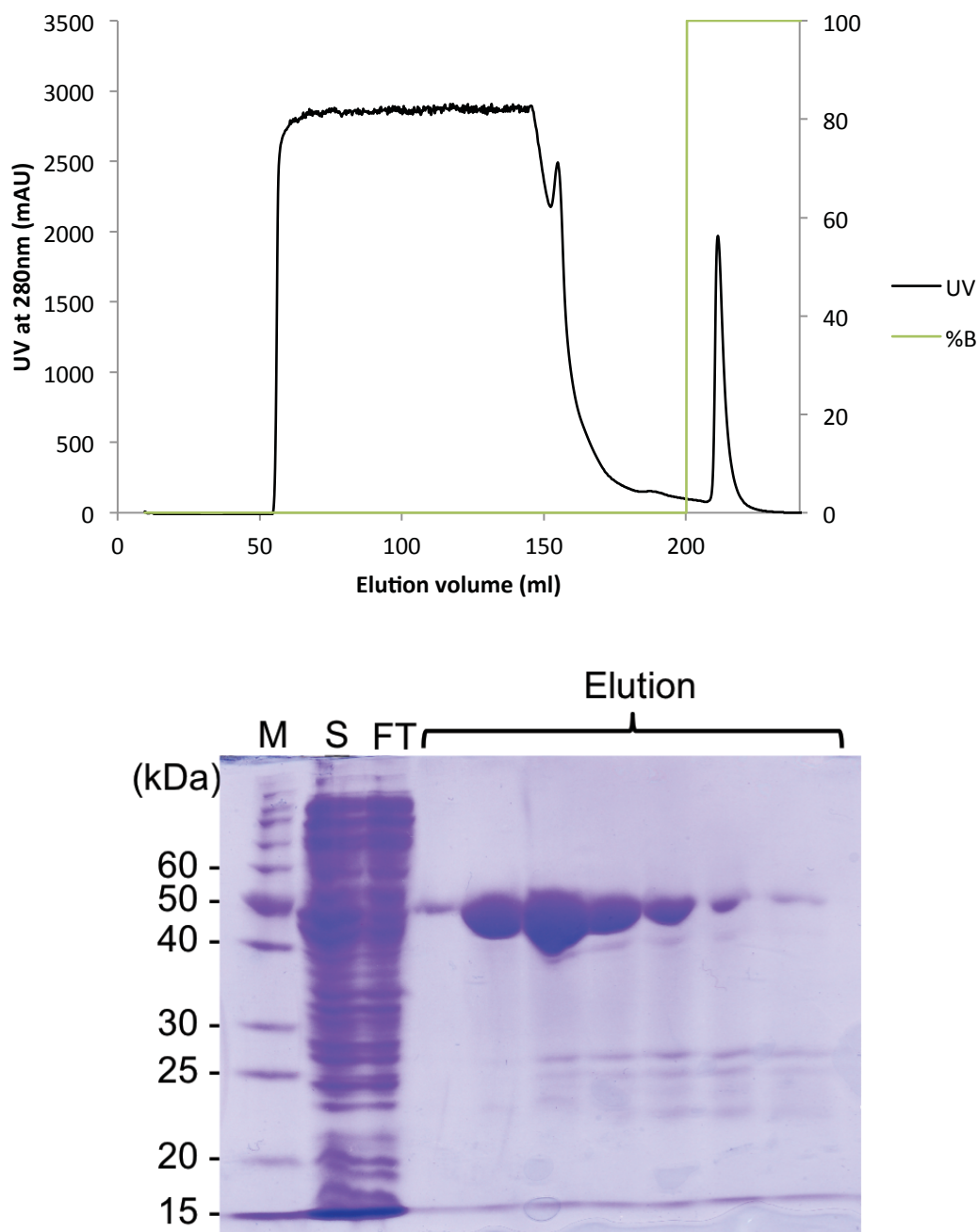


Figure 39. An example of IMAC of NisC. Upper panel: The IMAC chromatogram of NisC protein. Protein was eluted with 100% High IMAC buffer. Lower panel: The corresponding Commassie stained SDS-PAGE (15%) of NisC fractions.



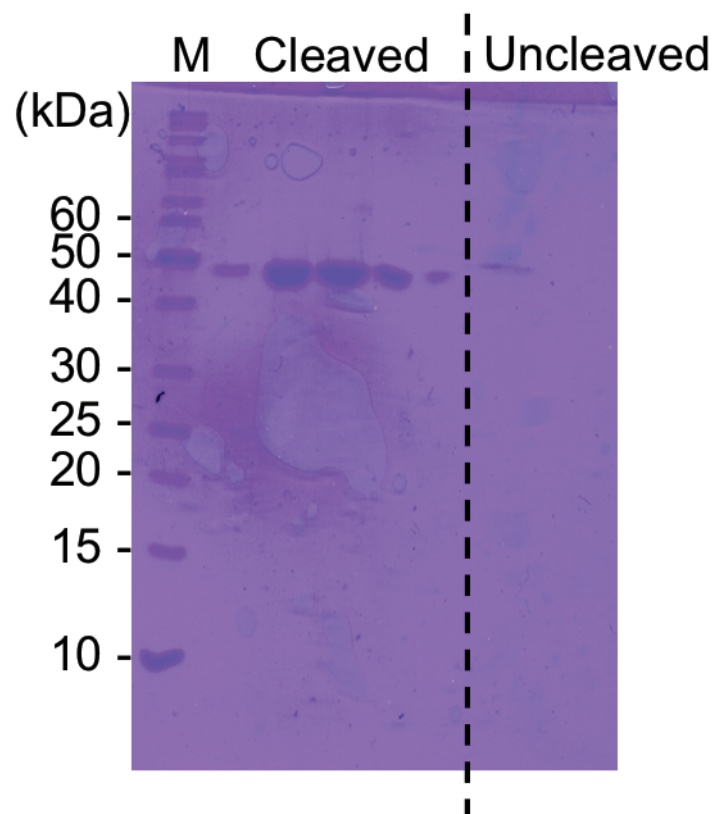
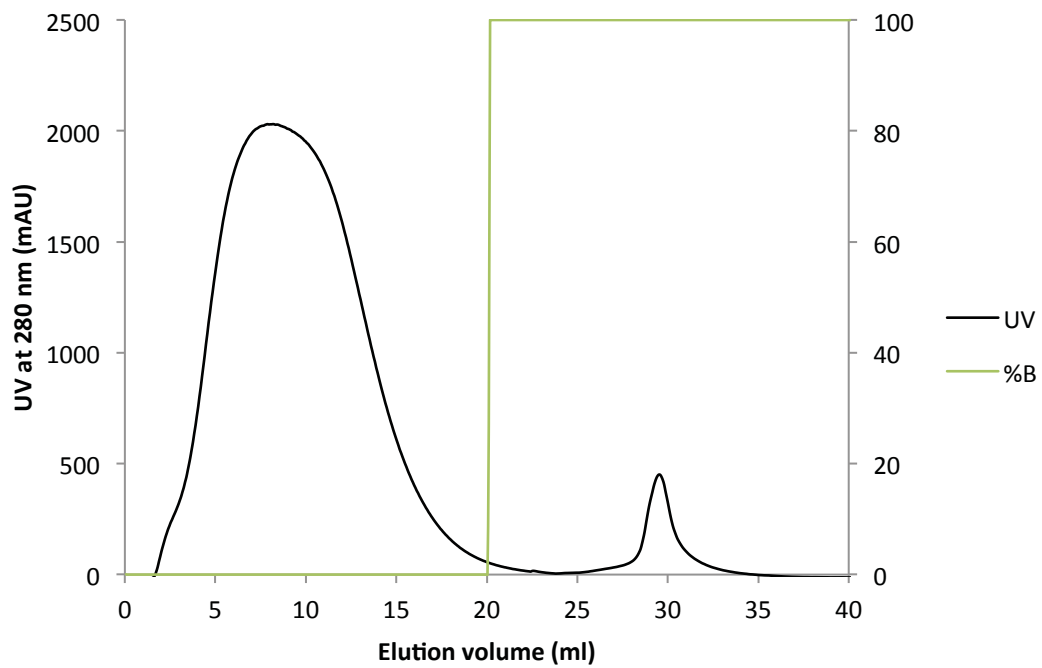


Figure 40. Thrombin cleavage of NisC. Upper panel: IMAC chromatogram after the thrombin cleavage reaction of NisC. Cleaved NisC, which has no his-tag, was not able to bind to the IMAC column. The non-cleaved NisC, with his-tag, was bound to the column and was eluted by 100% high IMAC buffer. Lower panel: 15%

Commassie stained SDS-PAGE after the thrombin cleavage reaction of NisC to detect cleaved and non-cleaved NisC, respectively.

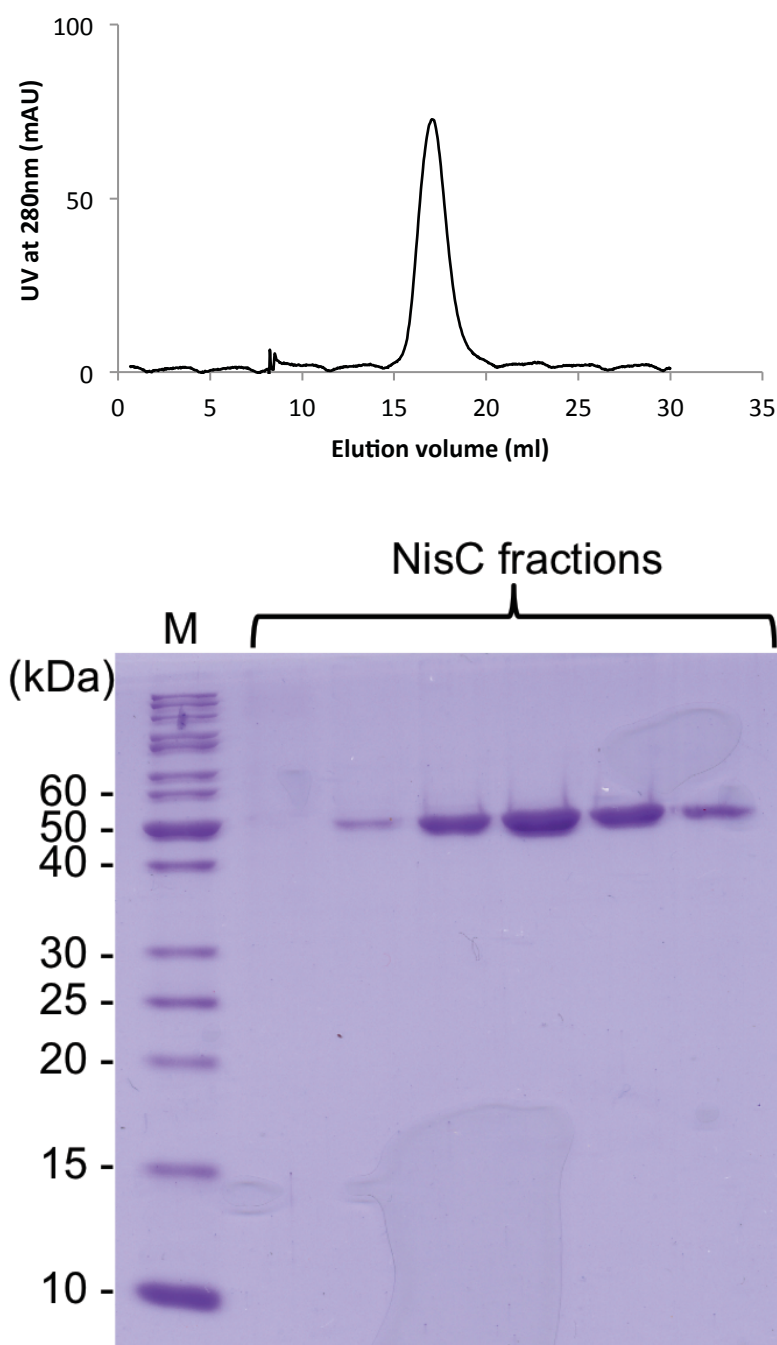


Figure 41. SEC of NisC. Upper panel: SEC chromatogram of NisC at pH 7.5. The void volume of the column is 8 ml. Lower panel: 15% Commassie stained SDS-PAGE of the corresponding NisC fractions.

#### 4.2.2 NisC with three $\text{Zn}^{2+}$ ions

#### 4.2.2.1 Crystallization

Initial crystal hits from the construct of NisC with a four amino acid spacer were obtained from two reservoir conditions (Figure 42): 40% ethylene glycol, 0.1 M HEPES (pH 7.5), 5% polyethylene glycol 3000 , 10 mg/ml NisC, 12 °C and 5% 2-methyl-2,4-pentanediol, 0.1 M HEPES (PH 7.5), 10% polyethylene glycol 6000, 10 mg/ml NisC, 12 °C. Optimized crystals (Figure 42 A) diffracted to a resolution of 1.82 Å.

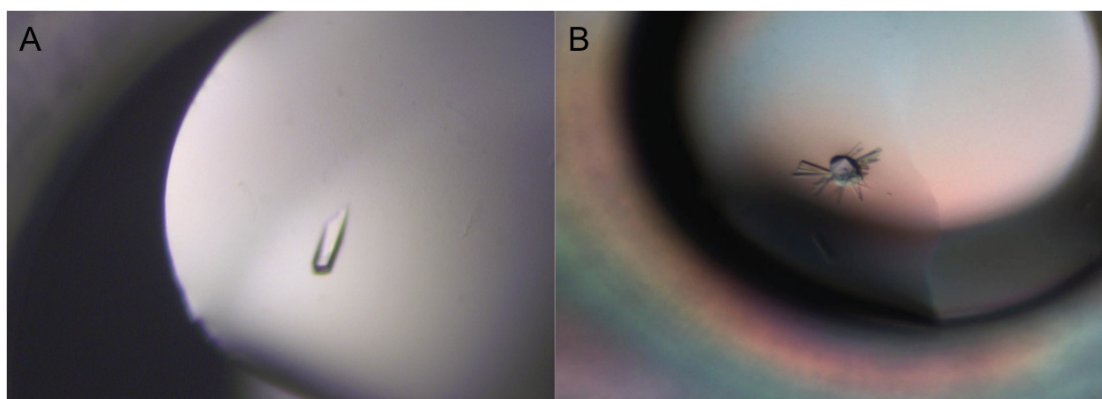


Figure 42. NisC crystals. A) Reservoir condition: 40% ethylene glycol, 0.1 M HEPES (PH 7.5), 5% polyethylene glycol 3000 , 10 mg/ml NisC, 12 °C. B) Reservoir conditions: 5% 2-methyl-2,4-pentanediol, 0.1 M HEPES (PH 7.5), 10% polyethylene glycol 6000, 10 mg/ml NisC, 12 °C.

#### 4.2.2.2 Data collection and processing

As the completeness and the  $I/\sigma$  in the highest resolution shell (1.96 - 1.82) for the obtained NisC crystal dataset (Figure 42A) were not satisfying, the data was cut at 1.96 Å for structure determination. It was phased using molecular replacement by using the published NisC structure (PDB code: 2G0D and reference) and resulted in a unique solution for one monomer in the asymmetric unit. Several rounds of manually model building using COOT and subsequent refinement by PHENIX were performed to establish the full models. The data statistics as well as the final R factors for the structure are summarized in the Table 1.

<b>Resolution range (Å)</b>	48.81 - 1.96 (2.03 - 1.96)
<b>Space group</b>	P 2 <sub>1</sub> 2 <sub>1</sub> 2 <sub>1</sub>
<b>Unit cell (a, b, c in Å; α, β, γ in °)</b>	63.4, 76.4, 85.3; 90.0, 90.0, 90.0
<b>Unique reflections</b>	30324 (2979)
<b>Completeness (%)</b>	99.67 (99.90)
<b>Mean I/sigma(I)</b>	15.07 (3.68)
<b>Wilson B-factor</b>	26.07
<b>R-work (%)</b>	0.1617 (0.2483)
<b>R-free (%)</b>	0.2081 (0.2934)
<b>Number of protein residues</b>	417
<b>RMS (bonds, Å)</b>	0.007
<b>RMS (angles, °)</b>	1.12
<b>Ramachandran favored (%)</b>	98
<b>Ramachandran outliers (%)</b>	0
<b>Clashscore</b>	2.43
<b>Average B-factor</b>	32.80

Table 1. Processing and refinement statistics for NisC crystal (shown in figure 42A) data set. The table is generated by PHENIX. Statistics for the highest-resolution shell are shown in parentheses.  $R_{work}$  is a measure of the agreement between the crystallographic model and the experimental X-ray diffraction data and  $R_{free}$  is used to assess possible overfitting of the data.  $R_{work} = \frac{\sum ||F_{obs}| - |F_{calc}||}{\sum |F_{obs}|}$ ,  $R_{free}$  is defined same as  $R_{work}$ , except 5% of the reflections were not included in the refinement for  $R_{free}$  calculations.

#### 4.2.2.3 Overall structure

By comparison, the packing and the overall fold of this NisC structure is nearly identical with the previously published model (Figure 11A). It also consists of 14  $\alpha$  helices, folded into two layers of  $\alpha$  toroid, and an extended SH2-like domain (Figure 43). However, the map quality was significantly improved because of the better resolution (1.96 Å compared to 2.5 Å), as a result, some features, which are not

visible before can be clearly seen now. In the former model published by Liu et al. [72] the N-terminal residues of the NisC (residues 1-6) are missing, whereas, in our model, the N-terminal is completely visible in the electron density.

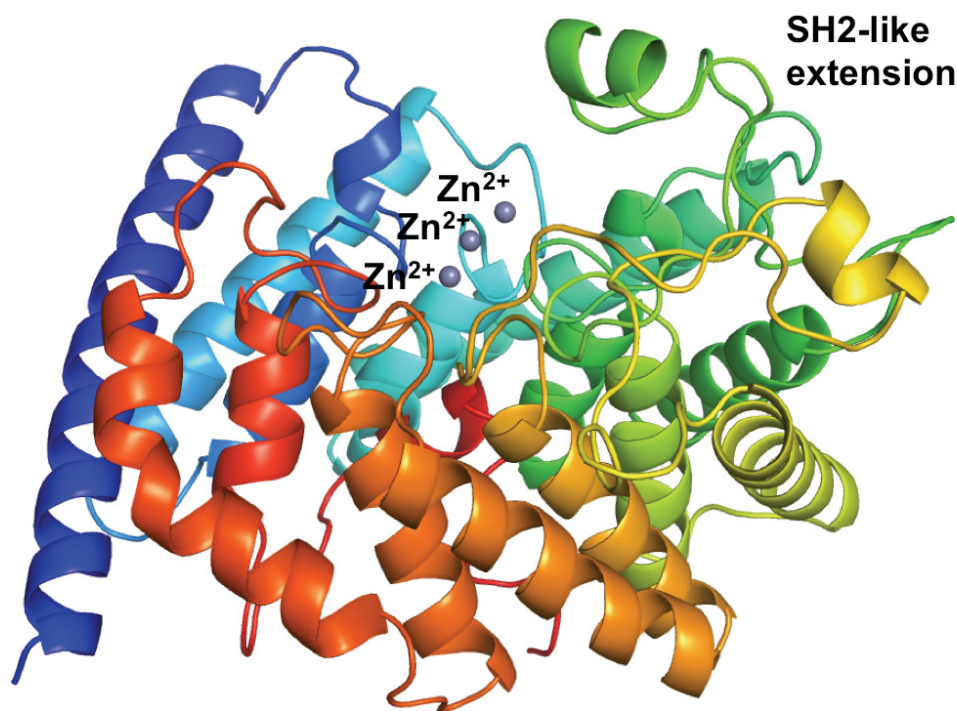


Figure 43. Overall structure of NisC protein. A two-layer toroid core consists of 14  $\alpha$ -helices. A SH2-like extension is observed adjacent to the  $\alpha$ ,  $\alpha$  barrel. Three  $\text{Zn}^{2+}$  ions are situated at the top of  $\alpha$ -toroid.

#### 4.2.2.4 Active site possessing three $\text{Zn}^{2+}$

It was demonstrated that NisC is a Zinc-dependent protein and previously published NisC model has revealed one Zinc ion binding to three other residues (Cys<sup>284</sup>, Cys<sup>330</sup>, and His<sup>331</sup>) and a water molecule, forming a tetrahedral coordination, in the active site (Figure 11B) [72]. Interestingly, the NisC structure from our crystals revealed three Zinc ions in the active site (Figure 43-44). As shown in Figure 44, each  $\text{Zn}^{2+}$  ion is supported by a tetrahedral coordination, respectively. One  $\text{Zn}^{2+}$  ion binds to the earlier mentioned coordinating residues plus one water molecule, reconstituting the earlier

mentioned active site. On the other hand, the middle  $\text{Zn}^{2+}$  is coordinated by the surrounding four water molecules. Furthermore,  $\text{His}^{212}$ , two  $\text{Cl}^-$  ions, and a water molecule support the third  $\text{Zn}^{2+}$ . This three- $\text{Zn}^{2+}$  status was further confirmed through atomic absorption spectroscopy.

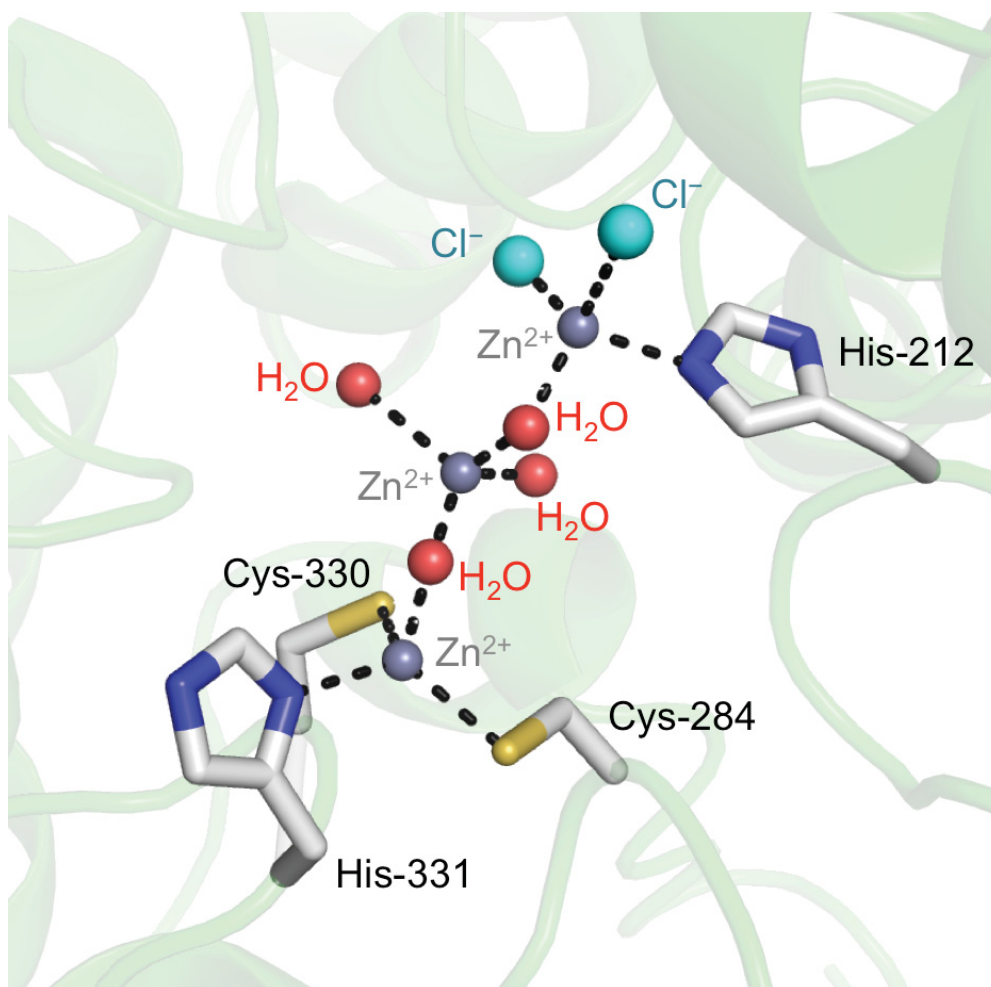


Figure 44. Active site of NisC revealing three  $\text{Zn}^{2+}$  ions. Four amino acids ( $\text{Cys}^{284}$ ,  $\text{Cys}^{330}$ ,  $\text{His}^{331}$ , and  $\text{His}^{212}$ ), as well as four water molecules (red) and two chloride ions (cyan), participate in localizing the three  $\text{Zn}^{2+}$  ions (gray).

#### 4.2.2.5 Crystal packing of NisC

An interesting phenomenon was discovered in the crystal packing of NisC. As shown in the Figure 45, these extra four amino acids (spacer) from the symmetry related molecule extend into a shallow groove, where the active site is located.



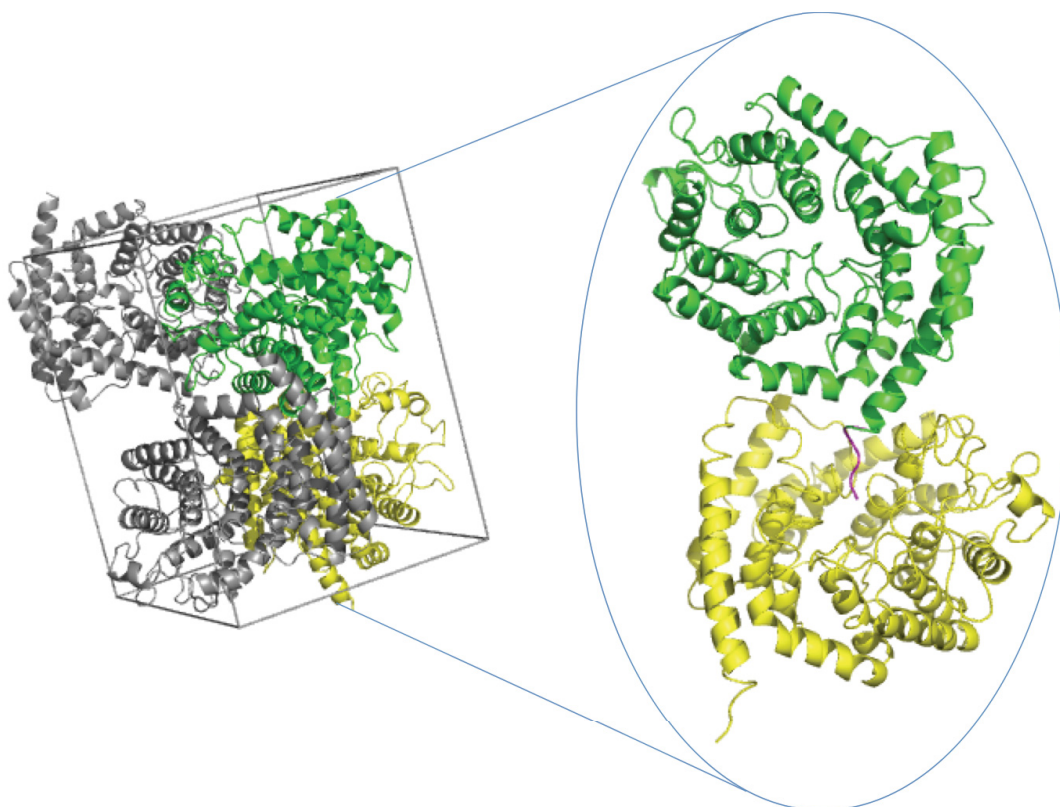


Figure 45. NisC packing in a unit cell. The pattern of NisC symmetry was enlarged to illustrate the crystal packing. The N-terminus of one NisC molecule (colored in magenta) extends into the groove of the symmetry related molecule (colored in yellow), where the prenisin binding site is suspected to be located.

### 4.2.3 Extra $\text{Zn}^{2+}$ ions removal

It was later discovered that two extra Zinc ions can be eliminated by using cobalt affinity column during the first step purification, suggesting they are not innately bound to NisC [28].

#### 4.2.3.1 Crystallization and data processing

NisC purified via the optimized protocol was used for crystallization trial. Initial crystal hits of NisC were obtained from several reservoir conditions at 12 °C. Two hits from two different conditions could be reproduced and optimized via hanging drop diffusion methods at 4 °C, 12 °C and room temperature (Figure 46), respectively. The best diffracting crystals were produced from 0.2 M calcium acetate, 0.1M sodium

cacodylate (pH 6.5), 40% PEG 600 (v/v) at 4 °C, which reached a diffraction of 1.6 Å. It was phased using molecular replacement by using the previously mentioned NisC structure (the one possessing three Zn<sup>2+</sup>) and resulted in a unique solution of monomer. Several rounds of manually model building using COOT and subsequent refinement by PHENIX were performed to establish the full models. Table 2 summarizes all the statistics as well as the final R factors.

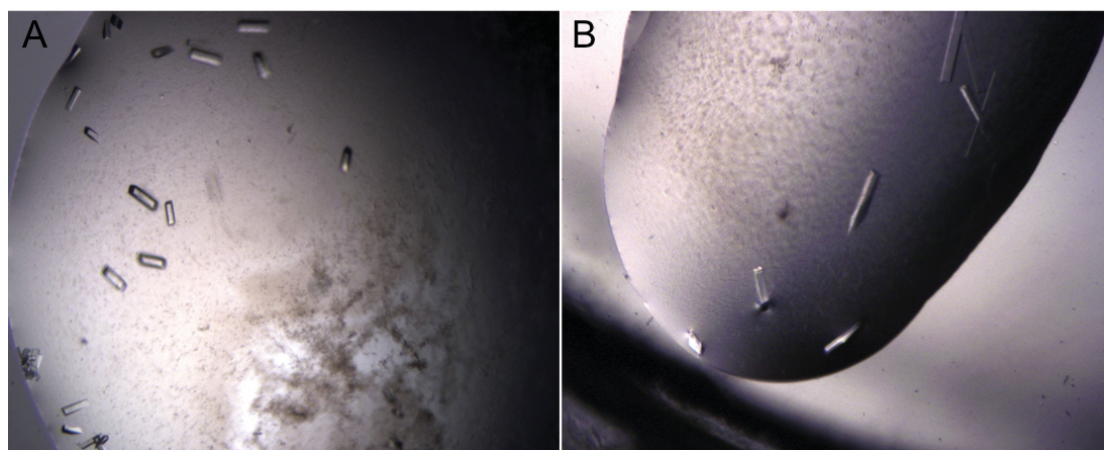


Figure 46. NisC crystals of fine screens derived from two initial crysallization conditions. A) 0.1 M HEPES pH 6.5, 10% (w/v) PEG 6000, final pH 7, 12 mg/ml; 12 °C. B) 0.025 M potassium phosphate, 12% (w/v) PEG 8000, 10% (w/v) MPD; 12 mg/ml, 12 °C.

<b>Resolution range (Å)</b>	48.37 - 1.6 (1.657 - 1.6)
<b>Space group</b>	P 2 <sub>1</sub> 2 <sub>1</sub> 2 <sub>1</sub>
<b>Unit cell (a, b, c in Å; α, β, γ in °)</b>	62.7 76.0 84.6 90.0 90.0 90.0
<b>Unique reflections</b>	53529 (5085)
<b>Completeness (%)</b>	99.11 (95.71)
<b>Mean I/sigma(I)</b>	15.92 (3.65)
<b>Wilson B-factor</b>	24.70
<b>R-work (%)</b>	0.1870 (0.3049)
<b>R-free (%)</b>	0.2073 (0.3204)
<b>Number of protein residues</b>	416
<b>RMS (bonds, Å)</b>	0.007



<b>RMS (angles, °)</b>	1.04
<b>Ramachandran favored (%)</b>	98
<b>Ramachandran outliers (%)</b>	0.24
<b>Clashscore</b>	2.40
<b>Average B-factor</b>	33.80

Table 2. Data collection and refinement statistics for NisC. The table is generated by PHENIX.  $R_{work}$  is a measure of the agreement between the crystallographic model and the experimental X-ray diffraction data and  $R_{free}$  is used to assess possible overfitting of the data.  $R_{work} = \frac{\sum ||F_{obs}| - |F_{calc}||}{\sum |F_{obs}|}$ ,  $R_{free}$  is defined same as  $R_{work}$ , except 5% of the reflections were not included in the refinement for  $R_{free}$  calculations.

#### 4.2.3.2 Overall structure

The new NisC model shows that only one zinc ion was observed (Figure 47), meaning extra zinc ions were successfully removed. All the other structural properties were identical as expected.

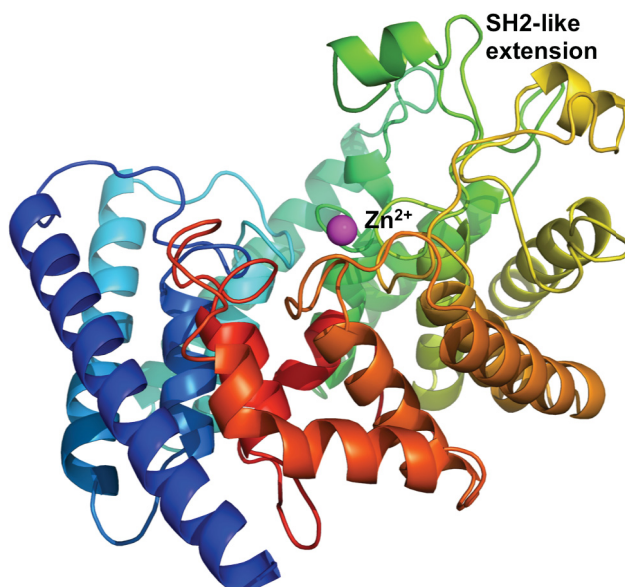


Figure 47. Overall structure of NisC. A two-layer toroid core consists of 14  $\alpha$ -helices. A SH2-like extension is observed adjacent to the  $\alpha$ ,  $\alpha$  barrel. One  $Zn^{2+}$  ion (magenta sphere) is located in the groove of the structure.

### 4.2.3.3 A structure revealing extra density

In the new NisC structure, the most worth-to-notice part is that a bulk of electron density that was observed right next to the zinc ion in the active site (Figure 48). In the published model [72], this bulk of left-over density was assigned to a water molecule. However, in our case, the amount of electron density is obviously overabundant for a water molecule. And given the significant improvement in resolution, we had reason to believe that this part of density is pointing to some other molecule binding to the zinc ion. And the subsequent analysis performed by ligand identification tool from PHENIX [95] suggested it could be a molecule called phosphoenol pyruvate (PEP). It is worth to know is that PEP has a high-energy phosphate group (-62 kJ/mol), which makes PEP a more-suitable co-factor for the reaction activation than water molecule [100].

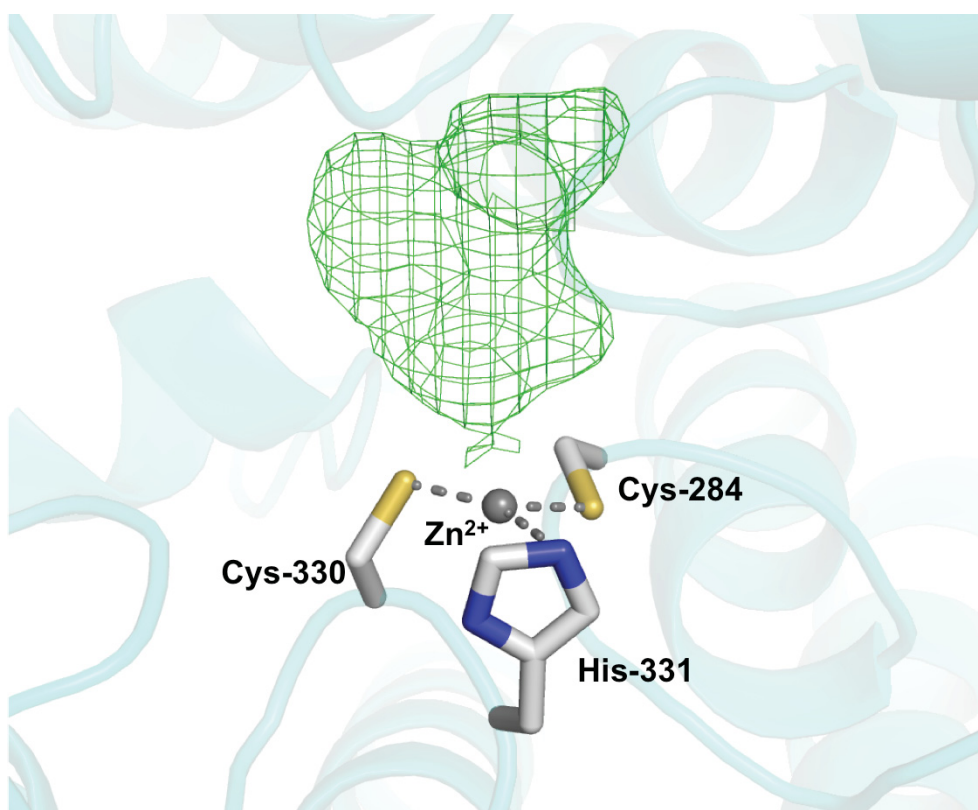


Figure 48. NisC model revealing extra density. A 1FoFc difference map for the extra density, contoured at 3.0 sigma, is located next to the Zinc site.

## 4.2.4 PEP binding to NisC

### 4.2.4.1 Co-crystallization of NisC in complex with PEP

To confirm if PEP is truly the cofactor binding to the zinc ion of the active site of NisC, two crystallization methods were performed. One was to use the same reservoir condition for single NisC crystal for co-crystallizing NisC with PEP, by incubating NisC with 10 mM PEP prior to setting up crystallization. Crystals were obtained, however with a smaller size as shown in Figure 49. The other method was to co-crystallize NisC with PEP, by pre-incubating NisC with 10mM PEP as well. Several crystal hits were observed from different conditions, but none of them were identical with the conditions of single NisC crystals, suggesting a different property of this batch of the crystals. During the crystal fishing, the crystals were found to be more delicate and fragile, compared to the crystals of NisC. Later, it turned out the condition of 0.1M CHES (pH 9.5), 30% (w/v) PEG 3000 produced the best-diffracting crystal, which achieved a resolution of 1.0 Å at the synchrotron.

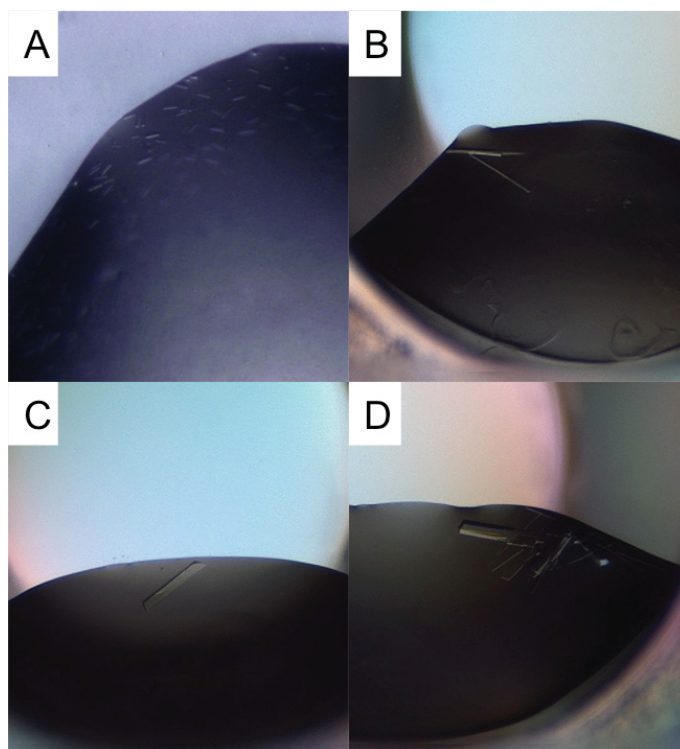


Figure 49. Crystals of NisC-PEP obtained from A) Same reservoir condition as single NisC, 10mM PEP, 16 mg/ml NisC; B) 20% (w/v) PEG 3350, 0.2M magnesium

acetate, 10 mM PEP, 16 mg/ml NisC); C) 0.1M CHES (pH 9.5), 30% (w/v) PEG 3000, 10mM PEP, 16 mg/ml NisC; D) 0.2 M magnesium chloride, 0.1 M TRIS pH 8.5, 30% (w/v) PEG 4000, 10mM PEP, 16mg/ml NisC.

#### 4.2.4.2 Data collection and processing

The dataset obtained for NisC-PEP crystals was phased using molecular replacement and resulted in a unique solution for a monomer. The earlier refined NisC model was used to phase the NisC-PEP data set. Upon the analysis of the data set, the unit cell and space group were identical with that of single NisC. Several rounds of manual model building using COOT and subsequent refinement by PHENIX were performed to establish the full models. For the dataset of NisC-PEP, the resolution limit was adjusted to 1.6 Å during refinement according to the values of data completeness and I/SIGMA. The data statistics as well as the final R factors for both of the structures are listed in Table 3.

<b>Resolution range (Å)</b>	37.12 - 1.6 (1.657 - 1.6)
<b>Space group</b>	P 2 <sub>1</sub> 2 <sub>1</sub> 2 <sub>1</sub>
<b>Unit cell (a, b, c in Å; <math>\alpha</math>, <math>\beta</math>, <math>\gamma</math> in °)</b>	62.5, 76.4, 84.9; 90.0, 90.0, 90.0
<b>Unique reflections</b>	53684 (5217)
<b>Completeness (%)</b>	98.62 (97.48)
<b>Mean I/sigma(I)</b>	13.02 (3.75)
<b>Wilson B-factor</b>	7.88
<b>R-work (%)</b>	0.1617 (0.1929)
<b>R-free (%)</b>	0.1908 (0.2177)
<b>Number of protein residues</b>	418
<b>RMS(bonds, Å)</b>	0.014
<b>RMS(angles, °)</b>	1.36
<b>Ramachandran favored (%)</b>	99
<b>Ramachandran outliers (%)</b>	0.23
<b>Clashscore</b>	3.81
<b>Average B-factor</b>	12.80

Table 3. Processing and refinement statistics for NisC in complex with PEP. The table is generated by PHENIX. Statistics for the highest-resolution shell are shown in parentheses.  $R_{work}$  is a measure of the agreement between the crystallographic model and the experimental X-ray diffraction data and  $R_{free}$  is used to assess possible overfitting of the data.  $R_{work} = \frac{\sum ||F_{obs}| - |F_{calc}||}{\sum |F_{obs}|}$ ,  $R_{free}$  is defined same as  $R_{work}$ , except 5% of the reflections were not included in the refinement for  $R_{free}$  calculations.

#### 4.2.4.3 PEP binding site

In the electron density map of the NisC / PEP co-crystal, as expected, the previously mentioned left-over density was still remaining, even possessing a sharper shape. Especially, the part of density close to the zinc ion was clearly pointing to a phosphate group. PEP molecule was added manually in coot according to the density, followed several times of alternative refinement by PHENIX and manual adjustment by coot. In the end, the final model was achieved with PEP a certain orientation as shown in Figure 49. More precisely, the phosphate group is interacting directly with the bound zinc ion, whereas the carboxyl group is pointing to the opposite side and, due to the reason of crystal packing, contacting with the N-terminal of the symmetry NisC molecule. Furthermore, by comparing with the earlier published NisC model, PEP, in here, is coordinating the zinc ion instead of water molecule in the active site (Figure 50), completing the tetrahedral coordination geometry with three other residues mentioned before. Based on the proximity of His<sup>212</sup> to PEP, it is possibly interacting with PEP, as well, in order to position the PEP molecule in the active site. Besides, we also believe PEP is possessing a certain level of flexibility, because the fixed position of PEP caused a relatively high clashes score in coot, suggesting a too close distance from PEP to His<sup>212</sup>, plus the first residues of the N-terminus are, in general, not visible, in which case, it would broaden the options about how PEP can be arranged (excluding the phosphate group). Based on the previously proposed mechanism, the high-energy phosphate group of PEP can work as an active site base to perform the deprotonation on the sulfur of Cysteine residue in nisin precursor, in which case it would possibly accelerate the reaction. [72]

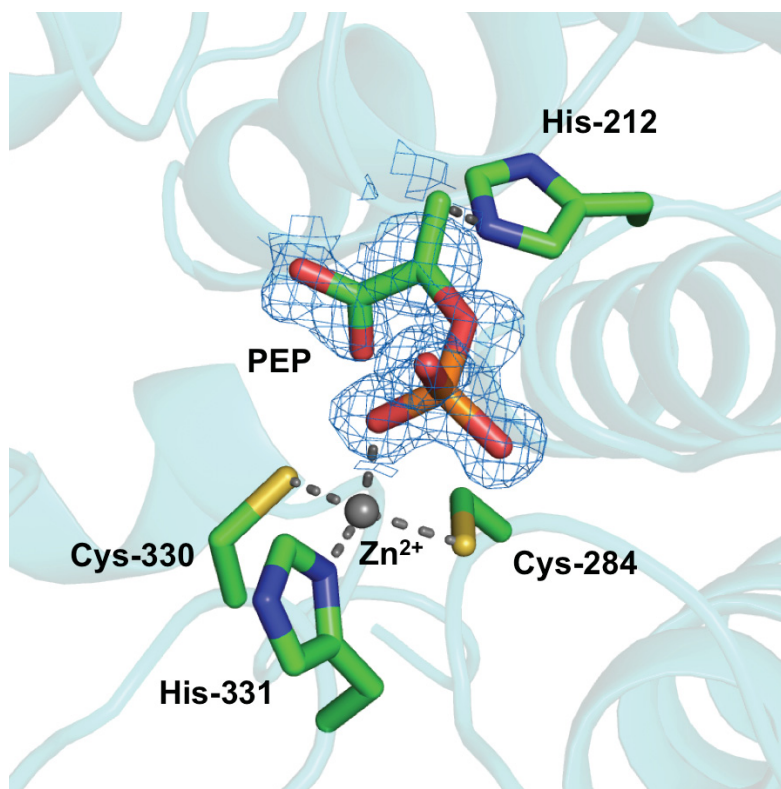


Figure 50. PEP binding site in NisC. The phosphate group of PEP participates in coordinating the Zn<sup>2+</sup> ion. His<sup>212</sup> plays a role in positioning PEP. A 2FoFc difference map (blue mesh), contoured at 1.0 sigma, is shown around PEP molecule.

#### 4.2.4.4 Binding property of NisC to PEP

Isothermal titration calorimetry (ITC) was applied to investigate the interaction between NisC and PEP. Here, the syringe was filled with a concentrated NisC solution (400  $\mu$ M), and the measuring cell was filled with the corresponding PEP solution (40  $\mu$ M). Here, the classic ITC setup was inverted, because the substance in the syringe is required to be prepared in the high concentration and the solubility of precursor peptides are not high enough to reach the requirement. During the measurement, NisC was gradually injected to the PEP containing measuring cell and the heat produced from each injection would be detected. In Figure 51, a preliminary curve was observed, suggesting binding of NisC to PEP. However, the curve was incomplete due to the reason that the concentration of NisC was not high enough to saturate PEP or PEP concentration was miscalculated, making it impossible to evaluate the  $K_D$  value. Moreover, several unusual signals were detected that might be caused by the presence of bubbles in the cell or a dirty cell.

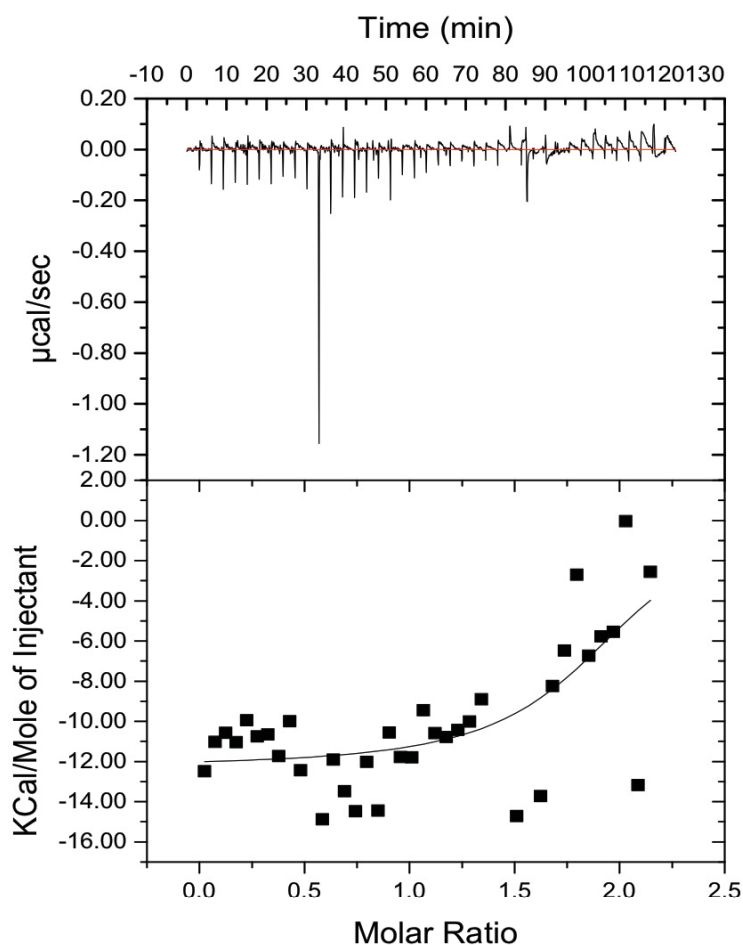


Figure 51. ITC for NisC titrating to PEP. The experiment was performed at room temperature. The points calculated from unreasonably high heat were removed manually.

## 4.2.5 Crystallization of NisC in complex with NisA

### 4.2.5.1 Expression of prenisin (NisA) in *L. lactis*

Dehydrated prenisin was expressed and purified by the protocol described in Materials and Methods. Since prenisin was secreted into the media during expression, supernatant would be the target to collect after centrifugation in this case. The concentration of prenisin was determined via RP-HPLC at 205 nm due to the fact that there is not aromatic amino acid present in prenisin molecule. In the chromatogram of



Figure 52, the peak eluted between 16-20 mins was assigned to be prenisin and the concentration was calculated based on the peak area.

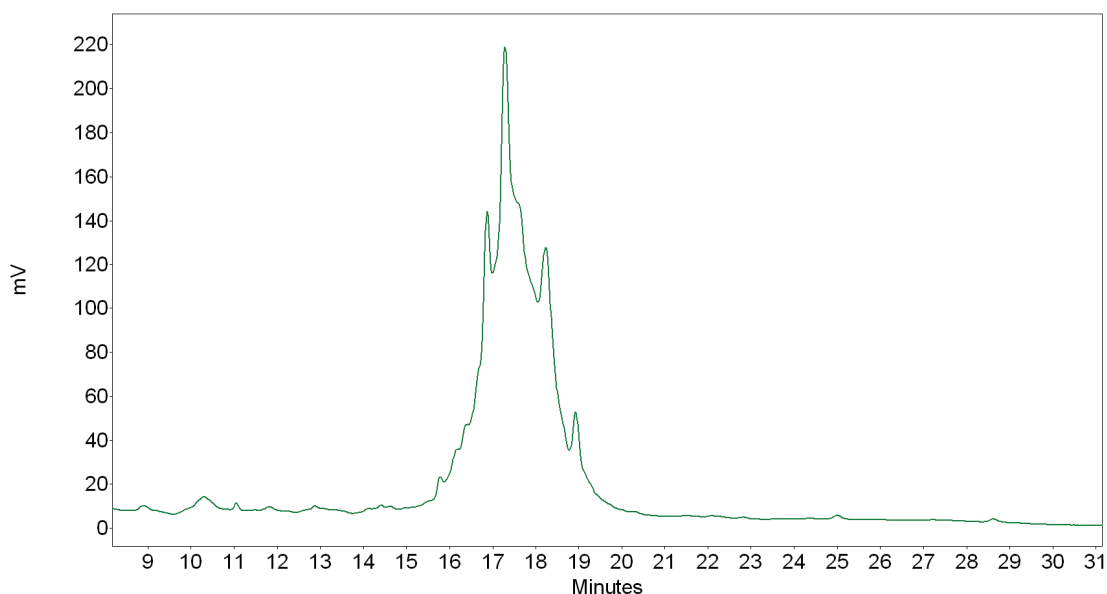


Figure 52. RP-HPLC of prenisin purification. The peak eluted between 16-20 mins was assigned to dehydrated prenisin.

#### **4.2.5.2 MALS-SEC analysis of AC complex formation and its stability**

The formation of AC complex was verified through Multiangle Light Sattering (MALS). By connecting MALC to SEC, it is possible to determine the molecular mass for each peak eluted by SEC. Having a prenisin molecule (NisA) binding to NisC (known as the AC complex) would result in a change of molecular mass. As shown in Figure 53, after incubating prenisin with NisC, the molecular mass was detected to be  $54.3 \pm 0.434$  kDa, which equals to a mass summation of NisC (48.5 kDa) and NisA (6 kDa) within the range of experimental errors.



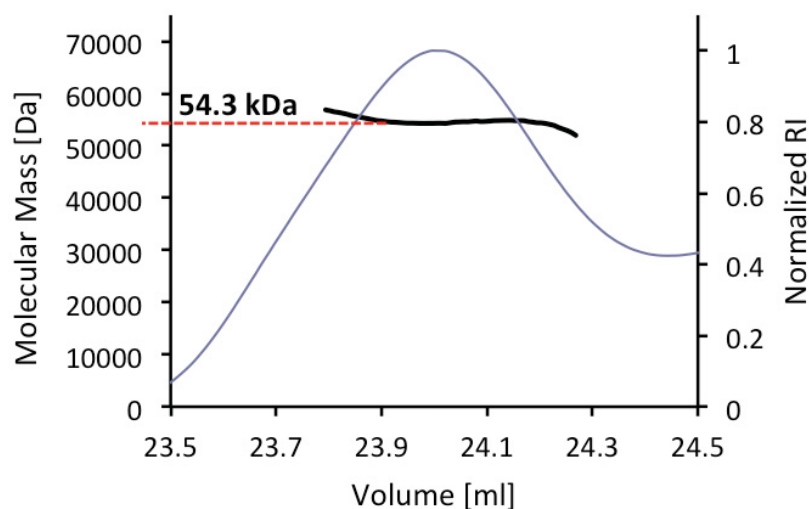


Figure 53. MALS-SEC of the AC complex. The position of the red dashed line indicates the detected molecular mass of NisC in complex with dehydrated prenisin.

Now that AC complex was successfully formed, and isolated, it is crucial to obtain a complex possessing long-term stability to crystallize a protein complex. In this case, the stability of the AC complex was studied through SEC combining SDS-PAGE and Western blot analysis. The freshly prepared AC complex was first purified with SEC and its presence was confirmed by the following SDS-PAGE and Western blot, the corresponding results of which were shown in Figure 54. The red arrow highlights the peak of the AC complex and the corresponding fractions were pooled and kept at 4 °C. After 24 hours, the previously collected AC complex fraction was re-injected to SEC column and the resulting peak was again verified to be the AC complex via SDS-PAGE and Western blot (Figure 55). The resulting fraction was again collected, re-injected and verified by following exactly the same protocol after 5 days, demonstrating the existence of AC complex in a time frame of least 5 days (data not shown).

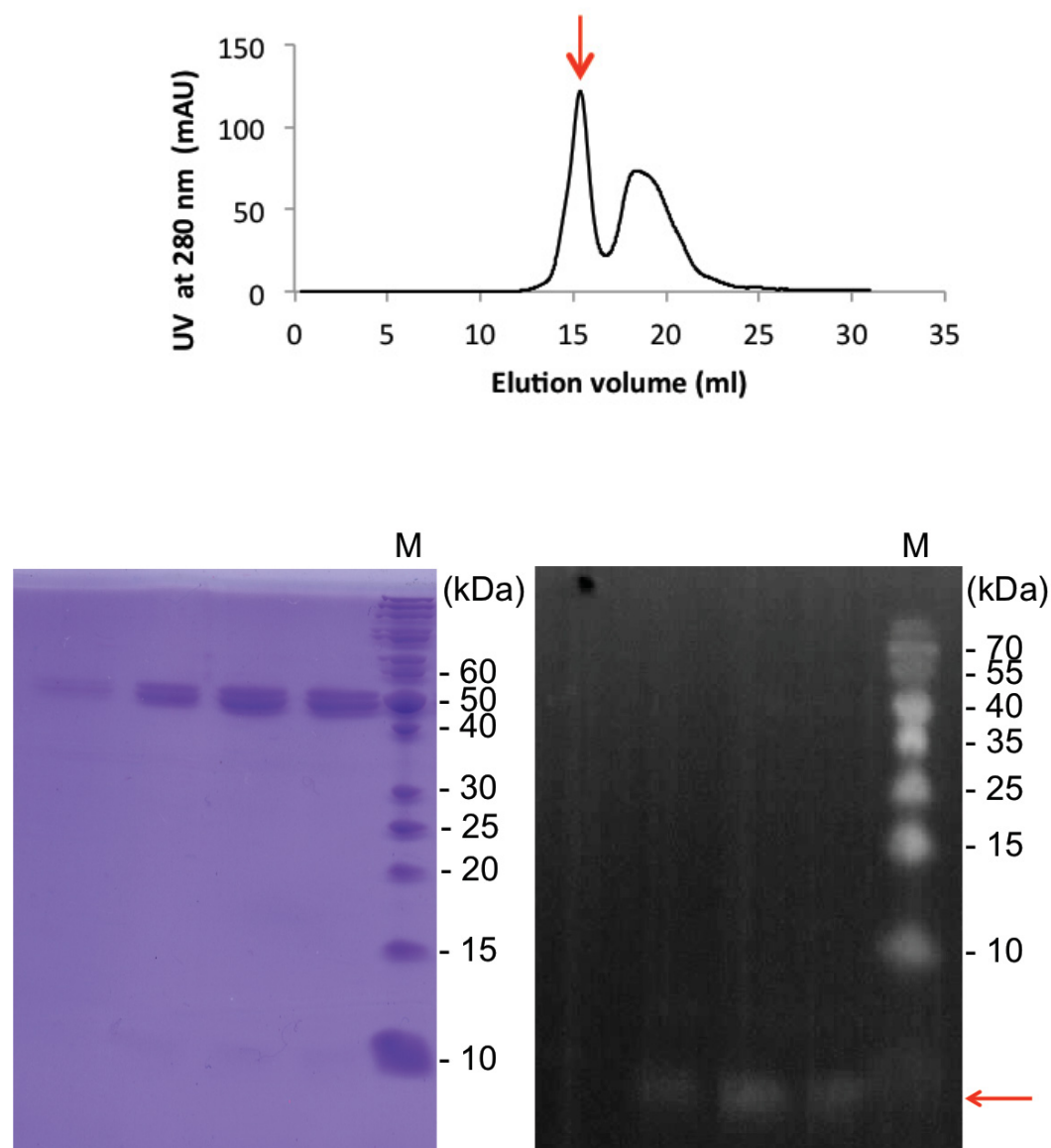


Figure 54. Detection of AC complex formation right after setting up the complex. Upper panel: SEC of AC complex right after the complex setting-up. The peak of AC complex is indicated by the red arrow. Lower panel: The corresponding Coomassie stained SDS-PAGE and Western blot of the AC complex. The red arrow points to the location of prenisin bands.

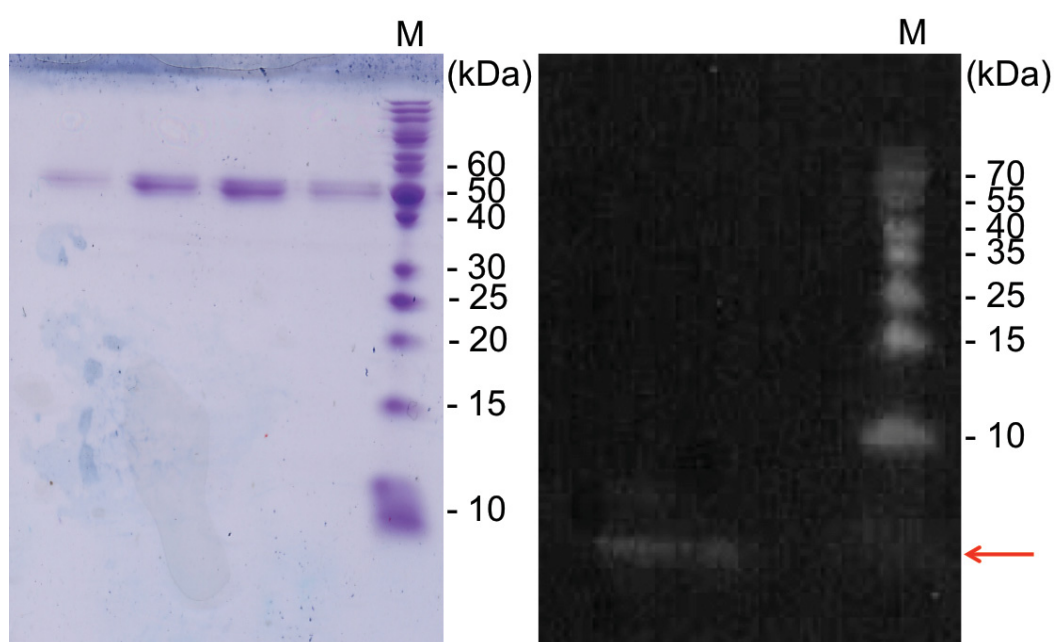
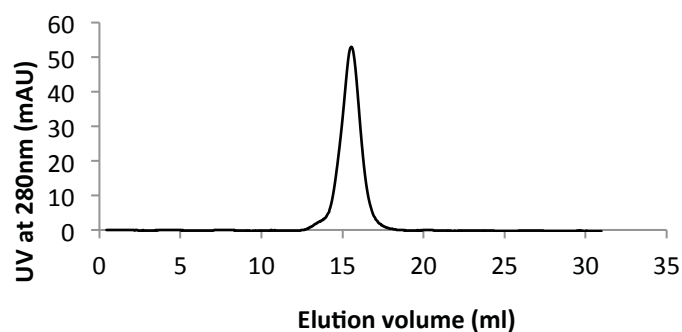


Figure 55. Detection of the AC complex after 24 hrs Upper panel: SEC of AC complex reinjection after 24 hrs. Lower panel: The corresponding SDS-PAGE and Western blot for AC complex.

#### 4.2.5.3 Crystallization of AC complex using the NisC construct with the four amino acid spacer

NisC with the four amino acid spacer was firstly used to perform AC complex co-crystallization trials, by pre-incubating NisC with NisA in molar ratios of 10: 1 and 2: 1, respectively. Unfortunately, no promising hits were observed from all the commercial initial screenings that had been tried.

On the other hand, leader peptide was used, instead of full length NisA, for crystallization trial of AC complex. The protocol for setting up the complex was the same except substituting the leader peptide for NisA. Both initial screening and fine screening, using the two reservoir conditions from which single NisC was crystallized, were performed. Crystals were obtained from the fine screen with a ratio of 1: 1 (Figure 56). However, the subsequent data collection and processing indicated there was no leader peptide present in the crystal, meaning no complex formation.

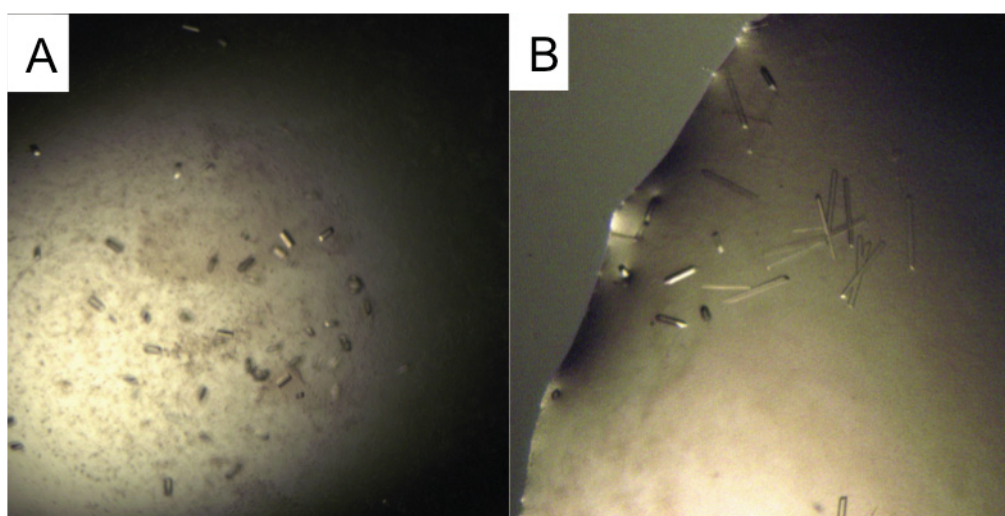


Figure 56. Crystals obtained from the fine screening of co-crystallization of NisC with the four amino acid spacer with leader peptide based on the original initial screening condition: A) 0.025 M potassium phosphate, 12% (w/v) PEG 8000, 10% (w/v) MPD; 12 mg/ml NisC; 12 °C; B) 0.2 M calcium acetate, 0.1 M sodium cacodylate pH6.5, 40% (v/v) PEG 600; 12 mg/ml NisC; 12 °C.

Later on, soaking of NisC crystal with prenisin was performed by adding prenisin stock solution to the drop to reach a final molar ratio of 10: 1 (NisA: NisC). After overnight incubation at 4 °C, compared with the original shape of NisC crystals, the shape of the crystals had changed (Figure 57). And crystals turned out to be quite difficult to mount in loops as well as it was very easy to physically harm the crystals. However, diffraction analysis indicated that the crystals did not diffract X-rays anymore.

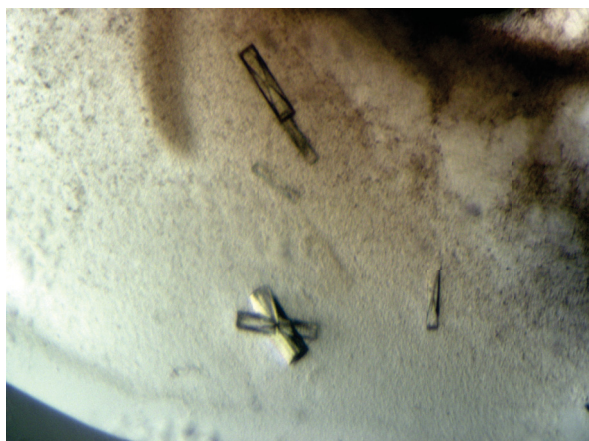


Figure 57. NisC soaking with leader peptide from the fine screening using the reservoir condition of 0.2 M calcium acetate, 0.1 M sodium cacodylate pH 6.5, 40% (v/v) PEG 600; 12 mg/ml NisC; 12 °C.

#### **4.2.5.4 AC complex crystallization using the NisC construct without spacer**

The idea of creating a NisC construct without the spacer appeared after analyzing the crystal packing of the structure of NisC containing a four amino acid spacer at the N-terminus (Figure 46). The spacer occupied the position where prenisin was suggested to bind [72], in which way, prenisin could be blocked from binding to the protein within the crystal due to lack of space, explaining why the crystal of NisC in complex with NisA was so difficult to obtain. Therefore, a new construct, spacer-less NisC, was prepared and the corresponding protein was obtained for a new set of crystallization trials, but no crystals were observed. This actually supports the hypothesis that this spacer takes an important role in the crystal formation process by strengthen the interactions within the crystal (“crystal packing”).

Both trials for co-crystallization and NisC protein crystallization for soaking were performed with a series of reservoir conditions, no promising hits, however, were observed.

#### **4.2.5.5 AC complex crystallization using NisC H331A**

It was speculated that reason why AC complex cannot be achieved is due to the limited stability of AC complex. To solve this issue, an AC complex with higher stability was demanded, which can be fulfilled by replacing NisC with its point mutation construct, NisC H331A [73, 101]. Several crystallization trials with NisC H331A were performed, and yet no crystals were observed.

#### **4.2.6 The stability of AC complex with PEP adding-in**

It was demonstrated that AC complex can be successfully formed in the absence of PEP. However, since PEP apparently binds to the active site of NisC, the question, whether or not PEP can influence the stability of the AC complex, was brought up. MALS-SEC was therefore used to study the stability of the AC complex. Three samples, NisC control, AC complex in the absence of PEP, and AC complex in the presence of PEP, were prepared from the same batch of protein and injected onto MALS-SEC right after day zero and day four, respectively. First of all, in Figure 58, even though a mismatch of the molecular weight of NisC was observed for this batch (due to the reason that MALS-SEC system contained impurities), a mass difference of 5 kDa (size of prenisin) between NisC and the AC complex (with and without the presence of PEP, respectively) still suggested the successful formation of an AC complex for all three samples. At day zero, if one compares the chromatograms of the AC complex with and without the PEP, a shoulder in the peak of AC complex was observed for both samples, however with PEP present, the peak appeared comparatively more homogeneous. This suggested that the AC complex was initially stabilized in the presence of PEP. Furthermore, by comparing the shoulder size of AC complex at day 0 with that of day 4, a trend of increasing amounts of the shoulder were discovered, suggesting that the complex becomes unstable over time. However, for the complex in the presence of PEP, the shoulder was found to be very small even after four days, supporting the hypothesis that PEP takes a roll in stabilizing the AC complex.

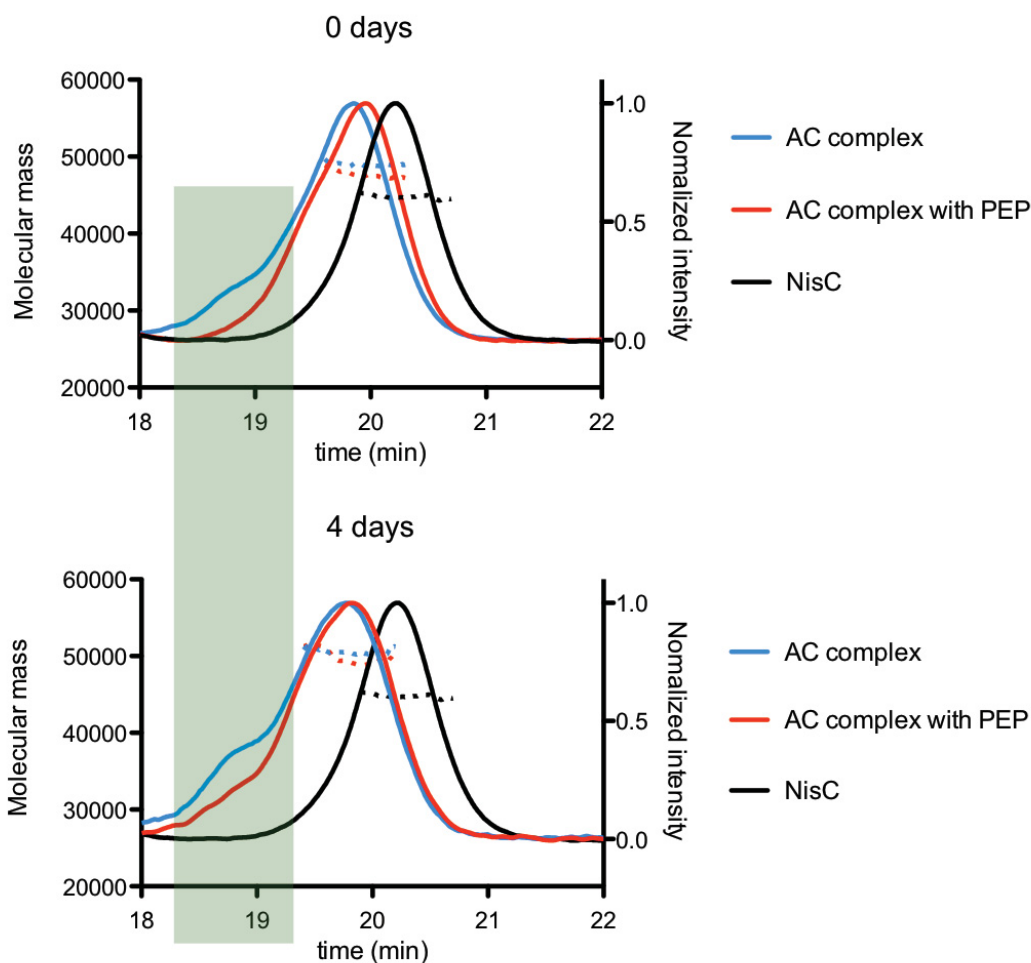


Figure 58. MALS-SEC of 1) NisC; 2) AC complexes in the absence of PEP; 3) AC complex in the presence of PEP at day 0 and day 4, respectively. Blue line: SEC for AC complex; blue dash line: detected molecular mass of AC complex. Red line: SEC of AC complex with PEP; red dash line: detected molecular mass of AC complex with PEP. Black line: SEC of NisC; black dash line: detected molecular mass of NisC.

## 5. Discussion

### 5.1 NisR

Although the NisR/NisK regulated NICE system has been used as an expression system for a long time [70], the structural information of NisR, as well as its *in vitro* activity, is still missing, hindering a thorough understanding of the molecular mechanism of NisR. On the other hand, the structure of NsrR, a response regulator



from the lantibiotic resistance strain, *Streptococcus agalactiae*, had been reported, revealing a typical helix-turn-helix motif [99]. Despite the fact that NisR and NsrR only share a sequence identity of 33% [102], they both belong to the OmpR/PhoB subfamily of response regulators [103, 104]. Thus, similar properties between these two proteins can be expected. A detailed comparison between these two proteins is provided in Table 4

	NisR	NsrR
<b>Sequence length</b>	229 aa	222 aa
<b>Molecular weight</b>	26.7 kDa	25.4 kDa
<b>Solubility</b>	Soluble	Soluble
<b>Family</b>	OmpR/PhoB	OmpR/PhoB
<b>Function</b>	To activate the transcription of genes within nisin operon	Not determined
<b>Binding property</b>	Binding to <i>nisA</i> and <i>nisF</i> promoter	Not determined
<b>Featured motif</b>	Not determined	Helix-turn-helix
<b>Important residues</b>	Not determined	Asp55, Ser82, Phe101, Lys104, Asp188
<b>Structure determined</b>	Not determined	X-ray crystallography

Table 4. Comparison between NisR and NsrR [99].

A homology model of NisR was built using NsrR as a template (Figure 59). The model is comprised by N-terminal receiver domain and C-terminal effector domain. The structure of NisR reveals a similar winged helix-turn-helix (wHTH) motif in effector domain (ED), which is the characteristic feature of OmpR/PhoB subfamily of RRs and responsible for DNA binding [99, 104]. Furthermore, the  $\alpha 7$ -loop- $\alpha 8$  region (labeled in Figure 59) in NisR builds up the helix-turn-helix motif and the helix of  $\alpha 8$  is expected to be the “recognition helix” for DNA binding, according to general feature of RRs [99, 104]. In NsrR, four positively charged residues, Arg198, Arg200, Lys201, and Lys202, are suggested to potentially interact with DNA. In comparison, Arg206 and Lys208 in helix  $\alpha 8$  of NisR model are highly conserved in RRs family and, as a result, might be important for DNA binding. In conclusion,



despite a small sequence identity of 33%, similar features, such as DNA-binding sites, might be still shared between NsrR and NisR.

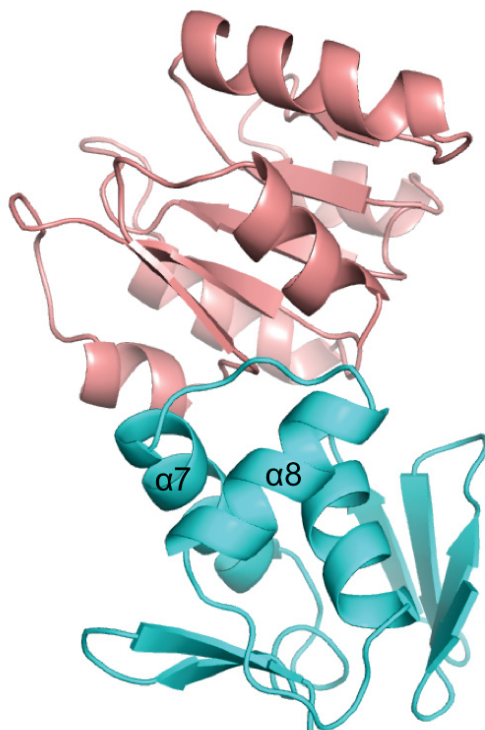


Figure 59. Homology model of NisR. The model is composed of two domains: the N-terminal receiver domain (colored in salmon) and C-terminal DNA-binding effector domain (colored in cyan).

### 5.1.1 NisR with N-terminal His-tag

The N-terminal His-tagged NisR purification at pH 11 was, at the beginning, well established, producing a homogenous species, which was shown to be a monomer through MALS. (Figure 26). However, given the fact that no crystal hits were obtained at pH 11, a pH screening was carried out to explore another potential pH for NisR. Due to the reason that protein would normally crystallize in its most native condition, three physiologically favored pHs were tested through native blue PAGE, as well as two salt concentration. As shown in the Figure 60, NisR at pH 9 with a salt concentration of 50 mM seems to be a suitable candidate, the feasibility of which was confirmed by the earlier mentioned SEC chromatogram (Figure 28).

The crystal hit obtained at pH 9 (Figure 35) with the first batch of purified protein furthermore suggested that this pH could be the suitable pH for NisR crystallization. However, the low reproducibility of the crystal hit might be due to the fact the SEC chromatogram from the first purification could not be reproduced, indicating the purification condition is still up for optimization and overnight dialysis against pH 9 buffer might not be the proper solution.

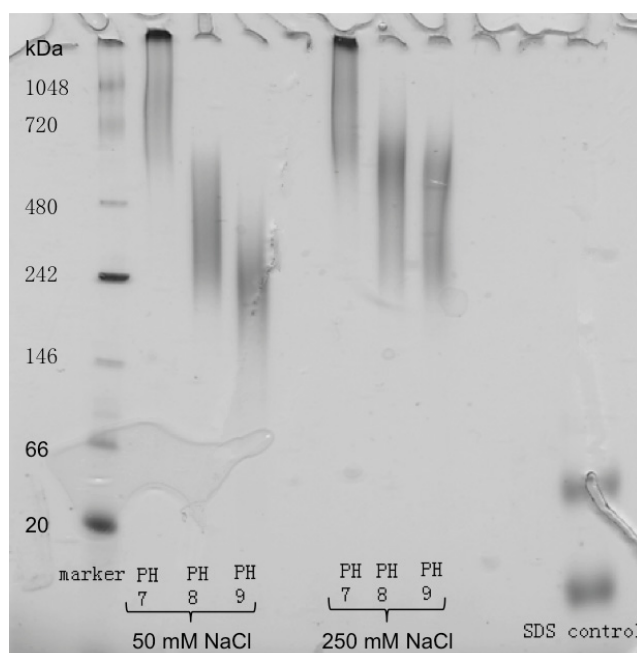


Figure 60. pH screening of NisR by blue native PAGE in a pH range of 7-9 at two different salt concentrations (50mM and 250mM NaCl). As pH decreases, NisR tends to form a higher degree oligomer. And at pH 9, NisR can stay homogeneous in 50mM NaCl, but not in 250 mM NaCl.

### 5.1.2 NisR with C-terminal His-tag

On the other hand, given that NsrR was successfully crystallized with a C-terminal His-tagged construct, a NisR construct with C-terminal His-tag was also used. The same phenomenon that protein would undergo inevitable proteolysis was expected and eventually observed [99]. This might be caused by the sensitivity of the linker region based on the observation that all of the cleavages from different RRs happen at this specific region [99, 105]. And given that both of the cleavages from NisR and NsrR can be only observed for the C-terminal His-tagged construct, the possibility

that this specific orientation can be recognized and used to activate some RR-targeting protease cannot be excluded.

Surprisingly, despite the shared degradation phenomenon, this version of NisR was not able to crystallize as NsrR did. And since pH 11 was used for purification, it is possible that this is not the optimal pH for crystallizing NisR. Besides, salt concentration also sometimes decide whether protein can crystalize or not, as it affects the solubility of protein. All in all, finding a buffer suitable is normally considered to be the most crucial step to achieve a successful crystallization [106].

### **5.1.3 Whether or not NisR can bind to its corresponding promoter?**

As mentioned earlier, NisR, as a response regulator protein, is responsible for regulating the transcription of nisin gene cluster through binding to its corresponding promoters upon activation by phosphorylation. This means that the characteristic property of NisR would be its binding ability to the promoter-involved DNA. Its binding affinity was thereby characterized via electrophoretic mobility shift assay (EMSA) as mentioned in Results. The contradiction between assay with the entire plasmid and that with the promoter region might be due to the reason that 20 fold size differences between pNZ-SV plasmid (6015 bps) and pNisA (341 bps), which means the shift of pNisA is not visible because of its tiny size compared to entire plasmid.

Furthermore, the NisR used for binding is not activated by phosphorylation, therefore the binding affinity, if any, would be dramatically lower than the activated version, which would result in only a small amount of binding and a shift even more difficult to detect. And the problem of visualizing small shifts can usually be solved by using radioactive labeling as it is much more sensitive than the standard ethidium bromide staining [107, 108].

## **5.2 AC complex**

As mentioned earlier, nisin is matured from its corresponding precursor (prenisin) by a series of posttranslational modifications. It is suggested that the process of nisin maturation occurs at a membrane-associated synthetase complex, containing the

proteins NisB, NisC, and NisT, however isolating this complex (NisBTC) has been proven to be very difficult [62, 101]. Yet, the assembly of the NisBC complex in the presence of the substrate was successfully achieved *in vitro*, which consists of a NisB dimer, a monomer of NisC and one prenisin molecule [74]. Furthermore, NisC in complex with NisA, as a much simpler system, was easily obtained and the binding properties were thoroughly studied.

Although NisC structure had already been published in 2006, the detailed information about how NisC interacts with its substrate NisA, which is quite important for peptides engineering studies, stays unknown. Until now, the only discovered detail is the highly conserved FNLD box on the leader peptide of prenisin is essential for NisC binding. To solve this puzzle, the most straightforward way would be obtaining the structural information of NisC in complex with NisA or NisC in complex with the leader peptide.

### **5.2.1 Formation of AC complex**

To ensure a successful AC complex formation, a ratio of 10: 1 (NisA: NisC) was demonstrated to be necessary. Insufficient amount of NisA would lead to the failure of AC complex formation, which might due to the reason that the  $K_D$  of the AC complex is, in the micromolar range, not considered strong enough compared to the nanomolar binding, and, in this case, excess amount of NisA is required to push the equilibrium to the other side.

### **5.2.2 Crystallization**

In general, there are two methods for protein complex crystallization: co-crystallization and soaking. In our case, both of these methods were performed with the goal to achieve crystals of AC complex.

As mentioned in the results, three types NisC constructs were used for co-crystallization. Crystal hits of NisC with leader peptide were obtained at the beginning for the NisC with spacer construct, however it was later discovered that no leader peptide was present in the crystals. The reason might be that the ratio used for crystallization was only 1: 1, which was not sufficient for complex formation.

Although given the concentration required for crystallization trial (minimum 5mg/ml), preparing leader peptide, which possesses a pI of 5, solution with a higher concentration at pH 7 was impossible. The non-spacer NisC construct was later used to substitute for NisC with spacer with a goal to prevent the active site from being blocked by the extra N-terminal amino acids. (Figure 59) Nevertheless, the continued failure of obtaining crystals of the AC complex led to the hypothesis that a mutated construct that is able to provide a NisC version lacking activity but still possessing the binding property would solve the problem as inactivated NisC will not release NisA and stay bound for longer time. The H331A mutation, capable of stabilizing the complex while losing the enzyme activity [73, 101], was considered to be an appropriate candidate, yet no promising crystal hits were observed from this version. In addition, since it was suggested that PEP is playing a role in stabilizing the AC complex, it is worth to try AC complex set-up with PEP adding-in for the crystallization trial.

On the other hand, crystals soaked with the leader peptide did not diffract. The failure was not surprising as soaking a large sized molecule such as a peptide of 23 amino acids normally means taking the high risk of cracking the original crystal. An alternative way would be to apply a shorter peptide, such as FNLD box to avoid the cracking problem.

### **5.2.3 Is AC complex stable enough?**

As a rule of thumb for protein complex crystallization, achieving a complex with long-term stability is essential. And all the above mentioned crystallization problems are clearly expressing a sign of AC complex not being stable enough. Therefore, a lot of effort was and still needs to be spent on studies of complex stability. The original version of AC complex (by using the NisC with spacer) was testified to be stable for at least 24 hours and still existed after 5 days, however the percentage of existence was not able to be quantified through regular SEC along with SDS-PAGE and Western blot. MALS-SEC would be an alternative method for complex stability study that is considered more accurate because of the high sensitivity of MALS. Especially for the NisC-H331A, although it has been reported the binding affinity was not

affected, the question regarding the stability of the complex has not been answered yet.

### **5.3 NisC with PEP**

It was proposed that a Lewis base is required in the deprotonation step and a ligand would be the best candidate for this purpose[72]. Although the discovery of PEP present in NisC structure is rather an accident at the beginning, it was later confirmed through co-crystallization.

#### **5.3.1 Crystallization**

The co-crystallization of NisC with PEP was at the beginning co-crystallized in a ratio of 1: 2 as using the same reservoir condition as single NisC. The electron density obtained from the achieved crystal was clearly showing some molecule is binding within the active site of NisC, however the calculated difference map was not of sufficient quality to confirm the molecule as PEP. In order to improve the sharpness of the density, 10-fold molar excess of PEP was added to the drop consisting NisC-PEP crystal, the resulting difference map obtained turned out to be much more clear and the residual density was assigned to be PEP. And the later newly obtained reservoir condition from co-crystallization trial implies a different crystal composition. The diffraction resolution from this new condition was a significant improvement (from 2.0 Å to 1.0 Å), suggesting a better crystal quality having NisC complexed with PEP.

#### **5.3.2 Why is PEP surely in the structure?**

As mentioned in the results, after the removal of two extra  $\text{Zn}^{2+}$ , the remaining unassigned density (Figure 49) is impossible to be a water molecule considering the size of the density. And the reason why it was initially assigned to be a water molecule in the published model [72] might be the insufficient resolution achieved (2.5 Å). In this case, the density of the active site, located in the groove of the NisC, might not be clear enough. This speculation is supported by the fact the N-terminal

residues (residues 1-6) was missing from the published model of NisC. By comparison, our NisC model achieved a resolution of 1.6 Å and, consequently, the assumption of having PEP binding to the active site, rather than water molecule, is highly plausible.

Furthermore, the previously published NisC structure reveals a tetrahedral Zinc coordination (Figure 11B). And a mechanism of NisC cyclization was proposed based on the structure, which is an intramolecular Michael-type addition of cysteines onto  $\alpha$ ,  $\beta$ -unsaturated amino acids [109]. It is noteworthy that, for this type of addition, the intrinsic reactivity of thiol (-SH) is  $10^{10}$ -fold less than thiolate ( $-S^-$ ), making deprotonation a necessary activation step at neutral pH [86, 110]. For this, a Lewis base is required, which was suggested to be either water or His<sup>212</sup> based on the NisC structure. However, neither of them can defeat the comparatively strong alkalinity of phosphate moiety of the PEP molecule, and this would make PEP a much more promising base for thiol deprotonation. Furthermore, since, in our structure, PEP is proposed to be anchored by His<sup>212</sup> (Figure 51), the demonstrated necessity of His<sup>212</sup> for NisC activity [28] can be considered as a strong support for the existence of PEP. In this way, His<sup>212</sup> mutation would cause the loss of PEP in the active site, eventually abolishing the activity of NisC.

On the other hand, the fact that PEP possesses a high energy phosphate group provides another possibility of using PEP as an energy donor upon its hydrolysis. Even though the binding pocket for the substrate is considered to be rather shallow, given the size of PEP molecule, having PEP in the active site should not be an obstacle either. Actually, PEP is not the first-time discovered to be involved in the reactions from non-phosphotransferase system. In 1988, The flavinylation of 6-hydroxy-D-nicotine oxidase was demonstrated to be PEP-dependent, where PEP was suggest to act as co-factor supporting the formation of the intermediate [111].

Although from the activity assay of NisC, no evidence shows that PEP is compulsorily required for the lanthionine rings formation, the excess electron density from the difference map of earlier published NisC model (PDB code: 2G02) supports the possibility of existing another molecule other than water. However, the limited resolution of the NisC model (2.5 Å) somehow hindered identification of the additional ligand. Our 1.6 Å model, on the other hand, solved this problem and ruled out the ambiguity, presenting a highly clear left-over density leading to PEP.

Interestingly, NisC-PEP is actually not the first co-crystal structure of a lantibiotic cyclase (or homolog) bound to a ligand. Another structure of LanC-like protein 1 (LanCL1), an eukaryotic lanthionine synthetase homologous to lanthionine cyclase, shows the similarity with our model by having a glutathione (GSH) binding to its zinc ion at the putative active site [112]. Although the effect of GSH for LanCL1 is not clear yet, from the complexed structure, it clearly reveals a participation in the tetrahedral coordination via thiol group binding to Zn ion. (Figure 61). It is similar with PEP participating in zinc coordination via phosphate group in NisC-PEP. Consequently, the observation of having PEP binding to NisC protein is not alone in the whole LanC/LanCL family, suggesting not an accident either.

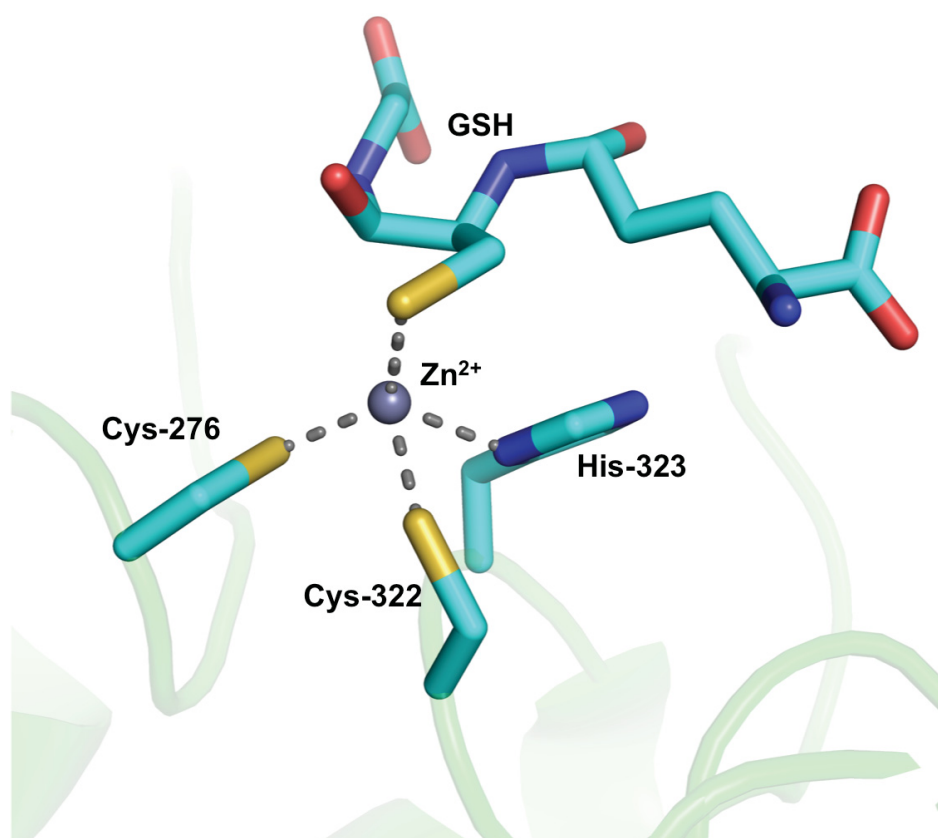


Figure 61. The putative active site of LanCL1. Zn ion was coordinated by GSH, Cys<sup>276</sup>, Cys<sup>322</sup> and His<sup>323</sup> in the tetrahedral geometry.



## 6. Summary

Recombinant NisR was successfully expressed in *E. coli*, purified and proved to be homogeneous at at least two pH values, both pH 9 and pH 11. Furthermore, its binding affinity was verified through EMSA assay, demonstrating the activity of purified NisR. Additionally, a series of crystallization trials were performed on NisR and a crystalline of NisR that illuminated under UV light was obtained at pH 9. Yet, it was not possible to re-produce the crystal.

Secondly, both co-crystallization and soaking were used to obtain the crystal of NisA /NisC complex. For co-crystallization, despite the effect of employing three constructs of NisC, no promising crystals were observed. For soaking, on the other hand, both full length NisA and the leader peptide were used. Crystals with leader peptide present diffracted nicely, nevertheless the data indicates no leader peptide present in the structure. In the meantime, crystals of NisC in complex with PEP were obtained and a data set was collected at the synchrotron. The structure of it revealed a PEP molecule located in the active site of NisC, being anchored by His<sup>212</sup>, and was therefore suggested to be an activating agent for the NisC catalyzed modification reaction.

## 7. Literature

1. Arnison, P.G., et al., *Ribosomally synthesized and post-translationally modified peptide natural products: overview and recommendations for a universal nomenclature*. Nat Prod Rep, 2013. **30**(1): p. 108-60.
2. Duquesne, S., et al., *Microcins, gene-encoded antibacterial peptides from enterobacteria*. Nat Prod Rep, 2007. **24**(4): p. 708-34.
3. Alvarez-Sieiro, P., et al., *Bacteriocins of lactic acid bacteria: extending the family*. Appl Microbiol Biotechnol, 2016. **100**(7): p. 2939-2951.
4. Klaenhammer, T.R., *Genetics of bacteriocins produced by lactic acid bacteria*. FEMS Microbiol Rev, 1993. **12**(1-3): p. 39-85.
5. Klaenhammer, T.R., *Bacteriocins of lactic acid bacteria*. Biochimie, 1988. **70**(3): p. 337-349.

6. Delves-Broughton, J., et al., *Applications of the bacteriocin, nisin*. Antonie Van Leeuwenhoek, 1996. **69**(2): p. 193-202.
7. McIntosh, J.A., M.S. Donia, and E.W. Schmidt, *Ribosomal peptide natural products: bridging the ribosomal and nonribosomal worlds*. Nat Prod Rep, 2009. **26**(4): p. 537.
8. Bosma, T., et al., *Bacterial display and screening of posttranslationally thioether-stabilized peptides*. Appl Environ Microbiol, 2011. **77**(19): p. 6794-801.
9. Yang, X. and W.A. van der Donk, *Ribosomally synthesized and post-translationally modified peptide natural products: new insights into the role of leader and core peptides during biosynthesis*. Chemistry (Easton), 2013. **19**(24): p. 7662-77.
10. Cotter, P.D., C. Hill, and R.P. Ross, *Bacteriocins: developing innate immunity for food*. Nature Reviews Microbiology, 2005. **3**(10): p. 777-788.
11. Jack, R.W., J.R. Tagg, and B. Ray, *Bacteriocins of gram-positive bacteria*. Microbiol Rev, 1995. **59**(2): p. 171-200.
12. Riley, M.A. and J.E. Wertz, *Bacteriocins: evolution, ecology, and application*. Annual Reviews in Microbiology, 2002. **56**(1): p. 117-137.
13. Carr, F.J., D. Chill, and N. Maida, *The lactic acid bacteria: a literature survey*. Crit Rev Microbiol, 2002. **28**(4): p. 281-370.
14. Arnison, P.G., et al., *Ribosomally synthesized and post-translationally modified peptide natural products: overview and recommendations for a universal nomenclature*. Nat Prod Rep, 2013. **30**(1): p. 108-160.
15. Suda, S., et al., *Lacticin 3147-biosynthesis, molecular analysis, immunity, bioengineering and applications*. Current Protein and Peptide Science, 2012. **13**(3): p. 193-204.
16. Willey, J.M. and A.A. Gaskell, *Morphogenetic signaling molecules of the streptomycetes*. Chem Rev, 2010. **111**(1): p. 174-187.
17. Meindl, K., et al., *Labyrinthopeptins: a new class of carbacyclic lantibiotics*. Angew Chem Int Ed, 2010. **49**(6): p. 1151-1154.
18. Goto, Y., et al., *Discovery of unique lanthionine synthetases reveals new mechanistic and evolutionary insights*. PLoS Biol, 2010. **8**(3): p. e1000339.

19. Goto, Y., A.e. Ökesli, and W.A. van der Donk, *Mechanistic studies of Ser/Thr dehydration catalyzed by a member of the LanL lanthionine synthetase family*. Biochemistry, 2011. **50**(5): p. 891-898.
20. Oman, T.J. and W.A. van der Donk, *Follow the leader: the use of leader peptides to guide natural product biosynthesis*. Nat Chem Biol, 2010. **6**(1): p. 9-18.
21. Plat, A., et al., *Requirements of the engineered leader peptide of nisin for inducing modification, export, and cleavage*. Appl Environ Microbiol, 2011. **77**(2): p. 604-611.
22. Neis, S., et al., *Effect of leader peptide mutations on biosynthesis of the lantibiotic Pep5*. FEMS Microbiol Lett, 1997. **149**(2): p. 249-255.
23. Nagao, J.-i., et al., *Mapping and identification of the region and secondary structure required for the maturation of the nukacin ISK-1 prepeptide*. Peptides, 2009. **30**(8): p. 1412-1420.
24. Patton, G.C., et al., *The Importance of the Leader Sequence for Directing Lanthionine Formation in Lacticin 481†*. Biochemistry, 2008. **47**(28): p. 7342-7351.
25. Chen, P., et al., *Effect of amino acid substitutions in conserved residues in the leader peptide on biosynthesis of the lantibiotic mutacin II*. FEMS Microbiol Lett, 2001. **195**(2): p. 139-144.
26. Müller, W.M., et al., *Leader peptide-directed processing of labyrinthopeptin A2 precursor peptide by the modifying enzyme LabKC*. Biochemistry, 2011. **50**(39): p. 8362-8373.
27. Xie, L., et al., *Lacticin 481: in vitro reconstitution of lantibiotic synthetase activity*. Science, 2004. **303**(5658): p. 679-681.
28. Li, B. and W.A. van der Donk, *Identification of essential catalytic residues of the cyclase NisC involved in the biosynthesis of nisin*. J Biol Chem, 2007. **282**(29): p. 21169-75.
29. Mavaro, A., et al., *Substrate recognition and specificity of the NisB protein, the lantibiotic dehydratase involved in nisin biosynthesis*. J Biol Chem, 2011. **286**(35): p. 30552-30560.
30. Furgerson Ihnken, L., C. Chatterjee, and W.A. van der Donk, *In Vitro Reconstitution and Substrate Specificity of a Lantibiotic Protease†*. Biochemistry, 2008. **47**(28): p. 7352-7363.

31. Rogers, L., *The inhibiting effect of Streptococcus lactis on Lactobacillus bulgaricus*. J Bacteriol, 1928. **16**(5): p. 321.
32. Rogers, L. and E. Whittier, *Limiting factors in the lactic fermentation*. J Bacteriol, 1928. **16**(4): p. 211.
33. Brötz, H., et al., *Role of lipid - bound peptidoglycan precursors in the formation of pores by nisin, epidermin and other lantibiotics*. Mol Microbiol, 1998. **30**(2): p. 317-327.
34. Breukink, E., et al., *Use of the cell wall precursor lipid II by a pore-forming peptide antibiotic*. Science, 1999. **286**(5448): p. 2361-2364.
35. Matsuzaki, K., et al., *Translocation of a channel-forming antimicrobial peptide, magainin 2, across lipid bilayers by forming a pore*. Biochemistry, 1995. **34**(19): p. 6521-6526.
36. van Kraaij, C., et al., *Pore formation by nisin involves translocation of its C-terminal part across the membrane*. Biochemistry, 1998. **37**(46): p. 16033-16040.
37. Breukink, E., et al., *Binding of nisin Z to bilayer vesicles as determined with isothermal titration calorimetry*. Biochemistry, 2000. **39**(33): p. 10247-10254.
38. Wiedemann, I., et al., *Specific binding of nisin to the peptidoglycan precursor lipid II combines pore formation and inhibition of cell wall biosynthesis for potent antibiotic activity*. J Biol Chem, 2001. **276**(3): p. 1772-1779.
39. Breukink, E., et al., *The orientation of nisin in membranes*. Biochemistry, 1998. **37**(22): p. 8153-8162.
40. Sahl, H.-G., M. Kordel, and R. Benz, *Voltage-dependent depolarization of bacterial membranes and artificial lipid bilayers by the peptide antibiotic nisin*. Arch Microbiol, 1987. **149**(2): p. 120-124.
41. van Heusden, H.E., B. de Kruijff, and E. Breukink, *Lipid II induces a transmembrane orientation of the pore-forming peptide lantibiotic nisin*. Biochemistry, 2002. **41**(40): p. 12171-12178.
42. Wiedemann, I., R. Benz, and H.-G. Sahl, *Lipid II-mediated pore formation by the peptide antibiotic nisin: a black lipid membrane study*. J Bacteriol, 2004. **186**(10): p. 3259-3261.

43. Breukink, E., et al., *Lipid II is an intrinsic component of the pore induced by nisin in bacterial membranes*. J Biol Chem, 2003. **278**(22): p. 19898-19903.
44. Bonev, B.B., et al., *Targeting extracellular pyrophosphates underpins the high selectivity of nisin*. The FASEB journal, 2004. **18**(15): p. 1862-1869.
45. Hasper, H.E., B. de Kruijff, and E. Breukink, *Assembly and stability of nisin-lipid II pores*. Biochemistry, 2004. **43**(36): p. 11567-11575.
46. Breukink, E. and B. de Kruijff, *Lipid II as a target for antibiotics*. Nature reviews Drug discovery, 2006. **5**(4): p. 321-323.
47. Hasper, H.E., et al., *An alternative bactericidal mechanism of action for lantibiotic peptides that target lipid II*. Science, 2006. **313**(5793): p. 1636-1637.
48. Nes, I.F., et al., *Biosynthesis of bacteriocins in lactic acid bacteria*. Antonie Van Leeuwenhoek, 1996. **70**(2-4): p. 113-128.
49. De Vos, P., et al., *Transient increase in obese gene expression after food intake or insulin administration*. 1995.
50. Kuipers, O.P., et al., *Autoregulation of nisin biosynthesis in Lactococcus lactis by signal transduction*. J Biol Chem, 1995. **270**(45): p. 27299-27304.
51. Siegers, K. and K. Entian, *Genes involved in immunity to the lantibiotic nisin produced by Lactococcus lactis 6F3*. Appl Environ Microbiol, 1995. **61**(3): p. 1082-1089.
52. Hols, P., et al., *Conversion of Lactococcus lactis from homolactic to homoalanine fermentation through metabolic engineering*. Nat Biotechnol, 1999. **17**(6): p. 588-592.
53. O'Connor, P.M., et al., *Nisin H is a new nisin variant produced by the gut-derived strain Streptococcus hyointestinalis DPC6484*. Appl Environ Microbiol, 2015. **81**(12): p. 3953-3960.
54. De Vuyst, L. and E.J. Vandamme, *Influence of the carbon source on nisin production in Lactococcus lactis subsp. lactis batch fermentations*. Microbiology, 1992. **138**(3): p. 571-578.
55. Parente, E. and A. Ricciardi, *Production, recovery and purification of bacteriocins from lactic acid bacteria*. Appl Microbiol Biotechnol, 1999. **52**(5): p. 628-638.

56. Kleerebezem, M. and L.E. Quadri, *Peptide pheromone-dependent regulation of antimicrobial peptide production in Gram-positive bacteria: a case of multicellular behavior*. *Peptides*, 2001. **22**(10): p. 1579-1596.
57. Cheigh, C.-I., et al., *Influence of growth conditions on the production of a nisin-like bacteriocin by Lactococcus lactis subsp. lactis A164 isolated from kimchi*. *J Biotechnol*, 2002. **95**(3): p. 225-235.
58. Buchman, A., et al., *Two DNA-binding factors recognize specific sequences at silencers, upstream activating sequences, autonomously replicating sequences, and telomeres in Saccharomyces cerevisiae*. *Mol Cell Biol*, 1988. **8**(1): p. 210-225.
59. Engelke, G., et al., *Biosynthesis of the lantibiotic nisin: genomic organization and membrane localization of the NisB protein*. *Appl Environ Microbiol*, 1992. **58**(11): p. 3730-3743.
60. Kuipers, O.P., et al., *Characterization of the nisin gene cluster nisABTCIPR of Lactococcus lactis*. *Eur J Biochem*, 1993. **216**(1): p. 281-291.
61. Van der Meer, J., et al., *Characterization of the Lactococcus lactis nisin A operon genes nisP, encoding a subtilisin-like serine protease involved in precursor processing, and nisR, encoding a regulatory protein involved in nisin biosynthesis*. *J Bacteriol*, 1993. **175**(9): p. 2578-2588.
62. Siegers, K., S. Heinzmann, and K.-D. Entian, *Biosynthesis of Lantibiotic Nisin POSTTRANSLATIONAL MODIFICATION OF ITS PREPEPTIDE OCCURS AT A MULTIMERIC MEMBRANE-ASSOCIATED LANTHIONINE SYNTHETASE COMPLEX*. *J Biol Chem*, 1996. **271**(21): p. 12294-12301.
63. Qiao, M. and P.E. Saris, *Evidence for a role of NisT in transport of the lantibiotic nisin produced by Lactococcus lactis N8*. *FEMS Microbiol Lett*, 1996. **144**(1): p. 89-93.
64. Immonen, T., et al., *The codon usage of the nisZ operon in Lactococcus lactis N8 suggests a non-lactococcal origin of the conjugative nisin-sucrose transposon*. *DNA Seq*, 1995. **5**(4): p. 203-218.
65. Stock, J., A. Ninfa, and A. Stock, *Protein phosphorylation and regulation of adaptive responses in bacteria*. *Microbiol Rev*, 1989. **53**(4): p. 450-490.
66. Abts, A., *The Nisin ABC: investigating the maturation process of the lanthipeptide nisin*. 2014.
67. Abts, A., et al., *NisC binds the FxLx motif of the nisin leader peptide*. *Biochemistry*, 2013. **52**(32): p. 5387-95.

68. Stock, A.M., V.L. Robinson, and P.N. Goudreau, *Two-component signal transduction*. Annu Rev Biochem, 2000. **69**(1): p. 183-215.
69. Kuipers, O.P., et al., *Quorum sensing-controlled gene expression in lactic acid bacteria*. J Biotechnol, 1998. **64**(1): p. 15-21.
70. Mierau, I. and M. Kleerebezem, *10 years of the nisin-controlled gene expression system (NICE) in Lactococcus lactis*. Appl Microbiol Biotechnol, 2005. **68**(6): p. 705-17.
71. Xie, L. and W.A. van der Donk, *Post-translational modifications during lantibiotic biosynthesis*. Curr Opin Chem Biol, 2004. **8**(5): p. 498-507.
72. Li, B., et al., *Structure and mechanism of the lantibiotic cyclase involved in nisin biosynthesis*. Science, 2006. **311**(5766): p. 1464-7.
73. Khusainov, R., et al., *Determining sites of interaction between prenisin and its modification enzymes NisB and NisC*. Mol Microbiol, 2011. **82**(3): p. 706-718.
74. Reiners, J., et al., *Stoichiometry and structure of a lantibiotic maturation complex*. Sci Rep, 2017. **7**.
75. Garg, N., L.M. Salazar-Ocampo, and W.A. van der Donk, *In vitro activity of the nisin dehydratase NisB*. Proceedings of the National Academy of Sciences, 2013. **110**(18): p. 7258-7263.
76. Ortega, M.A., et al., *Structure and mechanism of the tRNA-dependent lantibiotic dehydratase NisB*. Nature, 2015. **517**(7535): p. 509-512.
77. DeLano, W.L., *PyMOL*. 2002.
78. Ösapay, G., et al., *Lanthionine-somatostatin analogs: synthesis, characterization, biological activity, and enzymatic stability studies*. J Med Chem, 1997. **40**(14): p. 2241-2251.
79. Rew, Y., et al., *Synthesis and biological activities of cyclic lanthionine enkephalin analogues:  $\delta$ -opioid receptor selective ligands*. J Med Chem, 2002. **45**(17): p. 3746-3754.
80. de Vries, L., et al., *Oral and pulmonary delivery of thioether-bridged angiotensin-(1-7)*. Peptides, 2010. **31**(5): p. 893-898.
81. Zhu, Y., et al., *Biomimetic studies on the mechanism of stereoselective lanthionine formation*. Org Biomol Chem, 2003. **1**(19): p. 3304-3315.



82. Paul, M. and W.v. Donk, *Chemical and enzymatic synthesis of lanthionines*. Mini Rev Org Chem, 2005. **2**(1): p. 23-37.
83. Kuipers, O.P., et al., *Protein engineering of lantibiotics*. Antonie Van Leeuwenhoek, 1996. **69**(2): p. 161-170.
84. Chatterjee, C., et al., *Engineering dehydro amino acids and thioethers into peptides using lactacin 481 synthetase*. Chem Biol, 2006. **13**(10): p. 1109-1117.
85. Kluskens, L.D., et al., *Post-translational modification of therapeutic peptides by NisB, the dehydratase of the lantibiotic nisin*. Biochemistry, 2005. **44**(38): p. 12827-12834.
86. Li, B. and W.A. van der Donk, *Identification of essential catalytic residues of the cyclase NisC involved in the biosynthesis of nisin*. J Biol Chem, 2007. **282**(29): p. 21169-21175.
87. Chirgadze, D., *Protein crystallisation in action*. University of Cambridge, 2001.
88. TutorVista.com.
89. Klug, H.P. and L.E. Alexander, *X-ray diffraction procedures: for polycrystalline and amorphous materials*. X-Ray Diffraction Procedures: For Polycrystalline and Amorphous Materials, 2nd Edition, by Harold P. Klug, Leroy E. Alexander, pp. 992. ISBN 0-471-49369-4. Wiley-VCH, May 1974., 1974: p. 992.
90. Glusker, J.P., *Protein Crystallization. Techniques, Strategies, and Tips Edited by Terese M. Bergfors. International University Line, 1999. ISBN 0963681753*. 2003, ACS Publications.
91. Rupp, B., *Biomolecular crystallography: principles, practice, and application to structural biology*. 2009: Garland Science.
92. Kabsch, W., *Xds*. Acta Crystallogr D Biol Crystallogr, 2010. **66**(Pt 2): p. 125-32.
93. Read, R. *The phase problem: introduction to phasing methods*. 1999-2009.
94. Emsley, P., et al., *Features and development of Coot*. Acta Crystallogr D Biol Crystallogr, 2010. **66**(Pt 4): p. 486-501.



95. Adams, P.D., et al., *PHENIX: a comprehensive Python-based system for macromolecular structure solution*. Acta Crystallogr D Biol Crystallogr, 2010. **66**(Pt 2): p. 213-21.
96. Winn, M.D., et al., *Overview of the CCP4 suite and current developments*. Acta Crystallogr D Biol Crystallogr, 2011. **67**(Pt 4): p. 235-42.
97. Chen, V.B., et al., *MolProbity: all-atom structure validation for macromolecular crystallography*. Acta Crystallogr D Biol Crystallogr, 2010. **66**(Pt 1): p. 12-21.
98. Delano, W.L., *The PyMOL molecular graphics system*. 2002.
99. Khosa, S., et al., *Structure of the Response Regulator NsrR from Streptococcus agalactiae, Which Is Involved in Lantibiotic Resistance*. PLoS One, 2016. **11**(3): p. e0149903.
100. Berg, J.M., J. Tymoczko, and L. Stryer, *Glycolysis is an energy-conversion pathway in many organisms*. Biochemistry. 5th ed. New York: WH Freeman, 2002.
101. Lubelski, J., R. Khusainov, and O.P. Kuipers, *Directionality and coordination of dehydration and ring formation during biosynthesis of the lantibiotic nisin*. J Biol Chem, 2009. **284**(38): p. 25962-25972.
102. Khosa, S., *Nisin resistance in Streptococcus agalactiae*. 2016, Düsseldorf, Heinrich-Heine-Universität, Diss., 2016.
103. Kleerebezem, M., W. De Vos, and O. Kuipers, *The lantibiotics nisin in subtilin act as extracellular regulators of their own biosynthesis*. 1998.
104. Martínez-Hackert, E. and A.M. Stock, *Structural relationships in the OmpR family of winged-helix transcription factors*. J Mol Biol, 1997. **269**(3): p. 301-312.
105. Okajima, T., et al., *Response regulator YycF essential for bacterial growth: X - ray crystal structure of the DNA - binding domain and its PhoB - like DNA recognition motif*. FEBS Lett, 2008. **582**(23-24): p. 3434-3438.
106. Abts, A., et al., *Rational and irrational approaches to convince a protein to crystallize*. 2012: INTECH Open Access Publisher.
107. Fried, M. and D.M. Crothers, *Equilibria and kinetics of lac repressor-operator interactions by polyacrylamide gel electrophoresis*. Nucleic Acids Res, 1981. **9**(23): p. 6505-6525.

108. Garner, M.M. and A. Revzin, *A gel electrophoresis method for quantifying the binding of proteins to specific DNA regions: application to components of the Escherichia coli lactose operon regulatory system*. Nucleic Acids Res, 1981. **9**(13): p. 3047-3060.
109. Xie, L. and W.A. van der Donk, *Post-translational modifications during lantibiotic biosynthesis*. Curr Opin Chem Biol, 2004. **8**(5): p. 498-507.
110. Bednar, R.A., *Reactivity and pH dependence of thiol conjugation to N-ethylmaleimide: detection of a conformational change in chalcone isomerase*. Biochemistry, 1990. **29**(15): p. 3684-3690.
111. NAGURSKY, H., V. BICHLER, and R. BRANDSCH, *Phosphoenolpyruvate - dependent flavinylation of 6 - hydroxy - D - nicotine oxidase*. Eur J Biochem, 1988. **177**(2): p. 319-325.
112. Zhang, W., et al., *Structure of human lanthionine synthetase C-like protein 1 and its interaction with Eps8 and glutathione*. Genes Dev, 2009. **23**(12): p. 1387-92.

## 8. Curriculum vitae

### *Personal Data*

---

Date of Birth            November 29, 1986

Nationality            China

### *Research Experience*

---

**07/2013-present Characterization of Nisin-modifying Cyclase NisC through X-ray Crystallography**, Supervisor: Prof. Dr. Lutz Schmitt and Dr. Sander Smits, Heinrich-Heine-Universität Düsseldorf

**10/2010-5/2013 Characterization of tRNA-modifying MiaE Protein**, Supervisor: Assoc Prof. Dr. Brad Pierce, University of Texas at Arlington

**02/2008-02/2010 PEGylation of Recombinant Interferon- $\alpha$** , Supervisor: Prof. Dr. Jin-Feng Wang, Tianjin University

### *Academic Education*

---

07/2013-present **Ph. D.**, Heinrich-Heine-Universität Düsseldorf, Germany

Major: Biochemistry

08/2010-05/2013 **M. S.**, University of Texas at Arlington, USA

Major: Chemistry

09/2005-07/2009 **B. S.**, Tianjin University (“985-project”, “211-project”), China

Major: Pharmaceutical Science

### *Awards and Scholarships*

---

01/2016 Stipend for “BioStruct-X Mediterranean Macromolecular Crystallography Workshop”

07/2013-10/2016 Doctoral Scholarship of CLIB-Graduate Cluster Industrial Biotechnology

08/2012-05/2013 Graduate Teaching Assistantship, University of Texas at Arlington

08/2010-08/2012 Graduate Research Assistantship, University of Texas at Arlington

09/2007 “the Outstanding Student Leader”, School of Pharmaceutical Science and Technology, Tianjin University

### *Conferences and Symposiums*

---

02/2016 CLIB - Graduate Cluster 7<sup>th</sup> Annual Retreat, Herdecke, Germany

Oral presentation: “Characterization of Nisin-modifying Cyclase NisC through X-ray Crystallography”

08/2015 CLIB-GC & iGRASPseed 6<sup>th</sup> annual symposium “From Gene to Protein and Beyond”, Dusseldorf, Germany

03/2015 CLIB - Graduate Cluster 6<sup>th</sup> Annual Retreat, Wermelskirchen, Germany  
Poster presentation: “NisC in complex with NisA: A structural study through crystallization”

10/2014 4<sup>th</sup> Internal CLIB-GC Retreat HHU Düsseldorf, Mülheim, Germany  
Oral Presentation: “AC complex (NisC bound with NisA) structural study through crystallization”

09/2014 CLIB-GC & iGRASPseed 5<sup>th</sup> annual symposium “From Gene to Protein and Beyond”, Dusseldorf, Germany

02/2014 CLIB - Graduate Cluster 5<sup>th</sup> Annual Retreat, Lünen, Germany  
Poster presentation: “Characterization of a response transcriptional response regulator (NisR) involved in the two-component phosphoryl transfer signal transduction machinery from *Lactococcus lactis*”

11/2013 the International BioStruct Symposium "Biological Structures in Molecular Medicine and Biotechnology", Dusseldorf, Germany

10/2013 3<sup>rd</sup> Internal CLIB-GC Retreat HHU Düsseldorf, Kerkrade, Netherland  
Oral Presentation: “Modulation of the nisin-controlled expression system (NICE) in *lactococcus lactis*”

09/2013 CLIB-GC & iGRASPseed 4<sup>th</sup> Symposium “From Gene to Protein and Beyond”, Dusseldorf, Germany

### *Training*

---

06/2016 “X-ray Data Collection” by European Synchrotron Radiation Facility,  
Grenoble, France

01/2016 “Biostruct-X Mediterranean Macromolecular Crystallography Workshop”  
by Israel Institute of Technology, Haifa, Israel

10/2014 “Innovation management and patent Law” by CLIB<sup>2021</sup>, Wuppertal, Germany

10/2014 “Project Management” by CLIB<sup>2021</sup>, Wuppertal, Germany

08/2014 Summer School-“Advanced Post-genomics and Bioinformatics”, Bielefeld, Germany

### *Publications*

---

Bishnu P. Subedi, Andra L. Corder, **Siai Zhang**, Frank W. Foss Jr., and Brad S. Pierce “Steady-state kinetics and spectroscopic characterization of enzyme-tRNA interactions for the non-heme diiron tRNA-monooxygenase, MiaE” *Biochemistry*, **2015**. 54 (2): 363–376

Andra L. Corder, Bishnu P. Subedi, **Siai Zhang**, Amanda M. Dark, Frank W. Foss Jr., and Brad S. Pierce “Peroxide-shunt substrate-specificity for the *Salmonella typhimurium* O<sub>2</sub>-dependent tRNA modifying monooxygenase (MiaE)” *Biochemistry*, **2013**. 52 (36): 6182–6196

## **9. Acknowledgements**

I would like to express my greatest gratitude to Prof. Dr. Lutz Schmitt for offering me the opportunity to have my Ph. D study in his institute. I sincerely thank him for his supervising, encouragement, and academic advices. I’m really grateful that you are being extremely positive and always able to see something when I see nothing. As a busy guy, you are still there to try to help me solve all kinds of problem, even including some hands-on work. And I really appreciate it!

I especially thank Dr. Sander Smits for his guidance, scholarly suggestions, and motivations through out my Ph. D study. You are very generous with sharing me all your crystallography expertise, as well as the computational knowledge, which has

been invaluable for the progress of my project. And thank you very much for reviewing my thesis!

I would like thank Dr. Ulrich Schulte for his guidance and support while I'm doing practical course. I would also thank him for all the suggestions and comments that he made during Wednesday seminar.

I would give my gracious gratitude to Dr. Astrid Hoeppner for all her guidance, support and comforts. I'm always feeling thankful for having her company to ESRF and as well as for her constant patience with explaining me the crystallography 101. I feel extremely grateful that you are always there to help me whenever I come cross a problem.

I would also express my deep-hearted thanks to Stefanie for her special "magic" with my crystal. Thank you for your company in the crystallization room and for your support with my crystallization set-up. I'm very thankful that you take care of my plates, help me check my plates from time to time and keep me updated whenever you see something interesting.

I thank Dr. Diana Kleinschrodt and Iris for the guiding me through the cloning procedure and helping me with my primer designing, and of course for creating the spacer-less NisC construct for me!

I would express my special thanks to all the members of nisin group!

I firstly give my deepest thanks to Dr. Sakshi Khosa for her help and support through our my entire Ph. D. Thank you for introducing me to the Nisin world , teaching me purification and crystallography skills and patience for answering my endless, sometimes even annoying questions regarding crystallography. Thank you for accompanying me to my first synchrotron trip. I'm also very grateful to have your precious friendship in the institute. Thank you for taking me to the delicious Indian restaurants, sharing coffee and tea with me on the balcony and comforting me when I'm stressed and depressed.

Next, I would like to thank Jens for his collaboration on NisC project! Thank you for all the discussions, fruitful advices and helping me solve all the problems that I met for NisC. I really appreciate that you are always being patient with my questions regarding the HPLC, NisC protein and nisin molecule. Without you, it would take me ages to figure out how to deal with them. And I really appreciate that you helped me translate my abstract in to German version, which, for me, it's literally mission impossible...

And I also thank André, Zainab, Marcel and Rebecca for your collaborations on nisin project, as well as the discussions during every nisin meeting. Without your support and help, I would have gone through way more difficulties than I can imagine. Thank you all!

I would thank Kalpana for being my friend. Thank you very much for having lunch with me at small mensa, going to Vita together to have the delicious pizza, exploring the beauty of Duesseldorf. Also many thanks for being my translator when I feel frustrated with those German documents.

I give my special thanks and best wishes to the most lovely couple: Michael and Sven! I really appreciate both of your help with the SEC-MALS. Sometimes, you two even had to work late because of my samples, but you were always being supporting and considerate. Thank Sven for even taking care of my data when I'm too busy with my slides preparing and for telling me "it's OK" when I once screwed the MALS system. Thank Michael, my best neighbor ever, for all the cheer-up when I'm depressed, teaching me all kinds of softwares that I had no idea how to use them and walking me through the German history;-) Oh, and I highly appreciate that you went to the foreigner office with me for my VISA issue and it would never have been able to be solved so smoothly without your help!

Thank everyone else in how shared the same office with me! I would thank Martina for being generous with giving me new falcons, introductions about how to use the centrifuges and all the snacks. Thank Katja for her help and cooperation during the practical course. And welcome the new members: Isabelle and Julia! Hope you two would enjoy staying in this office as I do.

I would thank Katharina and Sandra, who basically joined the institute at the same time with me, for sharing the beginner feelings and also for having lunch and tea together.

Thank the rest of my dear colleagues: Tobias, Kerstin, Tim, Martin, Christian, Olivia and Manuel. Thank you all for discussions, advices, help, company outings and the parties! I also thank Kerstin for her translation from time to time. And Thank Manuel for the support and cooperation during the practical course.

I would specially thanks two of my friend I made at CLIB-GC: Anuseema and Daniel. Thank you two for accompanying me to all the retreats, trainings, for comforting me from the very start till the end of my Ph. D. Also thank you two too for showing me the computational side of biotechnology.

I thank Jessica, Jennifer, Sonja, Martina and Tatjana for the arrangement and management regarding all the CLIB-GC issues. Thanks a lot!

Last but not least, I would thank all my (old and new) friends and my family for believing in me all the time. In your eyes, I'm always the best even though we all know this is not true. For years, your support has been invaluable to me and helped me survive from all the frustrations and overcome all the obstacles. I'm not used to express my feelings, especially when I'm in depression, but you, all of you, can always understand me, stay on my side, be with me, tell me "everything is going to be fine." I'm stronger because of you all. You are the ones who make my life more colorful, beautiful and meaningful.

## **10. Declaration**

The dissertation presented here has been made independently and without unauthorized assistance. The dissertation has not been submitted in this or any similar form to any other institution. I have not taken any unsuccessful promotion exams so far.



---

(Siai Zhang)